PHYSICAL CHEMISTRY 2014

1st Workshop
on

# *Materials Science for Energy Related Applications*

## BOOK OF ABSTRACTS

September 26-27, 2014
University of Belgrade, Faculty of Physical Chemistry, Belgrade

KTH
ROYAL INSTITUTE OF TECHNOLOGY,
Stockholm, Sweden

UNIVERSITY OF BELGRADE,
FACULTY OF PHYSICAL CHEMISTRY,
Belgrade, Serbia

THE SOCIETY OF
PHYSICAL CHEMISTS OF SERBIA,
Belgrade, Serbia

1st WORKSHOP

on

# Materials Science for Energy Related Applications

held on September 26-27, 2014 at the University of Belgrade, Faculty of Physical Chemistry, Belgrade, Serbia

is a satellite event of

PHYSICAL CHEMISTRY 2014

*12th International Conference on Fundamental and Applied Aspects of Physical Chemistry*

organized by

**KTH**
**ROYAL INSTITUTE OF TECHNOLOGY**
**Stockholm, Sweden**

**UNIVERSITY OF BELGRADE**
**FACULTY OF PHYSICAL CHEMISTRY**
**Belgrade, Serbia**

in co-operation with

**THE SOCIETY OF PHYSICAL CHEMISTS OF SERBIA**

***Funded by***

***Swedish Research Council***

***Organizing Committee***

N. V. Skorodumova, KTH, Stockholm, Sweden
I. Pašti, University of Belgrade, Faculty of Physical Chemistry, Serbia
S. Mentus, University of Belgrade, Faculty of Physical Chemistry, Serbia
Š. Miljanić, University of Belgrade, Faculty of Physical Chemistry, Serbia
N. Gavrilov, University of Belgrade, Faculty of Physical Chemistry, Serbia
B. Simonović, University of Belgrade, Institute for General and Physical Chemistry, Serbia

PHYSICAL CHEMISTRY 2014

*12th International Conference on Fundamental and Applied Aspects of Physical Chemistry*

1st Workshop

# MATERIALS SCIENCE FOR ENERGY RELATED APPLICATIONS

September 26-67, 2014, University of Belgrade, Faculty of Physical Chemistry, Belgrade, Serbia

BOOK OF ABSTRACTS

BELGRADE, SERBIA 2014

1st WORKSHOP

on

Materials Science for Energy Related Applications

# BOOK OF ABSTRACTS

**Reviewers and Editors**

Prof. Dr. Natalia V. Skorodumova

Dr. Igor A. Pašti

**Publisher**

UNIVERSITY OF BELGRADE, FACULTY OF PHYSICAL CHEMISTRY,

Belgrade, Serbia

**For the Publisher**

Prof. Dr. Šćepan Miljanić

Printed by

University of Belgrade, Faculty of Physical Chemistry

Print run

40 copies

ISBN 978-86-82139-49-2

BELGRADE, SERBIA 2014

CIP - Каталогизација у публикацији
Народна библиотека Србије, Београд

66.017/.018(048)
621.315:66.017(048)
544.47(048)

WORKSHOP on Materials Science for Energy Related Applications (1st ; 2014 ; Beograd)
Book of Abstracts / 1st Workshop [on] Materials Science for Energy Related Applications, September 26-27, 2014, Belgrade, Serbia [within] 12th International Conference on Fundamental and Applied Aspects of Physical Chemistry - Physical Chemistry 2014 ; [organized by KTH Royal Institute of Technology, Stockholm, Sweden [and] University of Belgrade, Faculty of Physical Chemistry, Belgrade [and] the Society of Physical Chemistry of Serbia, Belgrade ; reviewers and editors Natalia V. Skorodumova, Igor A. Pašti]. - Belgrade : Faculty of Physical Chemistry, 2014 (Belgrade : Faculty of Physical Chemistry). - VI, 80 str. : ilustr. ; 29 cm

Tiraž 40. - Bibliografija uz svaki apstrakt.

ISBN 978-86-82139-49-2

1. International Conference on Fundamental and Applied Aspects of Physical Chemistry (12th ; 2014 ; Beograd) 2. Royal Institute of Technology (Štokholm)
a) Електротехнички материјали - Апстракти
b) Наука о материјалима - Апстракти c) Катализа - Апстракти

COBISS.SR-ID 209878028

# Table of Contents

**Session 1.3 – Electrocatalysis**



**Session 2.1 – Heterogeneous and Photocatalysis**



**Session 2.2 – Hydrogen storage**

# *Methods*

# *AB INITIO* NON-EQUILIBRIUM MOLECULAR DYNAMICS COMBINED WITH COLOR-DIFFUSION ALGORITHM: A THEORETICAL STUDY OF IONIC CONDUCTIVITY IN OXIDES

Olga Yu. Vekilova,[1] Johan O. Nilsson,[1] Olle Hellman,[2] Sergei I. Simak,[2] and Natalia V. Skorodumova[1, 3]

[1]*Multiscale Materials Modeling, Materials Science and Engineering,KTH - Royal Institute of Technology, Brinellvägen 23, 100 44 Stockholm, Sweden*
[2]*Department of Physics, Chemistry and Biology (IFM), Linköping University, SE581 83, Linköping, Sweden*
[3]*Department of Physics and Astronomy, Uppsala University, Box 516, 751 20 Uppsala, Sweden*

Non-equilibrium molecular dynamics is a powerful technique giving a possibility to theoretically study systems at high temperatures. In particular, it properly accounts for the effect of anharmonic lattice vibrations. Coupled with the color-diffusion algorithm it substantially decreases simulation time, allowing one to study diffusion from first principles. Understanding of the diffusion properties of electrolytic systems is of high practical importance for the modern development of fuel cells.

This approach has been successfully applied to study the oxygen diffusion coefficient and ionic conductivity in oxides, providing good agreement with the existing experiment data.

# THE KINETIC MONTE-CARLO APPROACH TO STUDY SLOW DIFFUSION PROCESSES IN ENERGY RELATED MATERIALS USING KMCLIB

Mikael Leetmaa

*Department of Physics and Astronomy, Uppsala University, Sweden*

Diffusion processes in solids and at interfaces are of fundamental importance in a wide range of areas in material science and technology, ranging from lithium ion batteries and defect diffusion and segregation in steels and alloys, to ion-conducting electrolytes in solid-oxide fuel cells and spillover phenomena in heterogeneous catalysis. These diffusion processes are typically studied either with ab initio techniques on short length and time scales, or at longer length and time scales using either continuum approaches or macroscopic models with parameters extracted from or fitted to experimental data. Bridging the gap between the details of the ab initio models with the time and length scales of the continuum approaches without sacrificing accuracy is one of the main contemporary challenges in computational materials science.

Ab initio kinetic Monte Carlo (KMC) modelling is in this respect a very appealing method, allowing simulations of large numbers of atoms over long times by only simulating rare events, where the need for describing fast vibrational motion explicitly is bypassed by treating the system as equilibrated each time a new rare event takes place. The input to a KMC simulation is the set of all possible elementary processes (or rare events) with their corresponding rate constants and the outcome of a KMC simulation is the trajectory of the simulated system evolving over time. Rate constants for the elementary reactions can be calculated with ab initio methods or estimated from other sources, and KMC thus provides a powerful tool for modeling slow diffusion processes over long time and length scales with the accuracy from ab initio techniques.

Despite the appeal of the method only a few general codes for performing KMC simulations exists, and they typically come with strict limitations on what types of systems and elementary processes can be used. We have recently developed a general framework for lattice KMC simulations, KMCLib,that has been made publicly available under the GPLv3 license [1]. This talk will give an overview of KMCLib and the features that make KMCLib unique, and I will show with examples from energy related materials science what you need to set up and run your own simulations using KMCLib.

**References**

[1] M. Leetmaa, N. V. Skorodumova, *Comput. Phys. Commun.* 185 (2014) 2340.

# MODELING OF ELECTROCHEMICAL DOUBLE-LAYER CAPACITORS

Petar Lauševića[1, 2], Vladimir Nikolić[1], Milica Marčeta Kaninski[1], Predrag Pejović[2]

[1] *Vinča Institute of Nuclear Sciences, Belgrade, Serbia*
[2] *School of Electrical Enginering, University of Belgrade, Serbia*

Electrochemical double-layer capacitors (EDLCs), or supercapacitors (SCs) as they are sometimes refer to, bridge the gap between batteries and conventional capacitors. Because of the wide range of EDLC applications, it is important to develop a model that can represent their behavior in all practical operations. This paper gives an owerviev of models used by scientist and engeeners and some models that attempt to link the two groups.

## Introduction

The operation of electrochemical double layer capacitors, being based on electrochemical principles, is normally better understood by scientists, but their operation also needs to be understood by electrical engineers. Electronic systems are generally very complicated, and simulation-based development methods are used to find better system architectures and optimal operation strategies. Accurate modeling is crucial for all components, and EDLCs, in particular, require a comprehensive model that is developed after a thorough understanding of its internal structure and characteristics. Developing a model that can explain the influence of voltage or temperature is of great importance. Self-discharge is crucial in acquiring accurate simulation results, for example, in simulation of driving cycles of fuel cell vehicles or electric cars.

For scientists, models have been used for determining the theoretical limits of supercapacitors energy and power densities and to generated new insights on methods to optimize supercapacitor design.

## Empirical Models

Engineers need a simplified equivalent circuit that manages to capture the characteristic behavior of supercapacitors under different operating conditions. Empirical models can be used to characterize parameters such as self-discharge and leakage current. Because the models are not developed on the basis of the physics of the device, the models cannot be used to predict the lifetime of a particular device.

A model which is commonly used for practical engineering was proposed by Zubieta [1] and is presented in figure 1. The model has three well distinct RC time constants covering the desired time range, resulting in an easily measurable model. The first branch (or the immediate branch), with the voltage-dependent capacitor $C_{i1}$ (in $F/V$), dominates the immediate behavior of the SC in the time range of seconds. The second branch or delayed branch dominates the terminal behavior in the range of minutes. Finally, the third branch determines the behavior for times longer than 10 minutes.

Modeling a two-terminal device using a circuit with eight parameters has unlimited possible solutions. Zubieta also proposed a procedure for the identification of the equivalent circuit parameters [1]. As a developed version of this model, Rafik formulated a model that takes into account frequency, voltage and temperature dependencies of capacitance, series resistance and leakage current to obtain a better agreement between simulations and experiments [2].

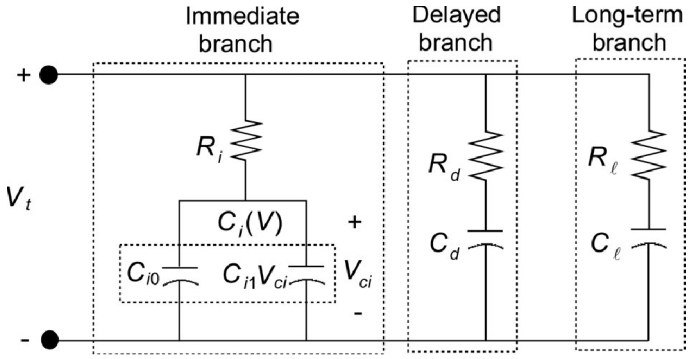


**Figure 1.** Zubieta three branch model.

**Equivalent Circuit Models for Detailed Physical Characterization**

Most of the SC models assume that the energy is stored purely by separation of charges at the electrode interface (the double layer) while neglecting or oversimplifying other aspects of EDLCs by not accounting for temperature dependency, the impact of pores, varying pore size, etc. One of the main reasons for the nonlinear rise of terminal voltage is the porous structure of the electrodes that prevents the movement of ions to interfacial sites located deep within a pore. So it is desirable to have a model that describes the transient and steady-state response of the porous electrode structure.

The first porous electrode model, developed by de Levie [3], treated the double-layer as a dissipative transmission line with a distributed double-layer capacitance and a distributed electrolyte resistance, by assuming a cylindrical pore electrode. The transmission line model is represented in figure 2. The main advantage of the transmission line model is its capability to provide a direct linkage between pore structures and the time (or frequency) response. It is based on the physical structure of the interface rather than on attempting to match the experimental

measurements through proper choice of passive circuit element combinations. However, the problem with these models is the complex determination of the different elements and the simulation time required, bounded by the large number of RC-branches.

Some new models take into account that the pores of activated carbon materials, used for EDLC electrodes, have a complex branch structure. These are known as multipore (MP) models. These models separate pores by their impedance time constant. The aim of this study is to show the impact of macro, meso and micro pores on the capacitance and to model the causes of SC ageing [4]. One approach is to group pores of the same individual impedance characteristics. Each group of pores can be modeled as a branch parallel to others. The resultant impedance of all the paralleled branches is the impedance of the whole porous structure. As this model is a generalization of de Levie's single pore model, the pores are considered to be cylindrical [5].

For all of these complex models, electrochemical impedance spectroscopy (EIS) analysis is performed in order to carry out the parameter identification [6]. From this analysis it has been observed that classical models need to be very complex in order to achieve a good match with experimental results.

Another important group of models are fractional order models. There are numerous different fractional order models. One of these models can be obtained by substituting the capacitor elements in the transmission line model of figure 2 with a constant phase elements (CPE). The impedance of a CPE is:

$$Z_{CPE} = \frac{1}{(j\omega)^{\gamma} \cdot C}. \tag{1}$$

Where C is the capacitance and $0 < \alpha \leq 1$, $\alpha = 1$ for an ideal capacitor. In addition, the use of fractional-order mathematical models instead of integer-order models can improve the behavior of the model towards the physical system [7].

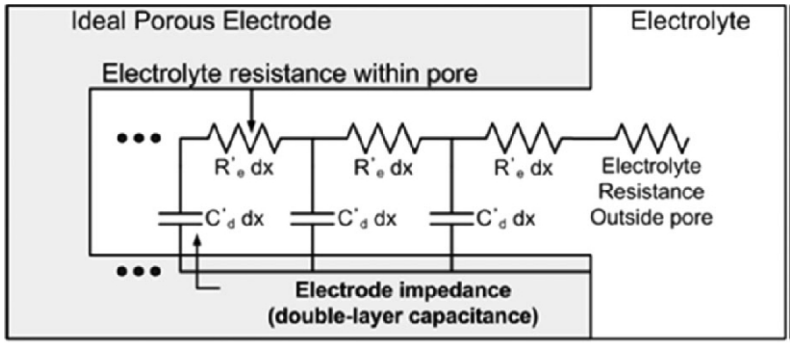


**Figure 2.** Model of the ideal porous electrode.

## Conclusions

A short overview of EDLC models was given in this paper. In spite of different modeling efforts no single model has yet emerged that is capable of representing the whole range of experimental results.

## References

[1] L. Zubieta R. Bonert, *IEEE Trans. Ind. Appl.* 36 (2000) 199.
[2] F. Rafik, H. Gualous, R. Gallay, A. Crausaz, A. Berthon, *J. Power Sources* 165 (2007) 928.
[3] R. de Levie, *Electrochim. Acta* 8 (1963) 751.
[4] R. German, P. Venet, A. Sari, O. Briat, J.-M. Vinassa, *IEEE Trans. Power Electron.* 29 (2014) 3669.
[5] M. Itagaki, S. Suzuki, I. Shitanda, K. Watanabe, H. Nakazawa, *J. Power Sources* 164 (2007) 415.
[6]S. Buller, S. Member, E. Karden, D. Kok, R. W. De Doncker, *IEEE Trans. Ind. Appl.* 38 (2002) 1622.
[7] S. Kim, W. Choi, K. Lee, S. Member, *IEEE Trans. Power Electron.* 26 (2011) 3377.

# NEW SYNTHETIC PROCEDURES FOR NANOMETRIC CARBIDES

Biljana Babić, Branko Matović

*Vinča Institute for Nuclear Sciences, University of Belgrade, P. O. Box 522, 11000 Belgrade, Serbia*

Carbon cryogel (CC) is a special class of porous carbon material which is usually formed from the sol-gel polycondenzation of resorcinol and formaldehyde, followed by freeze drying and subsequent pyrolysis. CC material possesses high specific surface and mesoporous structure, which can be controlled by varying the concentration of starting resorcinol - formaldehyde solutions and catalyst. In addition, carbon cryogel can be used as a source of carbon in synthesis of new nanomaterials such as metal carbides.

## Introduction

In 1989, Pekala [1] firstly described the synthesis procedure of organic gels with properties similar to silica gels. Synthesis procedure considers polycondenzation of resorcinol (R) and formaldehyde (F), in the presence of basic catalyst. To preserve the porous structure, wet RF gels can be dried by supercritical (aerogel) or freeze-drying (cryogel) method. Although carbon aerogel possess superior porous properties, their commercial applicability is quite limited mainly due to high cost of production. It has been shown [2] that mesoporous carbon, with appropriate characteristics, could be obtained by using, more economical, freeze-drying method.

In our previous work we have shown that, due to their characteristics such as: high specific surface (500-800 $m^2/g$), mesoporous structure and good electrical conductivity, CC can be used as a material for supercapacitors and catalyst support for fuel cells [3, 4]. Also, as a special form of active carbon, this material is a good adsorbent for organic compounds and metal ions from aqueous solutions.

Recently, we developed a new method for synthesis carbides of different metals, by using CC. This method is based on several facts:

- CC is obtained by sol-gel method, from aqueous solutions.
- If we consider that RF gel is a source of carbon, some liquid compound or solid compound soluble in water can be the source of other metal or nonmetal.
- Synthesis procedure starts from liquid phase which provide good mixing on molecular level.
- Thermal treatment in inert atmosphere will remove all traces of organic compounds and porous structure of gels and nanometric size of pores will provide that final material has particles in nanometric range.

## Experimental

SiC and WC were synthesized by polycondensation of resorcinol (R) with formaldehyde (F), with sodium carbonate (C) as a basic catalyst, in presence of different amounts of metal or nonmetal precursors. The source of Si and W were TEOS and ammonium metatungstate (AMT), respectively. The starting compositions were designed in order to yield different carbon/metal ratios. In all samples the concentration of the RF starting solution was 20 mass% and R/C ratio was 100. The mixture was poured into a glass tubes, sealed to prevent evaporation of water, and gelled by keeping for 2 days at 25 °C, 1 day at 50 °C, and 4 days at 85 °C. The RF cryogel was obtained by freeze-drying method. The exchange of water was done with *t*-butanol. The RF gels were pre-frozen and then freeze dried for 24 h under vacuum. The RF cryogel was further carbonized at 800 °C in nitrogen flow, and cooled to room temperature. In order to obtain desired materials, additional thermal treatment was performed. Samples were characterized by X-ray diffraction, SEM and TEM methods.

## Results and discussion

*Synthesis of nanometric silicon carbide*

The powders obtained after pyrolysis at 800 °C were amorphous and consisted of $SiO_2$ network with dispersed carbon. Subsequent heat treatment at higher temperatures initiated the formation of crystalline SiC. The effect of temperature of heat treatment on SiC crystallization is presented at figure 1a. As expected, the amount of β-SiC increase with an increase in temperature of the heat treatment. SEM image of sample obtained 1200 °C shows that powder is consisted of agglomerates of fine SiC crystallites with diameter about 20 nm (Fig. 1b).

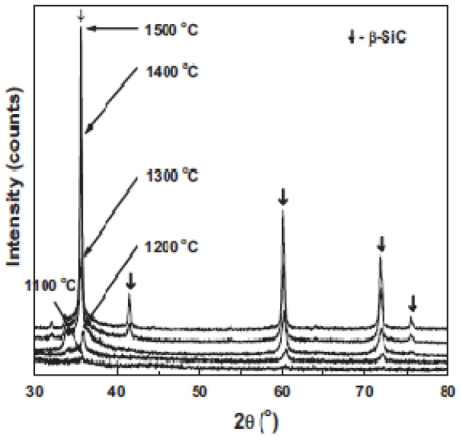


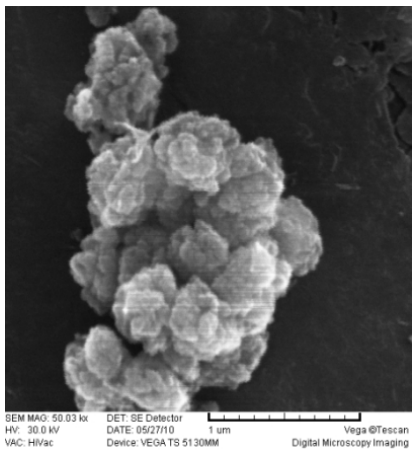


**Figure 1.** a) XRD patterns of samples heat-treated at different temperatures b) SEM image of SiC sample obtained at 1200°C.

*Synthesis of chore-shell tungsten carbide*

After pyrolysis, additional heat treatment was performed at 950 °C, in reducing atmosphere of $H_2$, for 2 h. Fig. 2a represents XRD pattern of obtained material. The diffraction peaks correspond to metallic W. These results indicate that tungsten support was converted to tungsten or to mixture of different carbides, in the quantity of few monolayers. TEM image (Fig. 2b) of material shows core–shell structure, containing W core and WC shell about 2–5 nm of thickness.

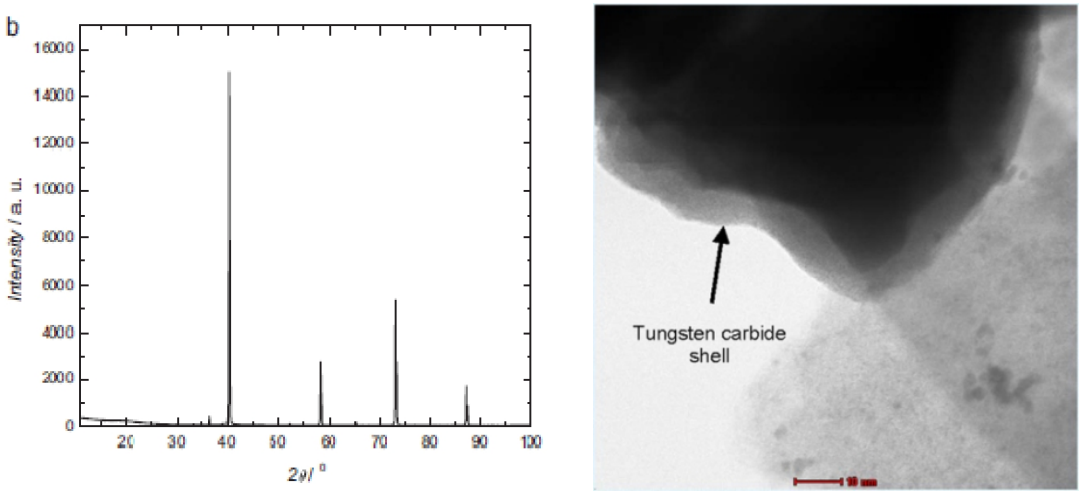


**Figure 2.** a) XRD pattern and b) TEM image of WC sample obtained at 950 °C, in $H_2$.

## Conclusion

A new method for preparation of metal carbides was proposed. Nanosized metal carbides were prepared by pyrolysis of resorcinole-formaldehyde gels, in presence of different metal precursors. Resorcinole and formaldehyde were found to be a promising source of carbon. To obtain desired materials, additional thermal treatment was performed, after carbonization.


## Acknowledgements

This work was supported by the Ministry of Science and Development, the Republic of Serbia, under Contract No. 45012.


## References


[1] R. W. Pekala, *J. Mater. Sci.* 24 (1989) 3221.
[2] H. Tamon, H. Ishizaka, T. Yamamoto, T. Suzuki, *Carbon* 37 (1999) 2049.
[3] B. Babić, B. Kaluđerović, Lj. Vračar, N. Krstajić, *Carbon* 42 (2004) 2617.
[4] B.M. Babić, Lj.M. Vračar, V. Radmilović, N.V. Krstajić, *Electrochim. Acta* 51 (2006) 3820.

# *Solid electrolytes and oxide materials for energy related applications*

# DESIGNING $Li_2Mn_xFe_{1-x}SiO_4$ AS A POTENTIAL Li-BATTERY CATHODE MATERIAL

Anton Kokalj,[1] Robert Dominko,[2] Gregor Mali,[2] Anton Meden,[3] Miran Gaberšček,[2] and Janez Jamnik[2]

[1]*Jožef Stefan Institute, Jamova 39, SI-1000 Ljubljana, Slovenia*
[2]*National Institute of Chemistry, Hajdrihova 19, SI-1000 Ljubljana, Slovenia*
[3]*Faculty of Chemistry and Chemical Technology, Askerčeva 5, SI-1000 Ljubljana, Slovenia.*

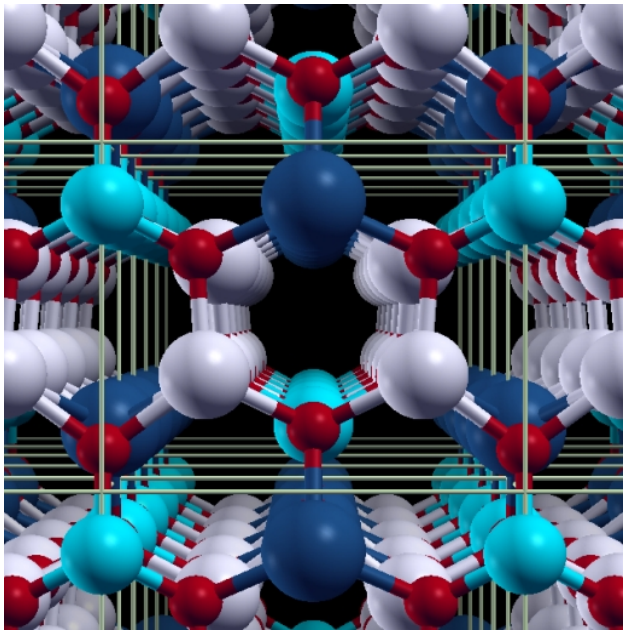

Two materials from a family of transition metal silicates, $Li_2FeSiO_4$ and $Li_2MnSiO_4$, have been successfully prepared and preliminary tested as potential positive electrode materials (cathodes) for lithium ion batteries [1,2]. The primary motivation for introduction of silicate-based materials in lithium batteries was their low price and safety. Among them, $Li_2MnSiO_4$ has been identified as one of the first cathode battery materials that, at least in principle, could exchange more than 1 lithium per redox-active transition metal ion [1]. However, actual experiments have not confirmed this expectation, and we demonstrate by a thorough analysis based on experiments and density-functional-theory (DFT) computer modeling why this is so [3]. In particular, $Li_2MnSiO_4$ is unstable upon delithiation, with a strong tendency to amorphize. Detailed DFT calculations further indicate that it might be possible to obtain a stable material with a reversible exchange of more than one Li per redox-active transition metal ion by using an appropriate Mn/Fe mixture with a general formula $Li_2Mn_xFe_{1-x}SiO_4$ [3].

**References**

[1] R. Dominko, M. Bele, M. Gaberšček, A. Meden, M. Remškar, J. Jamnik, *Electrochem. Commun.* 8 (2006) 217.
[2] A. Nytén, A. Abouimrane, M. Armand, T. Gustafsson, J. O. Thomas, *Electrochem. Commun.* 7 (2005) 156.
[3] A. Kokalj, R. Dominko, G. Mali, A. Meden, M. Gaberšček, J. Jamnik, *Chem. Mater.* 19 (2007) 3633.

# LITHIUM *VS.* SODIUM INTERCALATION MATERIALS IN AQUEOUS SOLUTIONS

Milica Vujković[1], Slavko Mentus[1,2]

[1]*Faculty of Physical Chemistry, University of Belgrade, Studentski trg 12-16, P.O. Box 137, Belgrade, Serbia.*
[2]*The Serbian Academy of Science and Arts, Knez Mihajlova 35, 11158 Belgrade, Serbia*

Several materials able to intercalate lithium ions, were synthesized, either chemically or electrochemically in their sodium forms: layered $Na_{1,2}V_3O_8$ and $Na_2V_6O_{16}$/C, olivine $NaFePO_4$/C and nasicon $NaTi_2(PO_4)_3$/C. Their intercalation capacity for both lithium and sodium ions was investigated in saturated aqueous solutions of $LiNO_3$ and $NaNO_3$ by potentiodynamic cycling. All materials can be recognized as excellent bifunctional materials. Lower sodium versus lithium storage capacity was found for vanadium based layered structure materials, whereas higher one was evidenced in the case of olivine and nasicon.

## Introduction

The Li-ion batteries with organic electrolytes possess the excellent electrochemical performances (high energy density) providing them a wide use in electronic communication devices and electric cars. In order to contribute to safely and simple production, many studies were devoted to the development of batteries with aqueous electrolytes. The suspect that the abundance of Li in Earth's core is satisfactory for grooving applications incited the researchers to develop Na-ion batteries. Although somewhat poorer in voltage, these batteries might replace Li ones in less demanding area of use (communication devices), and save Li for high-demanding area of use (electric cars). However, there is an important question whether Na intercalation materials may reach the capacity comparative to that of Li intercalation materials [1]. The aim of this study was to evaluate and compare the reaction kinetics and intercalation capacity in aqueous solutions, of several electrode materials known in literature as well Li-ion intercalated materials in organic solutions. For this purposes, layered $Li_{1,2}V_3O_8$ and $Li_2V_6O_{16}$/C, olivine $LiFePO_4$/C and nasicon $LiTi_2(PO_4)_3$/C were synthesized in their sodium forms, and investigated potentiodynamically in Li and Na aqueous nitrate solutions.

## Experimental

$Na_2V_6O_{16}$/C composite was synthesized hydrothermally, $Na_{1.2}V_3O_8$ was obtained by sol-gel process while the glycine-nitrate combustion process was employed for the synthesis of both $LiFePO_4$/C and $NaTi_2(PO_4)_3$ /C composites. $NaFePO_4$/C was obtained by electrochemical Li-Na

exchange of $LiFePO_4$/C. Used procedures are similar to those describe in references [2-5]. For electrochemical investigations, the working electrode was made as described in detail in ref. [2-5].

The cyclic voltammetric (CV) experiments were performed in a three-electrode type electrochemical cell, with the Pt as counter electrode, and saturated calomel electrode (SCE) as reference electrode, connected to Gamry PCI4/300 Potenstiotat/Galvanostat.

**Results and discussion**

By X-ray diffraction the structure of the synthesized samples was checked and confirmed, before than subjected to CV investigations.

Figure 1 shows the comparative CV's of vanadium-based oxides in aqueous electrolytes. Well defined peaks in both anodic and cathodic scan directions, at very high scan rate of 10 $mVs^{-1}$, indicate very fast kinetics of both lithium and sodium intercalation/deintercalation in sodium-based vanadium oxides. Since the charge storage is proportional to the area under CV curves, somewhat higher Li vs. Na storage capacity was measured, which may be due to smaller $Li^+$ than $Na^+$ ion. On the other hand, although the ionic radius of Na is higher than that of lithium, sodium intercalation/deintercalation kinetics of $LiFePO_4$/C and $NaTi_2(PO_4)_3$/C from aqueous electrolyte was evidenced to be faster than the lithium one, Fig.2. One of the reason may be weaker $Na^+$-$PO_4^{3-}$ bond compared to the $Li^+$-$PO_4^{3-}$ one. Different CV's of $LiFePO_4$/C and $NaTi_2(PO_4)_3$/C in $LiNO_3$ and $NaNO_3$ show the differences in the reaction kinetics of Na and Li interfacial reaction. Anodic and cathodic peaks of $LiFePO_4$ in both $LiNO_3$ and $NaNO_3$ correspond to the phase transition from $LiFePO_4$ (or $NaFePO_4$) to $FePO_4$ and vice versa, respectively. The phase transition during desodiation process occurred via intermediate phase $Na_{0.7}FePO4$ which is responsible for the splitting of anodic peak. Unlike vanadium-based oxide and olivine, where desodiation reaction occurred via more than one step, desodiation reaction from nasicon is one step process. Differences between CV curves of $NaTi_2(PO_4)_3$/C in

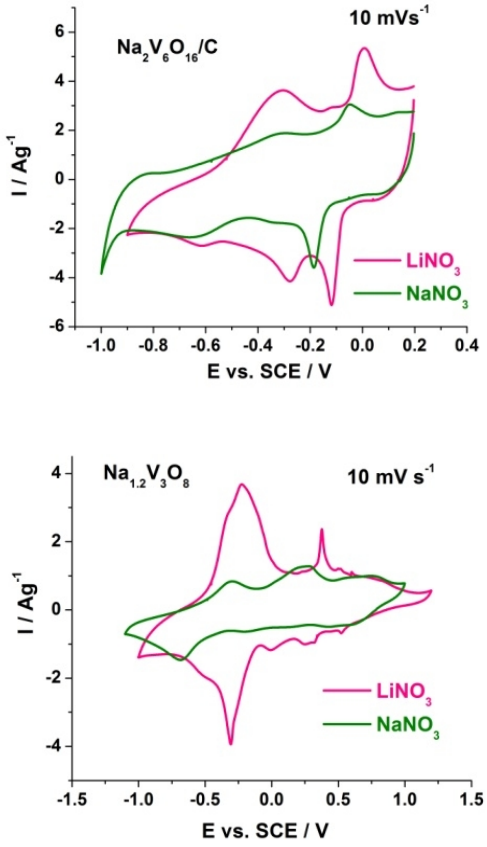


**Figure 1.** CV's of vanadium-based oxides measured in aqueous $LiNO_3$ and $NaNO_3$ solutions.

$LiNO_3$ and $NaNO_3$ originates from the different occupancy of crystallographic positions by intercalated ions. Namely, two redox peaks of nasicon in $LiNO_3$ correspond two non-equivalent crystallographic positions for Li ions, whereas this difference is almost absent for sodium ions.

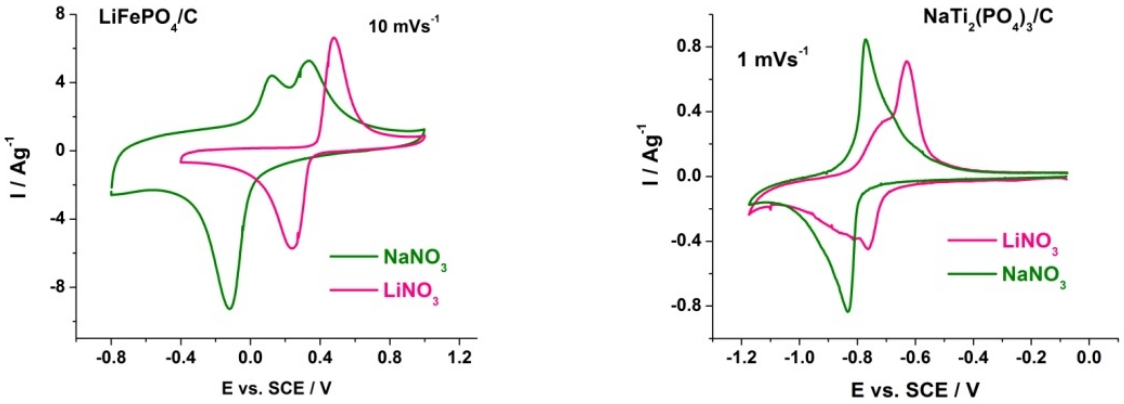


**Figure 2.** CV's of $NaFePO_4$/C (left) and $NaTi_2(PO_4)_3$/C (right) measured in aqueous $LiNO_3$ and $NaNO_3$ solutions.

## Conclusion

The crystal structure strongly influences to the reaction kinetics of material in aqueous solutions. The vanadium-based layered type oxides such as $Na_2V_6O_{16}$/C and $Na_{1.2}V_3O_8$ as well as olivine type $LiFePO_4$/C and nasicon type $NaTi_2(PO_4)_3$/C composites were evidenced to be excellent bifuncional intercalation materials in aqueous $LiNO_3$ and $NaNO_3$ solutions. Even faster intercalation of $Na^+$ ions relative to $Li^+$ ions was found for the $NaFePO_4$/C and $NaTi_2(PO_4)_3$/C composites, which make them very promising electrode materials for aqueous sodium-ion batteries.


## Acknowledgement

This work was supported by the Ministry of Sciences and Environmental Protection of Serbia through the Project III 45014.


## References


[1] D. Buchholz, A. Moretti, R. Kloepsch, S. Nowak, V. Siozios, M. Winter, S. Passerini, *Chem. Mater.* 25 (2013) 142.

[2] M. Vujković, I. Stojković, N. Cvjetićanin, S. Mentus, *Electrochim. Acta* 92 (2013) 248.

[3] M. Vujković, S. Mentus, *J. Power Sources* 247 (2014) 184.

[4] H. Wang, W. Wang, Y. Ren,K. Huang, S. Liu, *J. Power Sources* 199 (2012) 263.

[5] I. Stojković, N. Cvjetićanin, M. Mitrić, S. Mentus, *Electrochim. Acta* 56 (2011) 6469.

## TUNING IONIC CONDUCTIVITY IN CERIA BY VOLUME OPTIMIZATION

O. Hellman,[1] N. V. Skorodumova,[2,3] S. I. Simak[1]

[1] *Department of Physics, Chemistry and Biology (IFM), Linkoping University, SE-581 83, Linkoping, Sweden.*
[2] *Multiscale Materials Modelling, Department of Materials Science and Engineering, Royal Institute of Technology, SE-100 44 Stockholm, Sweden*
[3] *Division of Materials Theory, Department of Physics and Astronomy, Uppsala University, Box 516, S-751 20 Uppsala, Sweden*

Ceria is an important material in many environmentally benign applications. The characteristic high oxygen mobility is crucial to these applications. The optimization of this mobility has been the topic of many studies over the past decade. Attempts at improving the ionic conductivity usually revolve around choosing the correct kind and concentration of dopants. Here we approach the problem from a different direction: how does the conductivity depend on the lattice parameter? This question is valid as most external parameters carry with them a volume change. Effect of volume change on the ionic conductivity in ceria has been studied in the framework of the density functional theory. We show that varying the lattice constant of ceria one can change the topology of the energy landscape for the oxygen ion diffusion. We reveal the existence of the narrow range of lattice parameters, which optimize the ionic conductivity in ceria.

## IONIC CONDUCTION IN GADOLINIUM-DOPED CERIA

Johan O. Nilsson,[1] Olga Yu. Vekilova,[1] Olle Hellman,[2] Sergei I. Simak,[2]
Natalia V. Skorodumova[1,3]

[1] *Multiscale Materials Modeling, Materials Science and Engineering, KTH - Royal Institute of Technology, Brinellvägen 23, 100 44 Stockholm, Sweden*
[2] *Department of Physics, Chemistry and Biology (IFM), Linköping University, SE-581 83, Linköping, Sweden*
[3] *Department of Physics and Astronomy, Uppsala University, Box 516, 751 20 Uppsala, Sweden*

Rare-earth doped Ceria (CeO2) is considered a promising candidate for an electrolyte material in solid oxide fuel cells (SOFCs), owing to its relatively high oxygen-ion conductivity at intermediate temperatures (700 – 1000 K). We investigate the oxygen-ion conductivity in gadolinium-doped ceria with a non-equilibrium ab initio molecular dynamics method implementing the color force algorithm. We describe the preparatory steps of the approach, and how we have analyzed the data in practice. This includes among other things finding an appropriate color field and analyzing the ionic conductivity. We will also discuss our results for ceria doped with 6 % gadolinium at temperatures: 973 K, 1000K, 1073 K, 1173; and how they compare with results reported in the literature from both experiments and other computational studies.

# SYNTHESIS AND CHARACTERIZATION OF $Ce_{1-x}Bi_xO_{2-\Delta}$ SOLID SOLUTION FOR SOLID OXIDE FUEL CELLS APPLICATIONS

M. Prekajski[1], B. Matović[1] M. Stojmenović[1], G. Branković[2]

[1]*Institute of Nuclear Sciences "Vinca", Belgrade University, Belgrade, Serbia*
[2]*Institute for Multidisciplinary Research, University of Belgrade, Kneza Višeslava 1a, 11030 Belgrade, Serbia, Belgrade, Serbia*

Solid solution $Ce_{1-x}Bi_xO_{2-\delta}$ nanopowders with the composition of x = 0.1 - 0.5 were synthesized by using Self Propagating Room Temperature procedure (SPRT). The results obtained by XRPD show that synthesized samples were single-phase solid solution at room temperature. Powders were densified by using Conventional (CS) and Microwave (MS) Sintering techniques at different temperatures, in an air atmosphere for 1 h. Complex impedance method measurements were carried out on sintered samples. The highest conductivity was obtained for the ceramic composition $Ce_{0.80}Bi_{0.20}O_{2-\delta}$ sintered by microwave technique at 700 °C.

## Introduction

Ceria-based materials have been extensively studied as one of the most promising electrolytes for reduced temperature solid oxide fuel cell (SOFC) system due to their high ionic conductivity at moderate temperature [1-3]. $CeO_2$ system doped with $Bi^{3+}$ can be very interesting for application in SOFC's due to the high ion conductivity of $CeO_2$ and $Bi_2O_3$ phases [4]. Exactly that was a motivation for synthesis, characterization and study of sintering properties and ionic conductivity on this solid solution.

## Results and discussion

A series of nanocrystalline solid solutions $Ce_{1-x}Bi_xO_{2-\delta}$ (x = 0.1 – 0.5) were synthesized by cost and time SPRT method. The products were characterized by X-ray powder diffraction (XRPD), transmission electron microscopy (TEM) and Rietveld refinement procedure. The results showed that the solubility of $Bi^{3+}$ in ceria ($CeO_2$) can be as high as 50 mol% and all solid solutions crystallized in single-phase cubic fluorite type structure. The average crystallite size of synthesized powders was less than 5 nm.
Thermal stability of obtained solid solutions was investigated by thermogravimetric analysis (DTA/TGA). It was found that the sample with 10 mol% of $Bi^{3+}$ stays stable and monophased

even at temperature as high as 1400 $^{o}$C. On the other side, samples with higher concentration of bismuth are unstable at high temperature. Namely, $Bi^{3+}$ leaves the structure of ceria and forms $\beta$-$Bi_2O_3$ as a second phase which will start to evaporate at temperatures higher than 1100 °C.
Synthesized samples were sintered with two different methods. It appears that conventional sintering requires much higher temperatures for densification. However, at high temperatures there is significant loss of $Bi^{3+}$ content due to process of evaporation. This problem can be overcome by applying the microwave sintering technique. In this way high densified samples can be obtained at much lower temperatures (1050 ºC) without loss of $Bi^{3+}$ concentration.
The ionic conductivity measured by impedance spectroscopy showed that the samples with lower $Bi^{3+}$ content exhibited primarily the grain boundary conductivity, whereas the sample with composition $Ce_{0.5}Bi_{0.5}O_{2-\delta}$ depicted the bulk conductivity. In both cases conductivity increased dramatically with increasing temperature as well as with $Bi^{3+}$ concentration. The highest conductivity was obtained for the ceramic composition $Ce_{0.80}Bi_{0.20}O_{2-\delta}$ sintered by microwave technique at 700 °C.

## Conclusion

Solid solution $Ce_{1-x}Bi_xO_{2-\delta}$ powders in nanometric range (less than 4 nm) was successfully synthesized in range from 10 - 50% of $Bi^{3+}$ by SPRT method. Sintering of the obtained powders was performed by both conventional and microwave sintering. It appeared that the microwave sintering was more convenient to obtain dense samples. Ionic conductivity measurement showed that conductivity increased dramatically with increasing temperature as well as with $Bi^{3+}$ concentration. It seems that $Ce_{1-x}Bi_xO_{2-\delta}$ solid solution is promising material for application in IT-SOFC's.

## References

[1] H. Inaba, H. Tagawa, *Solid State Ionics* 83 (1996) 1.
[2] J. Van Herle, T. Horita, N. Kawada, N. Sakai, H. Yokakava, M. Dokiya, *Solid State Ionics* 86-88 (1996) 1255.
[3] K. Zheng, B.C.H. Sreele, M. Sahibzada, I.S. Metcafe, *Solid State Ionics* 86-88 (1996) 1221.
[4] Z.C. Li, H. Zhang, B. Bergman, *Ceram. Int.* 34 (2008) 1949.

# NOVEL FLUORINE-CONDUCTIONG SOLID ELECTROLYTES OF FLUORITE STRUCTURE IN THE $KYF_4$-$PbF_2$ SYSTEM

Yu.V. Pogorenko,[1] R.M. Pshenychnyi,[1] A.O. Omelchuk,[1] V.I. Lutsyk[2]*

[1]*Vernadskii Institute of General & Inorganic Chemistry of the Ukrainian NAS, prospekt Palladina 32-34, 03680 Kyiv 142, Ukraine*
[2]*Institute of Physical Materials Science, Siberian Branch, Russian Academy of Sciences,6, Sah'yanova str., Ulan-Ude 670047, Russia*
**e-mail: vluts@ipms.bscnet.ru*

The increasing interest in studying mass and charge transfer in fluoride compounds is due to good prospects for their practical use in electrochemical devices for different purposes, in particular as solid electrolytes in electrochemical power sources, for the creation of ion-selective electrodes and sensors, electrochemical generators of high-purity fluorine, etc [1, 2]. Among fluoride ion conducting solid electrolytes, lead difluoride and compounds based on it attract special attention. $PbF_2$-based aliovalent substitution solid solutions with fluorite structure have a high fluorine anion conductivity, which is due to the migration of fluoride sublattice defects. This makes it possible to use them for the creation of electrochemical devices for different purposes. References [3-5] present data on ion mobility in $(1 - x)\ PbF_2 \cdot xMF_n$ solid electrolytes (where M = Li, Na, K, Rb, Cs, Zr, Mg, Ca, Sr, Ba, Bi, Y). It has been found that at temperatures above 500 K, the conductivity of solid solutions is higher than that of lead fluoride of β-modification.

This paper presents the results of studies on the synthesis of fluorine-conducting phases in the quasi-binary $KYF_4 – PbF_2$ system and the investigation of their electrophysical properties.

The solid solutions were prepared by solid-state synthesis at 773 K according to the scheme:

$$xKYF_4 + (1–x)PbF_2 \rightarrow K_xPb_{1–x}Y_xF_{2x+2}$$

It has been found from the results of an X-ray phase analysis that single-phase compounds are formed in the $KYF_4 – PbF_2$ system at a $KYF_4$ content of 47-69 mol %. The unit cell parameter of the synthesized samples in the above concentration range are well approximated by the Vegard law. Outside this range, mixtures of starting substances with solid solutions or mixtures of two solid solutions are formed.

The electrophysical properties of the synthesized phases have been investigated (Table 1). For the solid electrolyte $K_{0,5}Pb_{0,5}Y_{0,5}F_3$, the plot of conductivity against temperature is approximated by the equation of a straight line in the $\lg \sigma$ - 1/T coordinates. The plots of conductivity against temperature for the samples with higher $KYF_4$ content have a more complex shape. Above 500 K, a sharp increase in conductivity is observed, followed by passage into straight line portion

(Fig ). This dependence may be due to an increase in defect concentration in the fluoride sublattice of fluorite structure through the compensation of the difference in charge between $Pb^{2+}$ and aliovalent $K^+$ and $Y^{3+}$ cations. According to the aliovalent substitution rule, $Pb^{2+}$ ions can be substituted by $K^+$ and $Y^{3+}$ ions according to the scheme:

$$2Pb^{2+} \rightarrow K^+ + Y^{3+}.$$

The conductivity of the synthesized phases at temperatures above 500 K is higher than that of β - $PbF_2$ ($\sigma = 2.6 \times 10^{-4}$ S/cm at 500 K). A sharp increase (of 2 – 2.5 orders of magnitude) in the electrical conductivity of the investigated samples on heating is observed in a rather narrow temperature range (500 – 570 K). This makes it possible to recommend them for the creation of thermistor materials with negative temperature coefficient.

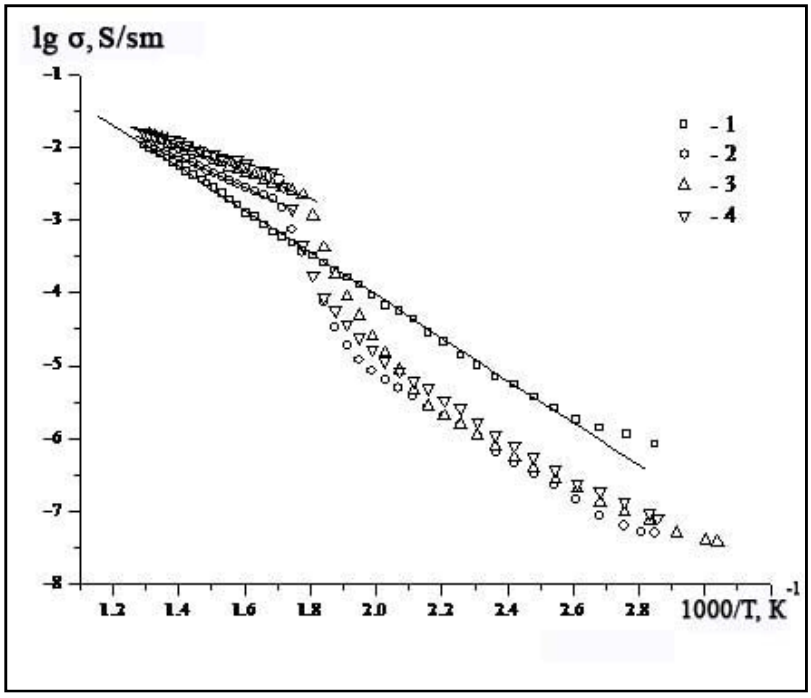


**Figure:** Plots of anion conductivity against temperature for the synthesized phases: (1) $K_{0,5}Pb_{0,5}Y_{0,5}F_{3,}$ (2) $K_{0,55}Pb_{0,45}Y_{0,55}F_{3\text{-}1}$, (3) $K_{0,6}Pb_{0,4}Y_{0,6}F_{3..2}$, (4) $K_{0,65}Pb_{0,35}Y_{0,65}F_{3.3}$

Thermal effects associated with polymorphic transformations of the synthesized phases have not been detected in the temperature range 293 -1073 K.

It was noted that the electrical conductivity of the synthesized solid solutions increases in direct proportion to the $KYF_4$ content of them, and that the activation energy decreases in inverse proportion. This dependence is typical of aliovalent substitution solid solutions (1 - *x*) $PbF_2$ -

$x$MF$_3$ and may indicate that the conductivity of the synthesized phases is realized mainly by the interstitial fluorine anions of the fluorite matrix.

**Table 1.** Ion conductivity parameters of solid solutions

| Sample | $\Delta T$ (K) | $\Delta E_a$ (eV) | lg ($A$) ((S / cm) · K) | $\sigma$ (S / cm) | $T$ (K) |
|---|---|---|---|---|---|
| $K_{0,5}Pb_{0,5}Y_{0,5}F_3$ | 350–773 | 0,61 ±0,01 | 4,86 | $1{,}1\cdot10^{-6}$ | 362 |
| | | | | $1{,}0\cdot10^{-2}$ | 773 |
| $K_{0,55}Pb_{0,45}Y_{0,55}F_{3,1}$ | 351–513 | 0,59 ±0,01 | 3,54 | $6{,}3\cdot10^{-8}$ | 363 |
| | | | | $1{,}2\cdot10^{-5}$ | 513 |
| | 583–773 | 0,45 ±0,01 | 3,88 | $1{,}5\cdot10^{-3}$ | 583 |
| | | | | $6{,}0\cdot10^{-3}$ | 773 |
| $K_{0,6}Pb_{0,4}Y_{0,6}F_{3,2}$ | 333–463 | 0,52 ±0,01 | 2,81 | $4{,}2\cdot10^{-8}$ | 333 |
| | | | | $4{,}0\cdot10^{-6}$ | 463 |
| | 563–773 | 0,43 ±0,01 | 3,72 | $2{,}2\cdot10^{-3}$ | 563 |
| | | | | $1{,}5\cdot10^{-2}$ | 773 |
| $K_{0,65}Pb_{0,35}Y_{0,65}F_{3,3}$ | 350–503 | 0,57 ±0,01 | 3,54 | $8{,}1\cdot10^{-8}$ | 350 |
| | | | | $1{,}7\cdot10^{-5}$ | 503 |
| | 593–773 | 0,30 ±0,01 | 2,99 | $4{,}6\cdot10^{-3}$ | 593 |
| | | | | $1{,}3\cdot10^{-2}$ | 773 |

The conductivity values obtained for solid solutions of fluorite structure in the $KYF_4$ – $PbF_2$ system in the temperature range 350 – 770 K give grounds to class the synthesized compounds as solid electrolytes with fluoride anion conductivity, which are close in conductivity to $La_{1-x}Ba_xF_{3-x}$ compounds [6] and can be recommended for use in different electrochemical devices.

**References**


[1] Yu.Ya. Gurevich, *Solid electrolytes* (in Russian), Nauka, Moscow (1986).

[2] A. K. Ivanov-Shits, I. V. Murin, *Solid-state ionics, vol 2 (in Russian)*, SPbGU Publishers, St.Petersburg (2010).

[3] V. Ya. Kavun, A. V. Slobodyuk, Ye. A. Tararako, Ye. Yu. Mikhteeva, V. K. Goncharuk, N. F. Uvarov, V. I. Sergiyenko, *Inorganic Mater.* 41 (2005)1388.

[4] V. Ya. Kavun, A. V. Slobodyuk, Ye. A. Tararako, Ye. Yu. Mikhteeva, V. K. Goncharuk, N. F. Uvarov, V. I. Sergiyenko, *Inorganic Mater.* 43 (2007) 352.

[5] Y. Ito, K. Koto, S. Yoshikado, T. Ohachi, *Solid State Ionics* 18–19 (1986)1202.

[6] M. Reddy, M. Fichtner, *J. Mater. Chem.* 21 (2011) 17059.

## FORMATION AND MOBILITY OF POLARONS IN OXIDES

N. V. Skorodumova

*Multiscale Materials Modelling, KTH Royal Institute of Technology, S-10044 Stockholm, Sweden; Department of Physics and Astronomy, Uppsala University, S-75120 Uppsala, Sweden*

The presence of oxygen vacancies, impurities and extended defects in oxides can lead to charge trapping and polaron formation. This is able to significantly modify the properties of oxide structures and influence their functionality in various energy related applications. Here I discuss how polarons and bipolarons can be modelled in first principle calculations, using $WO_3$, $CeO_2$ and MgO/CaO layered structures as examples.

# *Electrocatalysis*

# $NiFe_2O_4$ ELECTROCATALYST FOR THE HYDROGEN EVOLUTION IN ALKALINE WATER ELECTROLYSIS

Debabrata Chanda, Jaromír Hnát, Martin Paidar, Karel Bouzek

*Institute of Chemical Technology Prague, Technicka 5, 166 28 Prague 6, Czech Republic*

$NiFe_2O_4$ electrocatalyst for the hydrogen evolution reaction (HER) has been synthesized using the method of co-precipitation. After calcination of the precipitate at 475 °C the resulting metal oxide was characterized via scanning electron microscopy, energy dispersive X-ray spectroscopy, X-ray diffraction and nitrogen adsorption-desorption measurements to obtain information about its morphology, chemical composition, crystallographic structure and surface area respectively. The electrocatalytic activity towards HER in alkaline water electrolysis was investigated by linear sweep voltammetry using the rotating disk electrode. Cathode catalytic layer based on the catalyst was prepared with catalyst loading 10 mg $cm^{-2}$ by means of anion selective quaternized polyphenyleneoxide (qPPO) ionomer. Resulting membrane electrode assembly (MEA) was tested in alkaline water electrolyzer (10 wt. % KOH) at 50 °C. The current density obtained for 10 mg $cm^{-2}$ catalyst load was 125 mA $cm^{-2}$ at cell voltage 1.85 V and temperature of 50 °C. The stability of the qPPO binder containing MEA was examined with a continuous operation for 143 hours and subsequent 55 hours intermittent electrolysis at 250 mA $cm^{-2}$ and at 50 °C.

## Introduction

Hydrogen represents possible clean energy vector, which importance grows because of the serious shortage of fossil fuels and the problems of global warming [1]. It has been proposed that water electrolysis offers an attractive way to store momentarily excessive electric energy originating from the renewable energy sources (wind and solar) highly instable in time.
Electrolysis systems based on proton exchange membranes (PEMs) have a number of advantages over the commercial alkaline electrolyzers, such as substantially higher process intensity and efficiency, utilization of polymer electrolyte and thus application of demineralised water as a circulation media. Despite all these advantages, the PEM water electrolysis is being difficult for commercialization, because perfluorinated sulphonated acids used as a polymer electrolyte and precious metal catalysts, such as Pt and $IrO_2$, as the catalysts of the electrode reactions. The main target of water electrolysis development consists in improvement of the hydrogen production intensity and efficiency, while reducing the installation costs and at the same time enhancing the cell life time and flexibility.

Navarro-Flores et al have reported the binary Ni-Fe as a hydrogen evolution catalyst in acidic water electrolysis [2]. The results obtained indicate $NiFe_2O_4$ to be a promising candidate for the cathode production also in alkaline water electrolysis. But to our knowledge, no literature describes $NiFe_2O_4$ application as a HER catalyst in alkaline water electrolysis.
Anion selective membrane water electrolysis (ASMWE) systems are based on polymer anion selective membrane sandwiched between two gas diffusion electrodes (GDE) comprising a gas diffusion layer (GDL) ensuring mass and charge transfer and a catalytic layer (CL) accelerating the rates of electrochemical reactions. The most common approach for attaching CL to the GDL surface is being the use of a suitable polymeric binder.
The aim of this work is to synthesize and carefully characterize $NiFe_2O_4$ as a potential electrocatalysts of the HER in alkaline water electrolysis and to test its behavior in the laboratory ASMWE cell in order to assess this system efficiency and stability.

**Result and discussion**

During ASMWE process the hydrogen is produced on cathode via reaction written for the alkaline environment as:

$$2H_2O + 2e^- \rightarrow H_2 + 2OH^- \qquad (1)$$

HER starts with the proton discharge at the cathode (Volmer reaction, Eq. (2)) followed either by the electrodesorption step (Heyrovsky reaction, Eq. (3)), or by the hydrogen recombination step (Tafel reaction, Eq. (4)). The distinction between reactions (2), (3) and (4) as the rate-determining steps is usually accomplished in terms of evaluating Tafel slope of the reaction or by calculating the rate constants of the forward and backward reactions. According to the general model of the HER mechanism, if the Volmer reaction, Eq. (2), is the rate determining step, the resulting Tafel curve should yield a slope of 120 mV $dec^{-1}$ at 25 °C. If the Heyrovsky step, Eq. (3), is the rate determining one, the measured Tafel slope yields a value of about 30 mV $dec^{-1}$ in a low overvoltage region and 120 mV$dec^{-1}$ in a high overvoltage region. Tafel desorption step, Eq. (4), is characterized by a Tafel slope of 40 mV$dec^{-1}$ in a low overvoltage range.

$$M + H_2O + e^- \Leftrightarrow MH_{ads} + OH^- \qquad \text{Volmer} \qquad (2)$$

$$MH_{ads} + H_2O + e^- \Leftrightarrow M + H_2 + OH^- \qquad \text{Heyrovsky} \qquad (3)$$

$$MH_{ads} + MH_{ads} \Leftrightarrow H_2 + 2M \qquad \text{Tafel} \qquad (4)$$

The Tafel plot of HER is for the $NiFe_2O_4$ electrocatalyst together with this of commercial Vulcan XC-72R supported Pt catalyst shown in Fig. 1. The Tafel slopes of 52 mV $dec^{-1}$ and 95 mV $dec^{-1}$ were obtained for Pt/C and $NiFe_2O_4$ catalyst respectively. The Tafel slope of 52 mV $dec^{-1}$ (close

to 40 mV $dec^{-1}$) determined for Pt/C catalyst at low overpotential, indicates the HER to proceed predominantly through the Volmer-Tafel pathway (Eqs. 2 and 4). Recombination step (Eq. 4) is in this case the rate determining one. For $NiFe_2O_4$ surface with the Tafel slope 95 mV $dec^{-1}$ (close to 120 mV $dec^{-1}$) at high overpotential, the HER thus proceeds predominantly through the Volmer-Heyrovsky pathway (Eqs. 2 and 3). Electrochemical desorption is the rate determining step (Eq. 3). The exchange current densities ($j_0$) were $1.71\times10^{-5}$ A $cm^{-2}$ and $5.01\times10^{-6}$ A $cm^{-2}$ for Pt/C and $NiFe_2O_4$ respectively.

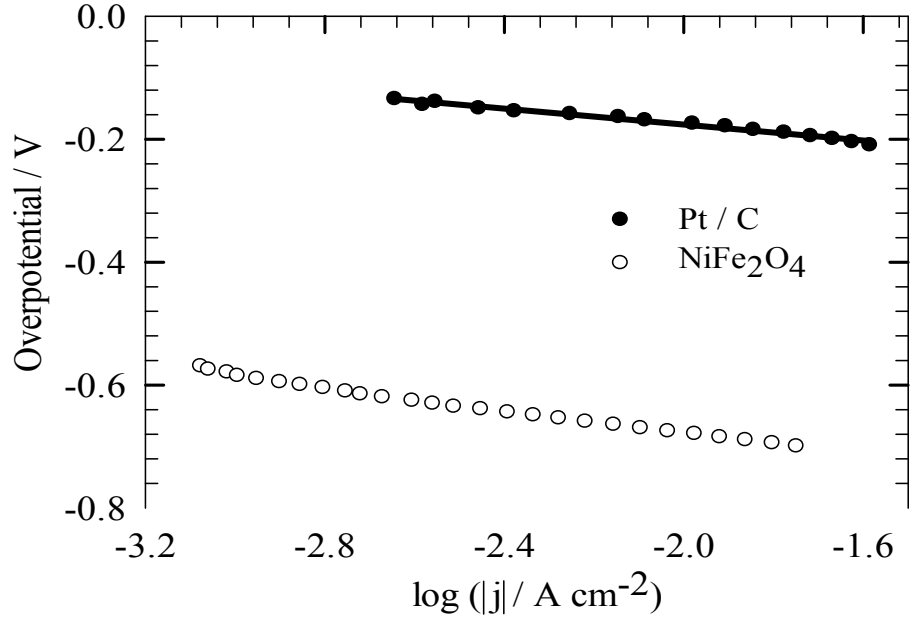


**Figure 1.** Tafel curves of hydrogen evolution. Experimental conditions: 22 °C; 1 mol $dm^{-3}$ KOH solution; working electrode: GC electrode modified with catalyst (Pt (60μg $cm^{-2}$), $NiFe_2O_4$ (200 μg $cm^{-2}$)) Hg/HgO reference electrode; Pt counter electrode; argon atmosphere; potential scan rate 10 mV $s^{-1}$; electrode rotating rate 2000 rpm.

## Conclusions

The $NiFe_2O_4$ spinel oxide electrocatalyst was investigated with respect to its potential utilization for the HER in alkaline water electrolysis. The material was found to be sufficiently stable and active under conditions of the investigation. The promising results have been explained in terms of the hydrogen adsorption-desorption on Ni-Fe surface, preferably on the Fe sites.

## Reference

[1] M. Daniel, D. E. Alessandro, *Int J Hydrogen Energy* 33 (2008) 3041.
[2] E. Navarro-Flores, Z. Chong, S. Omanovic, *J. Molecular Catal. A – Chem.* 226 (2005) 179.

# METAL OVERLAYER/TUNGSTEN CARBIDE HER ELECTROCATALYSTS: ELECTRONIC STRUCTURE AND SYNERGISM – A DFT APPROACH

Dragana D. Vasić Anićijević[1], Vladimir M. Nikolić[1], Milica P. Marčeta-Kaninski[1], Igor A. Pašti[2]

[1]*Vinča Institute of Nuclear Sciences, University of Belgrade, Mike Alasa 12-14, Belgrade*
[2]*Faculty of Physical Chemistry, University of Belgrade, Studentskitrg 12-16, Belgrade*

Influence of electronic structure to hydrogen binding energy (HBE) on WC-supported metal overlayers has been analyzed using DFT. Obtained results were then correlated to catalytic properties of these materials for hydrogen electrode reaction (HER). A particular attention was paid to the term and the origin of metal-support synergism, in light of obtained results.

## Introduction

Thin metal overlayers - primarilyPt - on WC, have been particularly investigated by the group of Chen [1], who postulated that the replacement of all but topmost layers of Pt with electronically similar material will result with HER activity more similar to Pt than to WC, with every Pt atom maximally exploited. In literature, experimentally obtained remarkable HER activity of such "Pt-group-metal/carbide(oxide) support" systems is often characterized as synergistic effect. However, the nature of the effect has never been explained unambiguously. We recently systematically studied a series of transition metal overlayers on WC support as HER catalysts using DFT calculations, and constructed a volcano curve to predict activity of systems that have never been examined experimentally [2]. According to obtained correlation between HBE and literature data for exchange current density, $Pt_{ML}$/WC, as well as $Pt_{2ML}$/WC, do not achieve the activity of clean platinum. On the other hand, some Pt-free systems, such as $Cu_{ML}$/WC and $Rh_{ML}$/WC, are predicted to have an activity that is very close to Pt(111). In this contribution a deeper analysis of these unexpected results, from the aspect of electronic structure, will be given.

## Results and discussion

Factors contributing to HBE change referred to clean (111) metal surfaces, and originating from the electronic structure, can be summarized as: 1) Charge transfer, clearly periodic (Figure 1) and occurring from (partially) filled metal high-energy s-states to adsorbate orbitals [3]. In general, interaction with sp-states is most expressed in cases of Cu, Ag and Au (filled d-bands), where it causes HBE increase in spite d-band center lowering, apparently unexpected from the point of view of simplified d-band center model; 2) Matrix element of interaction with d-states$V_{sd}$,

strongly depending on adsorbate-substrate distance, and determining density of adsorbate states near the Fermi level, which contributes to HBE decrease [4].For example, in case of $Pt_{ML}$/WC and $Pd_{ML}$/WC, an obvious contribution to HBE decrease is the weaker coupling between metal d- and renormalized adsorbate states, coming from strong interaction of metal with WC-support, and implying weaker separation of adsorbate states, i.e. low-energy states are less stabilized and high-energy ones become filled.

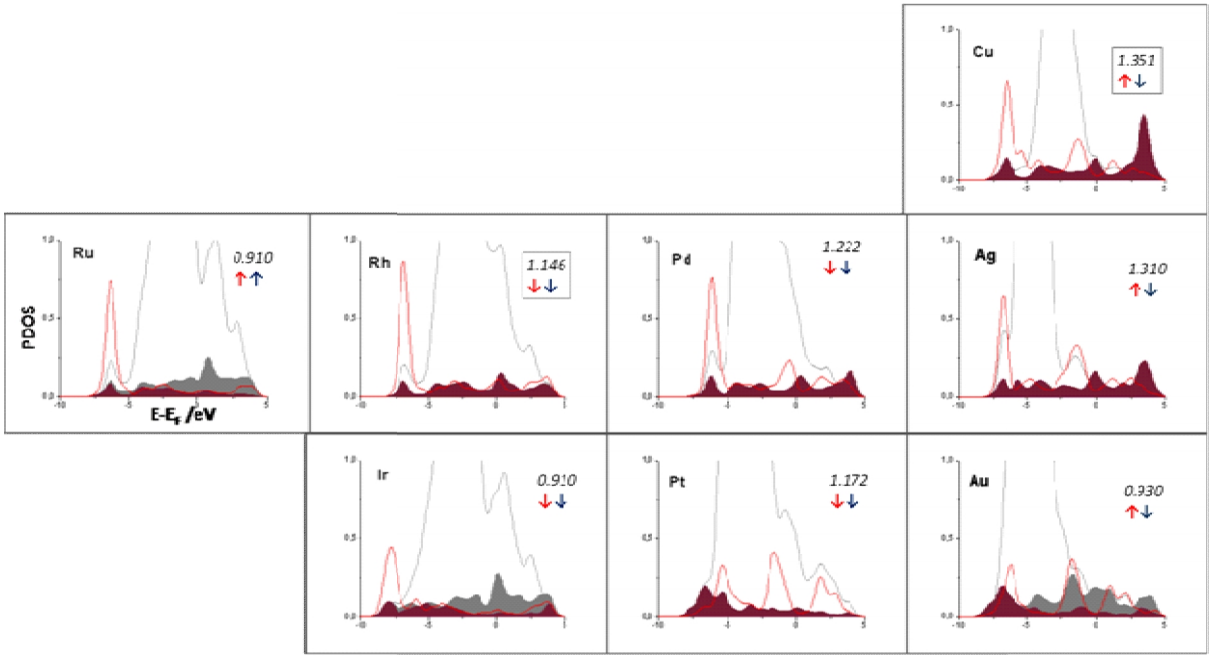


**Figure 1.** Projected density (PDOS) of d- (gray), s- (dark gray filled) and p- (light gray filled) states of metal and adsorbate (red line). Adsorbate Löwdin charges are shown in italic. Change directions of HBE strength referred to (111) metal surfaces are indicated by red, changes of d-band center by blue arrows (↑-increase,↓-decrease).

$Cu_{ML}$/WC and $Rh_{ML}$/WC examples illustrate synergy in terms of fundamental electronic factors. In case of $Cu_{ML}$/WC increase of HBE referred to Cu(111), that achieves 0.39 eV, actually comes from ionic contribution to the bond strength, as charge transfer to adsorbate, which is practically absent at Cu(111) [5], is maximized for $Cu_{ML}$/WC among all investigated monolayer systems. This gain in HBE resulted, according to [2], with an optimal value for HER catalysis, so in short, synergistic effect originates from metal sp-states modified by WC-support. In case of $Rh_{ML}$/WC, charge transfer to adsorbate is negligible, but the downshift of d-band center is now followed by optimal HBE weakening. There, the modification of d-band by WC-support gives the key contribution to the synergy.

## Conclusion

Although similarity in d-band structure between Pt and WC is not enough to maintain $Pt_{ML}$/WC activity, there is a sum of factors, originating from periodic properties of d-, as well as sp-substrate states, that may contribute to HBE in a way to optimize it for HER catalysis, illustrating possibilities in investigating different metal/support combinations.

## References

[1] D. V. Esposito, J. G. Chen, *Energy Environ. Sci.* 4 (2011) 3900.
[2] D. D VasićAnićijević, V. M. Nikolić, M. P. Marčeta-Kaninski, I. A. Pašti, *Int. J. Hydrogen Energy* 38 (2013) 16071.
[3] Z. P. Liu, J. P. Hu, *J. Am. Chem. Soc.* 123 (2001) 12596.
[4] B. Hammer, J. K. Norskov, *Nature* 376 (2002) 238.
[5] S. Sakong, A. Gross, *Surf. Sci.* 471 (2001) 59.

# BOROHYDRIDE OXIDATION AT Ni-Cu NANOSTRUCTURED FOAMS

D. M. F. Santos,* S. Eugénio, D. S. P. Cardoso, B. Šljukić, and M. F. Montemor

*Institute of Materials and Surfaces Science and Engineering, Instituto Superior Técnico, Universidade de Lisboa, 1049-001 Lisboa, PORTUGAL.*
**e-mail: diogosantos@tecnico.ulisboa.pt*

Nickel-copper (Ni-Cu) metallic foams have been prepared by electrodeposition using a dynamic hydrogen template. Subsequently, they were tested as electrode materials for the borohydride oxidation reaction (BOR) in alkaline media for application in direct borohydride fuel cells. Preliminary study of their activity for BOR was performed using cyclic voltammetry, chronoamperometry, and chronopotentiometry, allowing evaluation of main reaction parameters, including number of exchanged electrons, and providing information on their stability.

## Introduction

Sodium borohydride ($NaBH_4$) is seen as a promising fuel of the future due to its chemical stability, storage and handling simplicity, non-toxicity of its oxidation products and possibility of their recycling [1]. Additionally, fuel cells operating with $NaBH_4$ as the anodic fuel and oxygen ($O_2$) or hydrogen peroxide ($H_2O_2$) as the oxidant, known as direct borohydride fuel cells (DBFCs) or direct borohydride-peroxide fuel cells (DBPFCs), respectively, have higher energy density compared to other types of fuel cells [2].However, at most electrode materials, parallel with borohydride oxidation reaction (BOR) proceeds borohydride ($BH_4^-$) hydrolysis reaction that results in lower BOR coulombic efficiency (Eq. 1) [3].

$$BH_4^- + x\ OH^- \rightarrow B(OH)_4^- + (x - 4)\ H_2O + (4 - x/2)\ H_2 + x\ e^- \quad (1)$$

where $x$ is the coulombic number, i.e., the actual number of electrons released by a $BH_4^-$ ion, that is determined by anode material. Consequently, there is a wide search for materials for DBFCs that can catalyse only BOR and suppress $BH_4^-$ hydrolysis.
Three-dimensional (3D) nanostructured metallic foams (NMFs) are structures of interconnected pores with nano-ramified walls formed of metallic particles, dendrites or other morphologies that combine the good electrical and thermal conductivity of metals with a high surface area and low density, inviting an array of new technological possibilities. These materials are particularly interesting for applications such as catalysis and electrodes for energy storage devices [4]. Electrodeposition provides a one-step, low-cost method for the fabrication of NMFs by taking

advantage of the dynamic template formed by hydrogen bubbling that often occurs simultaneously to metal deposition [5,6]. In this way, self-supported nano-ramified foam structures with properly tailored architectures can be designed, enhancing mass and charge transfer processes. Application of 3D materials for BOR was previously reported to be advantageous [7], as enhanced BOR was observed at vitreous carbon coated with gold nanoparticles as well as at silver porous sponge material. Among low-cost, non-noble metals, Ni and Ni-based materials have been studied for BOR, including Ni alloys with rare-earth metals [8] as well as Cu/Ni/AuNi electrodes [9].

## Experimental

Nickel-copper(Ni-Cu) nanostructured foams were electrodeposited on AISI 304 stainless steel from an electrolyte solution containing 0.5 M $NiSO_4$, 1.5 M $H_2SO_4$, 1M HCl and 0.01 M $CuSO_4$, using a two-electrode cell connected to a power source (Kikusui Electronics, Model PAB 32-3). A platinum (Pt) plate was used as counter electrode. Electrodeposition was carried out in galvanostatic mode by applying a current density of 1.5 A $cm^{-2}$ for 90 (NiCu-90) or 180 (NiCu-180) seconds. Working electrodes thus prepared were of 1 $cm^2$ geometric surface area.
Surface morphology and chemical composition of the metallic foams were assessed by scanning electron microscopy (SEM, Hitachi S2400) and energy dispersive X-ray spectroscopy (EDS, Rontec standard detector), respectively.
All BOR studies were done using PAR 273A potentiostat (Princeton Applied Research Inc.) with PowerSuite software, in a three-electrode cell of 80 $cm^3$ volume. Pt mesh (100 $cm^2$area, Johnson Matthey) served as counter electrode with saturated calomel electrode (SCE, Metrohm) completing the circuit. All potentials in this study are given relative to the SCE. Electrolyte solution with 0.03 M $NaBH_4$ (98%, Merck) in 2 M sodium hydroxide (NaOH, 99% AnalaR NORMAPUR) was prepared immediately prior to the measurements in order to avoid any $BH_4^-$ losses due to hydrolysis. The studies were performed using cyclic voltammetry (CV), chronoamperometry (CA) and chronopotentiometry (CP) at temperature of 25 ºC.

## Results and Discussion

*Characterization of the Ni-Cu Metallic Foams*

SEM images of two Ni-Cu metallic foams (Figure 1) showed uniform foams morphology presenting a 3D structure with nearly-circular micropores with non-compact walls formed of dendrites. This conferred an enhanced surface area of the foams since their porosity arises not only from the existence of pores but also from the empty space in pore walls due to the open dendritic structure.

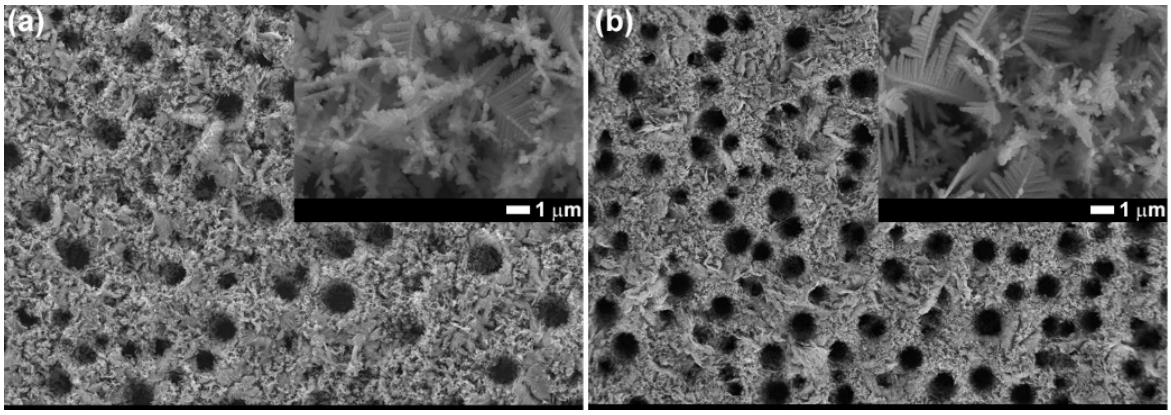


**Figure 1.** SEM images of Ni-Cu foams deposited at 1.5 A $cm^{-2}$ for 90 s (NiCu-90, a) and for 180 s (NiCu-180, b). Images insets show higher magnifications.

The 3D structure of the foams was favored with increasing the deposition time, due to the increase of the foam thickness and mass. EDS analysis showed that the NiCu-90 foam had higher Ni content (72 at.%) thanNiCu-180 foam (60 at. % ).

*$BH_4^-$ oxidation at the Ni-Cu Metallic Foams Electrodes*

$BH_4^-$ oxidation at Ni-Cumetallic foam electrodes was first investigated by CV measurements in 2 M NaOH solution, in the presence and in the absence of 0.03 M $NaBH_4$,at temperature of 25 ºC. Figure 2 shows voltammograms recorded at the two electrodes at scan rate of 50 $mVs^{-1}$.Several peaks appearing in the -1.2 to -0.6 V region are attributed to the oxidation of $BH_4^-$ as well as to the oxidation of its hydrolysis products [8,9]. The currents at more positive potentials are attributed to the oxidation of the electrode surface itself [8], as confirmed by the CVs obtained in the absence of $NaBH_4$. Higher currents were obtained at NiCu-180 electrode in the whole potential range scanned. To evaluate kinetic parameters such as charge transfer coefficient, α, and number of exchanged electrons, n, voltammograms of the studied electrodes were recorded using different scan rates, ν, ranging from 0.005 to 1 $Vs^{-1}$(Figure 3a).With increase of ν, peak potential, $E_p$, was observed to shift towards more positive values accompanied with increase of peak current, $i_p$.

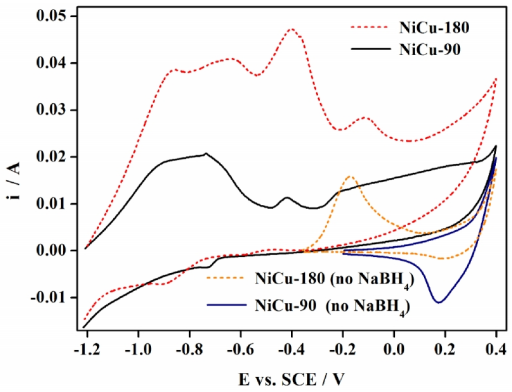


**Figure 2.** CVs of the Ni-Cu electrodes in 2 M NaOH solution in the presence and in the

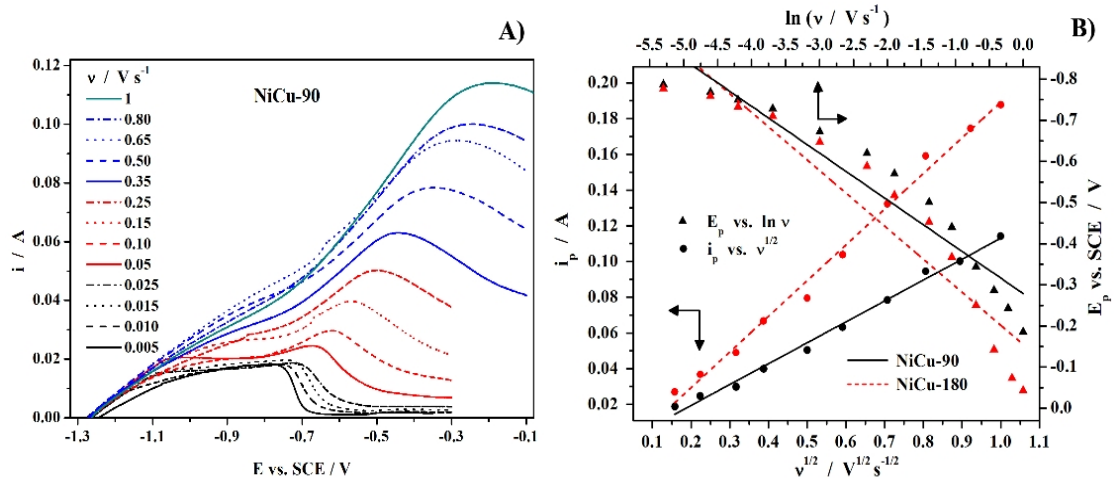


**Figure 3.** Voltammograms obtained for NiCu-90 electrode at ν ranging from 0.005 to 1 $Vs^{-1}$ (A) and corresponding peak analysis as a function of ν for both Ni-Cu electrodes (B).

Using the modified Randles-Sevcik equation for irreversible processes (Eq. 2) [10] it was possible to calculate n from the slope of the $i_p$ vs. $\nu^{1/2}$ plot (Figure 3b).

$$i_p = 2.99 \cdot 10^{-5}[(1-\alpha)n_a]^{1/2} n A C_0 (D_0 \nu)^{1/2} \quad (2)$$

where $n_a$ is the number of electrons transferred in the rate determining step (most likely 1 in this case), A is the electrode surface area ($cm^2$), $C_0$ is the bulk $NaBH_4$ concentration (mol $cm^{-3}$) and $D_0$ is $BH_4^-$ diffusion coefficient (2.42 x $10^{-5}$ $cm^2$ $s^{-1}$ at 25 ºC [11]). α could be determined from the $E_p$ vs. lnν plot (Figure 3b) using Eq. 3.

$$E_p = E^0 + \frac{RT}{(1-\alpha)n_a F}\left[0.78 + \ln\left(\frac{D^{1/2}}{k_s}\right) + \ln\left(\frac{(1-\alpha)n_a F \nu}{RT}\right)^{1/2}\right] \quad (3)$$

where $E^0$ is the formal potential (V), R is the universal gas constant, T is the temperature (K), F is the Faraday constant and $k_s$ is the standard heterogeneous rate constant (cm $s^{-1}$). High α values of 0.89 and 0.91 were obtained for NiCu-90 and NiCu-180 electrodes, respectively, as expected for irreversible processes. Subsequently, n values of 7.2 and 5.5 were evaluated for NiCu-90 and NiCu-180 electrodes, respectively. The lower n value calculated for NiCu-180 was obtained by normalization of the catalyst mass, since it is approximately double of that for NiCu-90. Still, it is worth noticing that these n values are higher compared to those reported in the literature for other Ni-based electrodes (n between 2 and 4)[8].

Next, CA studies were performed in 0.03 M $NaBH_4$ + 2 M NaOH solution applying several different potential. NiCu-180 electrode gave higher currents compared to NiCu-90 electrode at all applied potentials(Figure 4a), which is in agreement with CV data. Practically no decrease of current was observed during 20 min measurements, indicating good stability of the Ni-Cu

electrodes activity for BOR. Complimentary CP measurements (Figure 4b) clearly show three oxidation steps, in agreement with previous CV studies. The two first steps can be attributed to the oxidation of $BH_4^-$ and to the oxidation of its hydrolysis products [8,9], and the potential step observed at about 0.4 V concerns the electrode material oxidation.

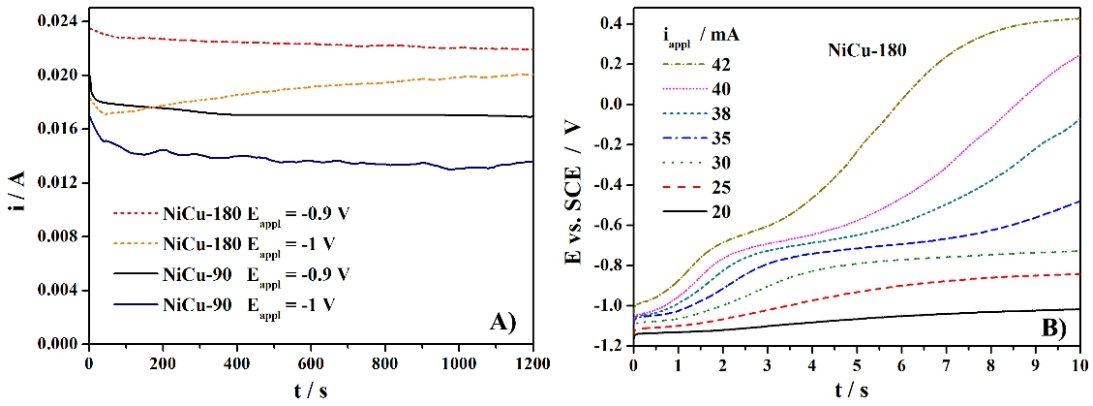


**Figure 4**. CAs of Ni-Cu electrodes applying potentials of -0.9 V and -1 V (A) and CPs recorded for NiCu-180 electrode for currents ranging from 20 to 42 mA (B). All measurements done in 0.03 M $NaBH_4$ + 2 M NaOH solution.

## Conclusion

3D Ni-Cu metallic foams were prepared by electrodeposition and their activity for BOR was tested. n values ranging from 7.2 to 5.5 were achieved for foams obtained using different deposition times. They have also shown high stability in the tested conditions. In this way, Ni-Cu foams seem to be promising materials for BOR. Moreover, they can be produced using a low cost, single step synthesis procedure, making them a viable alternative to conventional catalytic materials.


## Acknowledgement

D.M.F. Santos and B. Šljukić would like to thank the Portuguese Foundation for Science and Technology (FCT) for postdoctoral research grants SFRH/BPD/ 91853/2012 and SFRH/BPD/77768/2011, respectively. D.S.P. Cardoso thanks FCT for a research grant within project PTDC/SENENR/121265/2010.


## References


[1] D. M. F. Santos, C. A. C. Sequeira, *Renew. Sustain. Energy Rev.* 15 (2011) 3980.

[2] D. M. F. Santos, P. G. Saturnino, R. F. M. Lobo, C. A. C. Sequeira, *J. Power Sources* 208 (2012) 131.

[3] B. Šljukić, J. Milikić, D. M. F. Santos, C. A. C. Sequeira, *Electrochim. Acta* 107 (2013) 577.

[4] B. C. Tappan, S. A. Steiner, E. P. Luther, *Angew. Chem. Int. Ed.* 49 (2010) 4544.

[5] H. C. Shin, J. Dong, M. Liu, *Adv. Mater.* 15 (2013) 1610.
[6] S. Eugénio, T. M. Silva, M. J. Carmezim, R. G. Duarte, M. F. Montemor, *J. Appl. Electrochem.* 44 (2014) 455.
[7] C. Ponce de Leon, A. Kulak, S. Williams, I. Merino-Jimenez, F. C. Walsh, *Catal. Today* 170 (2011) 148.
[8] D. M. F. Santos, B. Sljukic, L. Amaral, D. Maccio, A. Saccone, C. A. C. Sequeira, *J. Electrochem. Soc.* 161 (2014) F594.
[9] M. Ghasem Hosseini, M. Abdolmaleki, F. Nasirpouri, *Electrochim. Acta* 114 (2013) 215.
[10] A. J. Bard, L. R. Faulkner, *Electrochemical methods: fundamentals and applications*, 2nd ed., John Wiley & Sons, New York, 2001.
[11] K. Wang, J. Lu, L. Zhuang, *J. Electroanal. Chem.* 585 (2005) 191.

# EXPLORATION OF FACTORS GUIDING ORR ACTIVITY IN BORON DOPED ORDERED MESOPOROUS CARBONS

Nemanja Gavrilov[1], Igor Pašti[1], Milan Momčilović[2], Marija Stojmenović[2], Biljana Babić[2], Slavko Mentus[1,3]

[1]*Faculty of Physical Chemistry, University of Belgrade, Studentski trg 12-16, P.O. Box 137, Belgrade, Serbia*
[2]*Institute of Nuclear Sciences "Vinča", University of Belgrade,P.O. Box 522, Belgrade, Serbia*
[3]*The Serbian Academy of Science and Arts, Knez Mihajlova 35, 11158 Belgrade, Serbia*

Series of boron doped ordered mesoporous carbons (B-OMCs) were synthesized by an evaporation induced self-assembly method with boric acid as the doping agent. The obtained products were characterized by $N_2$ sorption measurements, X-ray photoelectron and Raman spectroscopies accompanied with cyclic voltammetry measurements. Effective ORR electrocatalysis of B-OMCs in alkaline media was evidenced, with onset potential amounting to −0.10 V vs. saturated calomel electrode, an improvement upon pure OMC of around 80 mV. Enhanced activity is verified even for minute doping levels and attributed to highly active boron surface sites. However, no linear relationship between ORR activities and doping level is found. Additionally, it is established that the appropriate pore structure decidedly influences ORR activity through enabling fast reactant/product diffusion to/from the boron active sites.

## Introduction

Increasing demand for portable/stationary devices that deliver electrical energy on demand presents a principal motive for full cell research. Their development promises an efficient and eco-friendly way of producing electric energy through redox reactions using hydrogen and lower alcohols as fuel. Hindered commercialization of these devices arises from the use of Pt-group metals, for reduction of $O_2$ at the cathode, which significantly increases their cost. Hence further progress is expected through replacing these expensive metals with new electrocatalytic materials with high catalytic activity towards oxygen reduction reaction (ORR). This objective is realized through the use of carbon-based ORR catalysts which display high intrinsic ORR activity in alkaline media [1]. In addition, doping with different heteroatoms (nitrogen, boron, sulfur, etc.) their activity can be altered to reach Pt-based catalysts in terms of ORR activity [2].

## Experimental

Doped OMC materials were prepared using evaporation-induced self-assembly (EISA) method. Initially, Pluronic F127 (EO106PO70EO106) was dissolved in the equal volume mixture of

deionized water and ethanol and vigorously stirred for 15 min at room temperature. Then, resorcinol was added and stirred for the next 30 min when the mixture was acidified with HCl (37 wt. %). This step was followed by B dopant introduction. Various amounts of boric acid (Merck) were used in order to obtain various mass ratios in the final material. After 2 h, formaldehyde (37 wt. %) was slowly added dropwise, stirred for another hour, aged, covered at room temperature for 3 days and dried at 85 °C for two days. Obtained polymeric cakes were carbonized under nitrogen at 800 ºC for 3 h at a ramping rate of 5 ºC/min, cooled down in the same atmosphere and used for further examination.

The cyclic voltammetric (CV) experiments were performed in a three-electrode type electrochemical cell in $N_2/O_2$ purged 0.1M KOH solution, with the Pt as counter electrode and saturated calomel electrode (SCE) as reference electrode, connected to Gamry PCI4/300 Potenstiotat/Galvanostat.

**Results and Discussion**

Raman spectra of investigated materials (Fig. 1a) display typical features of carbonaceous materials with two major bands commonly designated as G and D, centered around 1592 $cm^{-1}$ and 1332 $cm^{-1}$, respectively. Following the B-doping into OMC shift, in both the position and width of G and D band, is observed. Namely, the G band for pure OMC located at 1588 $cm^{-1}$ shifts up with the progressive B doping while D band shifts down from 1337 $cm^{-1}$. This observation is well documented and is associated with the modification of phonon and electron structures of carbon layers due to boron doping [3].

Fitting the B1s spectra was accomplished using only two components (Fig. 1b) located at 188.7 and 190.5 eV ascribed to $BC_3$ and $BC_2O$ species, respectively. B doped content increased with the increase in amount of boric acid added in the synthesis while the incorporated content remained under 1 at. % which is in line literature data [4].

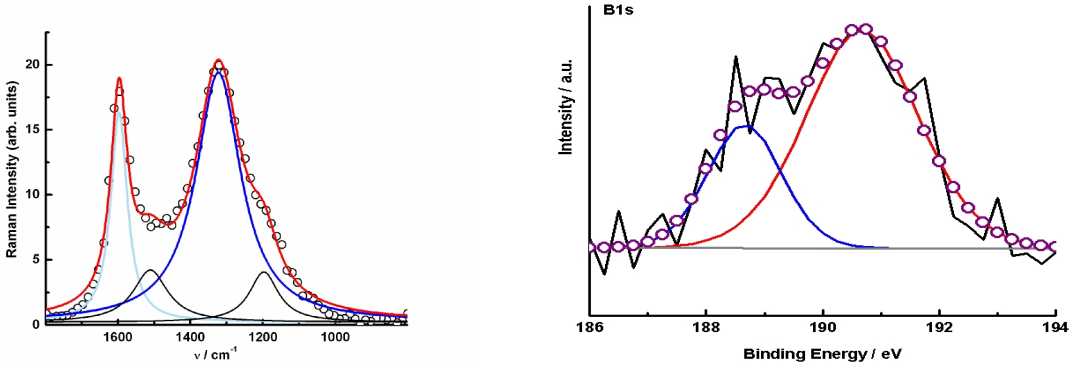


**Figure 1.** (a) De-convoluted Raman spectra of selected B-OMC sample in 1800-800 $cm^{-1}$ wavenumber window. (b) B1s spectra of selected B-OMC indicating peaks atributed to $BC_3$ and $BC_2O$ species.

Results derived from $N_2$ sorption measurements are given in Table 1 and are augmented by boron surface concentration from XPS measurement for clarity.

**Table 1.** Results of $N_2$ sorption and XPS-B1s measurements

| **Sample** | $S_{BET}$, $m^2\ g^{-1}$ | $S_{meso}$, $m^2\ g^{-1}$ | $S_{micro}$, $m^2\ g^{-1}$ | $V_{micro}$, $m^3\ g^{-1}$ | ***B* at. %** |
|---|---|---|---|---|---|
| OMC | 712 | 320 | 392 | 0.190 | 0.00 |
| 2B-OMC | 509 | 324 | 185 | 0.051 | 0.13 |
| 4B-OMC | 532 | 312 | 220 | 0.087 | 0.48 |
| 6B-OMC | 578 | 178 | 300 | 0.229 | 0.42 |
| 8B-OMC | 533 | 200 | 333 | 0.171 | 0.84 |

For the studied B-OMCs the onset potential for ORR is around –0.10 V vs. SCE (Fig. 2), which is comparable to or higher than the values found in literature for various types of carbon materials [5]. High ORR onset potential can be explained by a relatively large number of surface defects, as evidenced by Raman spectroscopy and the presence of ORR active boron surface species as evidenced by XPS. These defect sites can enhance $O_2$ adsorption energetics and charge transfer kinetics which corresponds with high ORR onset potentials observed. Although three samples show very similar onset potentials and limiting currents the most active materials is not one with the highest boron content but one with the highest mesopore/micropore ratio. This led us to conclude that appropriate pore structure is essential for fast reactant/product diffusion to/from the boron active sites which results in more favorable activity.

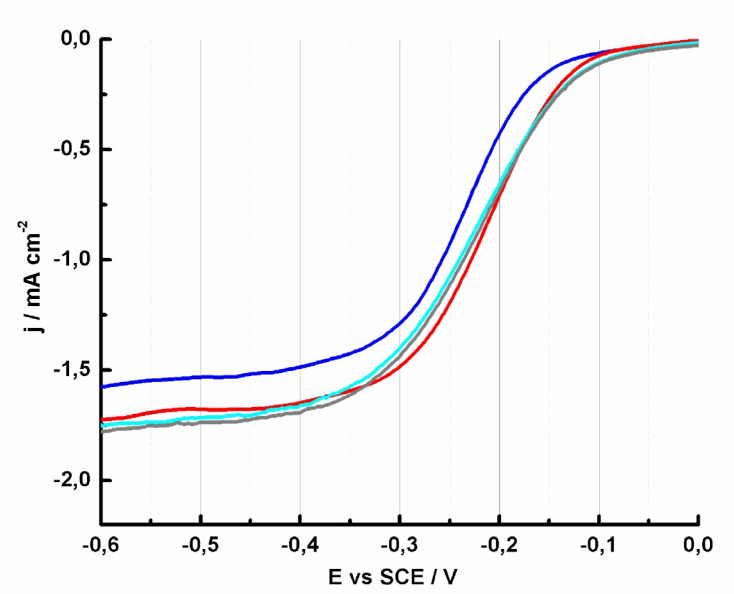


**Figure 2.** RDE polarization curves of oxygen reduction on B-OMC electrodes at rotation rate of 600 rpm. Measurements were performed in $O_2$-saturated 0.1 mol $dm^{-3}$ KOH and potential sweep rate was 20 mV $s^{-1}$.

## Conclusion

Based on the Raman spectra of investigated materials it was concluded that B-doped OMCs have highly disordered phases with shifts in peak positions evidencing succesfull doping while XPS measurements provided information present surface grups and their realtive content. In comparison to non-doped sample, boron doping leads to a reduction in mesopore surface area, while microporous domain initially drops but rises with increased doping. Boron doping was found to be beneficial regarding the ORR performance of investigated materials in alkaline media. Measurements of ORR in alkaline media revealed the onset potentials of B-OMCs sligtly above −0.10 V vs. SCE, pointing to high intrinsic catalytic activity of investigated materials towards ORR. The most active ORR catalysts in investigated series of materials has the highest specific surface area. Obtained results indicated that doping of OMC with small amounts of boron enhanced significantly the ORR activity.

## Acknowledgement

This work was supported by the Ministry of Sciences and Environmental Protection of Serbia through the projects III45012, III 43009 and III 45014.

## References

[1] K. Tammeveski, K. Kontturi, R. J. Nichols, R. J. Potter, D. J. Schiffrin, *J. Electroanal. Chem.* 515 (2001) 101.
[2] D. S. Yang, D. Bhattacharjya, M. Y. Song, J. S. Yu, *Carbon* 67 (2013) 736.
[3] Q.-H. Yang, P.-X. Hou, M. Unno, S. Yamauchi, R. Saito, T. Kyotani, *Nano Lett.* 5 (2005) 2465.
[4] X. Bo, L. Guo, *Phys. Chem. Chem. Phys.* 15 (2013) 2459.
[5] N. Alexeyeva, E. Shulga, V. Kisand, I. Kink, K. Tammeveski, *J. Electroanal. Chem.* 648 (2010) 16

# ON THE WAY OF IMPROVING CO TOLERANCE OF ANODE CATALYST IN PEM FUEL CELL

Vladimir M. Nikolić[1*], Ivana M. Perović[1], Danka D. Aćimović[1], Biljana M. Babić[1], Igor A. Pašti[2], Milica P. Marčeta Kaninski[1]
[1]*University of Belgrade, Vinca Institute of Nuclear Sciences, 11000 Belgrade, Serbia*
[2]*University of Belgrade, Faculty of Physical Chemistry, 11000 Belgrade, Serbia*
**e-mail: nikolicv@vinca.rs*

The central component of the μCHP (Micro Combined Heat and Power) system is PEM fuel cell. High cost and decline in performance are slowing their wide application. In order to increase CO tolerance, Pt-Ru catalyst was deposited onto tungsten carbide nanoparticles. Electrochemical characterisations were performed in order to investigate the electrochemical activity towards HOR, in both pure $H_2$ and $H_2$+ 2% (vol) CO mixture. PtRu/WC catalyst was utillized as an anode catalyst in PEMFC, and performance of such single PEMFCs are compared to commercial catalyst.

## Introduction

Hydrogen fuel cells (Proton Exchange Membrane Fuel Cell, PEMFC) are fueled by hydrogen and oxygen to generate electric power with following products water and heat [1]. As the central component of the μCHP system is PEM fuel cell. Platinum catalyst is the most commonly used for both, anode and cathode electrodes in PEMFC. Increase of CO tolerance of the anode catalyst [2], as well as replacement of commonly used high surface area carbon catalyst support, is of great research interest. Tungsten carbide (WC) has been in the focus of researchers and industry for over two decades, due to the Pt-like behavior of WC which was explained by the change of electron distribution in tungsten by the addition of carbon [3]. WC plays an important role as a catalyst support with improved CO tolerance [4].

## Experimental

The preparation of the nanosized WC powder and the deposition of the Pt and Ru was described elsewhere [5]. Commercial anode catalyst PtRu/C (30%) (Sigma Aldrich) was used as a reference material. Linear sweep (LSV) and cyclic voltammetry curves were recorded using Gamry PCI4/750, Au rotating disk electrode, 0.328 $cm^2$, 0.5 M $HClO_4$ saturated with $H_2$ and $H_2$+ 2% CO. The anode catalyst layer was with total metal loading (Pt) of 0.2 $mg/cm^2$. Cathodes were prepared using Pt/C powders (Alfa Aesar, 40 wt.% Pt), Pt loading of 0.2 $mg/cm^2$. Arbin FC hardware and HepasMini150 test station was used for performance measurements.

**Results and disscusion**

Investigations of the HOR kinetics in the presence CO are presented at Fig 1.

Fig 1. shows that the oxidation of the adsorbed CO on the prepared PtRu/WC is two-step reaction, starting at lower overvoltage of 0.15 V vs RHE, while the second step is similar to the behavior of the commercial PtRu/C catalyst, starting at 0.4V. This effect could be attributed to the interactive nature of the WC support with the deposited Pt particles. This is quantified via calculation of the mass activities, for the HOR, Table 1.

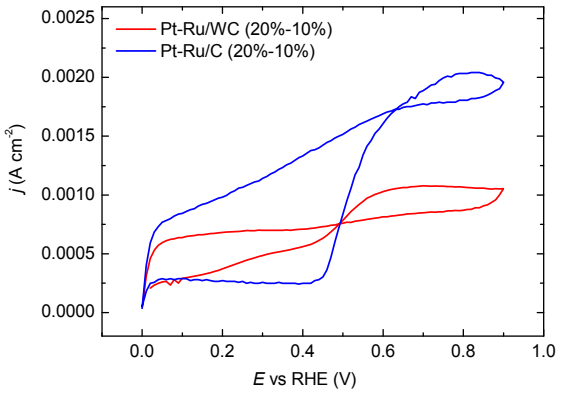


**Figure 1.** The HOR in the $H_2$+2%CO mixture for: blue- commercial PtRu/C and red-PtRu/WC catalysts obtained at 2000rpm RDE rotation speeds at room temperature.

**Table 1.** Summarized results of electrochemical measurements and PEMFC performance.

| Catalyst | $I_{mass}$ ($A/mg_{Pt}$) | $I_{massCO}$ ($A/mg_{Pt}$) | OCV (V) | $J_{@0.6V}$ ($A/cm^2$) | Catalyst utilization ($g_{Pt}$/ kW) |
|---|---|---|---|---|---|
| Pt-Ru/WC (30%) | 0.210 | 0.121 | 0.946 | 0.234 | 1.81 |
| Pt-Ru/C (30%) | 0.197 | 0.043 | 0.996 | 0.271 | 1.80 |

Results show that the mass activities for the HOR in pure $H_2$ are very close for both, PtRu/WC and commercial catalyst, while the mass activity towards the HOR in the presence of 2% CO is about 3 times higher for prepared PtRu/WC catalyst. These findings are of the great importance, proving increase in CO tolerance, when the PtRu/WC catalyst is used. These catalysts were utilized as anode catalysts in the MEA preparation, and determination of the PEM fuel cell performance, Fig. 2.

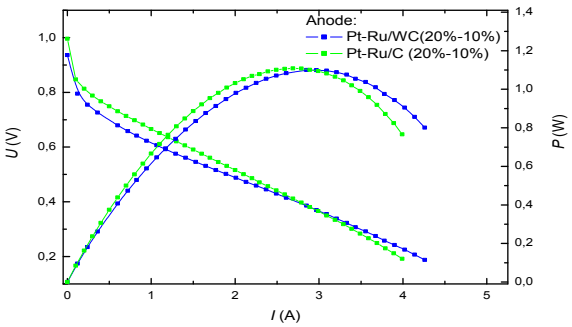


**Figure 2.** PEMFC polarisation curves: blue- 0.2 $mg_{Pt}/cm^2$ from PtRu/WC at the anode and green-0.2 $mg_{Pt}/cm^2$ from commercial PtRu/C catalyst.

Performance parameters presented in the Table 1, show slightly lower OCV value and the operating current at 0.6V, in the case of PtRu/WC anode catalyst. This fact is due to the higher density of the WC catalyst support, which resulted in the lower catalyst dispersion onto the GDL. Both catalysts show similar catalyst utilization values.

## Conclusions

The results on the characterization of PtRu/WC catalyst were compared to the commercial catalyst. Both catalysts show excellent behavior towards HOR, when pure $H_2$ is used. Mass activity towards the HOR in the presence of CO for PtRu/WC is found to be about 3 times higher, compared to the commercial catalyst. Obtained performance of PEM fuel cells were found to be similar, which opens the possibility of the replacement of commercial catalyst with much tolerant PtRu/WC.

**Acknowledgements**
Authors would like to acknowledge the financial support through the FP7 FCH-JU project, acronym „EURECA“, Grant Agreement No 303024.

**References**

[1] R. P. O'Hayre, Suk- Won Cha, W. G. Colella, F. B. Prinz, *Fuel Cell Fundamentals*, John Wiley & Sons, INC., 2008.
[2] G. Postole, A. Auroux, *Int. J. Hydrogen Energy* 36 (2011) 6817.
[3] R. Levy, M. Boudart, *Science* 181 (1973) 547.
[4] V. M. Nikolic, D. L. Zugic, I. M. Perovic, A. B. Saponjic, B. M. Babic, I. A. Pasti, M. P. Marceta Kaninski, *Int. J. Hydrogen Energy* 38 (2013) 11340.
[5] N. R. Elezovic, B. M. Babic, P. Ercius, V. R. Radmilovic, L. M. Vracar, N. V. Krstajic, *Appl. Catal. B* 125 (2012) 390.

# SYNTHESIS OF Pd-Ni/C ELECTROCATALYST AND ITS ELECTROCATALYTIC ACTIVITY FOR ALCOHOLS OXIDATION IN ALKALINE MEDIA

Zdenka Stancic*

*Faculty of Technology and Metallurgy, University of Belgrade, Serbia*
**e-mail: zdenka_stancic@hotmail.com*

Focus of this paper is the catalyst synthesized using the method of galvanic changes with core of the Ni and shell of Pd, supported on high area carbon, Pd-Ni/ C. Energy dispersive X-ray Spectroscopy was used to determine the atomic ratio of metals Pd: Ni=0.4:0.6 in the catalyst, considering this atomic ratio with thermo-gravimetric analysis it was found that the mass percentage of Pd in the catalyst is 6.4 wt. %. The electrocatalytic activity of the Pd-Ni/C for the oxidation of methanol and ethanol in alkaline media were examined with cyclic voltammetry and chronoamperometry. It was shown that Pd-Ni/C is not a promising catalyst for methanol oxidation in an alkaline medium. However, Pd-Ni/C showed higher activity for the oxidation of ethanol, as compared to the commercial Pd powder.

## Introduction

Direct alcohol fuel cells (DAFCs) are attracting much attention because of its unquestionable advantages over analogue devices that use hydrogen as fuel [1]. Pure hydrogen and hydrogen-rich gases are obtaining a higher electrical efficiency in fuel cells with proton exchange membrane as electrolyte (PEMFCs), but the problem of their production, storage and distribution are major brake on further development [2]. Using alcohol, which can be presented as hydrogen carriers, in direct alcohol fuel cells, can solve the flaws of hydrogen, in the way that these substances have two significant advantages such as: they are in the liquid state (solving the problem of storage and distribution) and their theoretical mass energy density is rather high(for methanol is 6.1 kWh/kg for ethanol is 8.0 kWh / kg) [3].The most common DAFC is direct methanol fuel cell (DMFC)which can be already found in commercial use. DMFCs operate mainly in acidic media with anode catalyst made of platinum or its alloys and they use solid electrolyte in the form of a proton exchange membrane. However, DMFCs have a few disadvantages: CO poisoning of Pt-based catalysts, degradation of the membrane and corrosion of the carbon support and cell hardware [4].Pt-based catalyst are studied a lot in the recent years for methanol and ethanol oxidation in acid media. It is known that platinum has a highest catalytic activity for the methanol oxidation of any of the noble metals both in acid and in the alkaline media. However, high prices and limited resources of this noble metal don't give a hope for greater industrial commercialization [9]. None of so far known Pt-based catalysts showed good capacity to produce an acceptable current density in direct ethanol fuel cells (DEFCs). With the emergence of alkaline anion exchange membrane, in recent years, the development of

catalysts for alkaline media is gaining a lot of importance. The better kinetics of alcohol oxidation and oxygen reduction is an advantage of an alkaline environment. Therefore, the study of the catalytic activity of electrodes made from materials that are less expensive and abundant in nature than platinum becomes much more important. Palladium is one of the noble metals which in recent years attracted much attention due to its high stability in alkaline media and the good activity to oxidize lower alcohols in this environment. In order to develop less expensive and more efficient catalyst, it is necessary to combine noble metal with a transition metal, in order to reduce the amount of used noble metal, and in order to obtain a catalyst with improved activity through the bifunctional and electronic effects.

**Results and discussion**

Pd-Ni/C catalyst, synthesized by combination of reduction process with $NaBH_4$ and spontaneous galvanic replacement [6, 7, 8], was investigated as potential anode catalyst in DMFCs and DEFCs. The physicochemical characteristics of Pd-Ni/C catalysts were tested by energy dispersive spectroscopy (EDS), and thermo-gravimetric analysis (TGA). EDS analysis revealed that the atomic ratio of metals are Pd:Ni = 0.4:0.6; and by thermogravimetric analysis, taking into account the EDS analysis, it was found that the mass percentage of Pd in the catalyst is 6.4 mass%. Electrochemical properties of Pd-Ni/C were compared with the Pd powder and polycrystalline Ni electrode. The aim of electrochemical characterization of the catalysts is to identify the processes on the surface that occur in the same potential region as well as the oxidation of methanol and ethanol, to estimate the surface composition of the synthesized catalyst Pd-Ni/C and to determine the electrochemical active surface of Pd on the Pd powder and on the Pd-Ni/C catalyst. Synthesized Pd-Ni/C and Pd powder were deposited on a glassy carbon electrode as a thin film for electrochemical testing. The catalysts were tested in a 0.1 M NaOH, saturated by $N_2$. Investigated potential range was 0.13 to 1.2 V vs. RHE. Tests on Pd-Ni/C were performed by cyclic voltammetry and the result was, taking into account tests on Pd powder and polycrystalline Ni electrode, voltammogram with shape similar to the voltammogram of Pd powder [9], but with tiny differences that are attributed to the presence of Ni. Cyclic voltammograms of polycrystalline Ni electrode in alkaline media does not show any voltammetric peaks in the potential range of 0.13 to 1.2 V, which indicates the inertia of β-Ni $(OH)_2$ [10].The electrochemical active surface area of the catalyst Pd-Ni/C or Pd powder were determined based on the charge transfer in the metal reduction region, and assuming the charge of 420 μA $cm^{-2}$ needed for the reduction of oxide monolayer on the catalyst surface [11]. Oxidation of methanol and ethanol was investigated in electrolyte containing 0.5 M methanol and 0.5 M ethanol, by recording potentiodynamic polarization curves, at the sweep rate of 50 mV $s^{-1}$ and chronoamperometric curves at potentials 0.8 V vs. RHE for methanol and 0.7 V vs. RHE for ethanol oxidation. The results show that the modest activity of Pd for methanol oxidation does not increase, but on the contrary decreases by the addition of Ni, indicating that Pd-Ni/C is not a promising catalyst for the oxidation of methanol in an alkaline media. However, Pd-Ni/C

showed a higher activity for the oxidation of ethanol, as compared to the Pd powder. It is interesting that the activity of the Pd-Ni/C catalyst becomes higher under the potential cyclization conditions. This result was obtained based on the examination of ethanol oxidation in potentiodynamic conditions during 250 cycles of potential change where was revealed that until the second cycle presence of Ni has no effect on the rate of ethanol oxidation on Pd. However, further cyclization to the 50th cycle current density on Pd decreases, while on the Pd-Ni/C rises to the maximum current twice bigger than on the Pd. After that, there is gradual decrease of the current density on the Pd-Ni/C, but in $250^{th}$ cycle its activity remains high, approximately 50% higher than that of pure Pd. Influence of cyclization of the electrode potentials on their stability was tested under the same conditions over the 250 cycles, but the in the basic electrolyte (0.1 M NaOH), and it was found the identical 31% decrease of the electrochemical active surface area of the both catalyst. Measurement of the current density of ethanol oxidation on the Pd-Ni/C and Pd under potentiostatic conditions have shown that the Pd-Ni/C catalyst is more active, which corresponds with the results obtained under the conditions of potential cyclization. It should be noted that the decrease in activity during the 25 min is significant for both catalyst and it was about 60%.

## Conclusion

Because of the demonstrated good activity for the oxidation of ethanol and the ability to be activated during the potential cyclization Pd-Ni/C catalyst should be taken into consideration for application in direct alcohol fuel cells, and with further improvements and testing in order to become a competitive commercial catalyst.

## References


[1] C. Bianchini, P. K. Shen, *Chem. Rev.* 109 (2009) 4183.
[2] J. W. Gosselink, *Int. J. Hydrogen Energy* 27 (2002) 1125.
[3] C. Lamy, J.-M. Léger, *J. Phys.*IV 4 (1994) C1.
[4] R. Dillon, S. Srinivasan, A. S. Arico, V. Antonucci, *J. Power Sources* 127 (2004) 112.
[5] Y. Zhao, X. Yang, J. Tian, F. Wang, L. Zhan, *Int. J. Hydrogen Energy* 35 (2010) 3249.
[6] K. A. Kuttiyiel, K. Sasaki, D. Su, M. B. Vukmirovic, N. S. Marinkovic, R. R. Adzic, *Electrochim. Acta* 110 (2013) 267.
[7] M. Liao, Q. Hu, J. Zheng, Y. Li, H. Zhou, C.-J. Zhong, B. H. Chen, *Electrochim. Acta* 111 (2013) 504.
[8] M. Ren, J. Chen, Y. Li, H. Zhang, Z. Zou, X. Li, H. Yang, *J. Power Sources*, 246 (2014) 32.
[9] M. Grden, M. Lukaszewski, G. Jerkiewiczb, A. Czerwinski, *Electrochim. Acta* 53 (2008) 7583.
[10] M. Grden, K. Klimek, A. Czerwinski, *J. Solid State Electochem.* 8 (2004) 390.
[11] M. Wang, W. Zhang, J. Wang, D. Wexler, S. D. Poynton , R. C. T. Slade, H. Liu, B. Winther-Jensen , R. Kerr , D. Shi , J. Chen. *ACS Appl. Mater. Interfaces* 5 (2013) 12708.

# A LIFE TIME MODEL FOR PEM FUEL CELLS BASED ON VOLTAGE DEGRADATION

Petar Laušević, Vladimir Nikolić, Đorđe Šaponjić, Milica Marceta Kaninski

*Vinča Institute of Nuclear Sciences, Belgrade, Serbia*

Durability of proton exchange membrane fuel cells (PEMFCs) is one of the major obstacles in the comercialization of these systems for statianary and mobile applications. The objective of this paper was to develop a semi-empirical model that would simulate the performance of fuel cells without extensive calculations. The model was validated with data from several 500 h single cell durability tests.

## Introduction

The main barriers to market acceptance of PEM fuel cells are: endurance and reliability. Voltage degradation will be the main factor governing the life of the FC stack in terms of time in service, performance and reliability. The goal of this paper is the development of a generalized electrochemical degradation model with voltage degradation (ageing) terms. Much work has been done on modeling of PEM fuel cell performance, but few models address voltage degradation over time. Many mechanistic and empirical models can be found in literature and the complexity of these models varies [1,2]. The model presented in this paper is a semi-empirical electrochemical model, combining theoretically derived differential and algebraic equations with empirically determined relationships. The main parameters known to influence PEM FC performance and life are: water management, corrosion of the catalyst and membrane degradation [3]. Also the operational history of the FC will have a great influence on degradation and performance.

## Model

The expression for the voltage of a single cell is given by:

$$V_{cell} = E_{Nernst} + \eta_{actA} + \eta_{actC} + \eta_{ohmic}\,, \tag{1}$$

where $E_{Nernst}$ is the thermodynamic (open-circuit) potential of the cell, $\eta_{actA}$ and $\eta_{actC}$ are the anode and cathode activation overvoltages (a measure of the voltage losses associated with the anode and cathode), and $\eta_{ohmic}$ is the ohmic overvoltage, a measure of the IR losses associated with the proton conductivity of the polymer electrolyte and electronic internal resistances.

In order to have a single expression, the activation overvoltages can be combined and given in a parametric form [4,5]:

$$\eta_{act\ A+C} = \xi_1 + \xi_2 T + \xi_3 T \cdot \ln\left(C_{O_2}\right) + \xi_4 T \cdot \ln(i). \quad (2)$$

The terms $\xi_i$ are semi-empirical coefficients. The use of such semi-empirical coefficients gives a significant degree of flexibility when modeling a specific fuel cell. In equation 2: T is the cell temperature, *i* the cell current and $C_{O_2}$ the oxygen concentration at the cathode membrane/gas interface. The terms $\xi_i$ can be obtained by a fitting procedure based on the measured polarization curve of a single cell or a stack. At the same time, these coefficients have a significant mechanistic background.

For developing a voltage degradation model the most important of these parameters is $\xi_2$ because a degradation term can be introduced in the equation: $\xi_2 = k_{cell} + 197 \cdot 10^{-6} \ln A + 4.3 \cdot 10^{-5} \ln C_{H_2}$, where $k_{cell}$ represents the measure of apparent catalytic activity [4]. The active surface area or catalyst activity will be one of the main parameters that will degrade over the operational time of the cell. So it is this parameter that will change in the model to represent the degradation of the voltage associated with the loss of catalyst activity in the FC.

The ohmic losses result from the resistance to electron transfer in the collector plates and electrodes, combined with the resistance to proton transfer in the polymer electrolyte membrane. For high purity graphite plates the electron resistance can be neglected. The proton resistance is defined based on the membrane parameters: $R^{proton} = \left(r_m \cdot l\right)/A$, where $r_m$ is the membrane specific resistance ($\Omega \cdot cm$), *l* the thickness of the proton exchange membrane and *A* is the cell active area. For Nafion membranes, used in our experiments, the following empirical expression was proposed in literature [1,5]:

$$r_m = \frac{181.6 \cdot \left(1 + 0.03(i/A) + 0.062(T/303)^2 (i/A)^{2.5}\right)}{(\lambda - 0.634 - 3(i/A)) \cdot \exp(3.25(T - 303)/T)}. \quad (3)$$

The parameter λ is a function of membrane water content and as such it is strongly correlated with the overall cell management, but it is also a function of the cells age.

Changes in catalytic activity and the degradation parameter associated with the conductivity loss are modeled by a first order degradation rates:

$$k_{cell} = k_0 \cdot age / T + k_1 \text{ and } \lambda = \lambda_0 + \lambda_1 \cdot age\ . \quad (4)$$

## Experimental

The model response has been validated with data from several 500 h durability tests of a single cell with 25 $cm^2$ active area at 90$^oC$ with reformate at the anode side (10ppm CO) and air at the cathode side conducted under different load conditions. The membrane electrode assembly (MEA) has been developed and provided by CEA/Liten, France. The tests were conducted using the Hepas test station, programmable load and Hepas eLoad test software. The model was implemented in MATLAB. Figure 1 shows that the model can be used to accurately predict the FC performance over time and to estimate the life span of a FC.

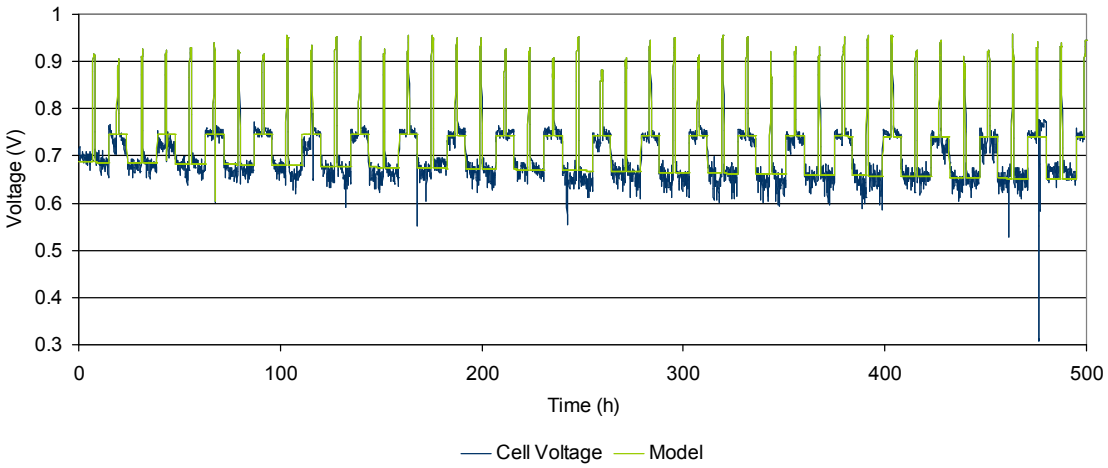


**Figure 1.** Experimental and model results of a 500h durability test.

## Conclusions

The model is based on the cell voltage degradation data obtained from several 500h durability test. The objective of the modeling effort is to model the observed behavior in performance looking at different degradation mechanisms. The model takes into account the main variables of the FC operation: the operating temperature, the current density, cathode and anode pressures. Other model parameters are the cell active area and membrane thickness. The model has a significant degree of flexibility when modeling a specific fuel cell. The mechanistic basis of the model gives it flexibility over a wide range of operating conditions.


## Acknowledgment

The authors would like to acknowledge the financial support through the FP7 FCH-JU project, acronym „EURECA“, Grant Agreement No 303024.


## References


[1] A. Saadi, M. Becherif, A. Aboubou, M. Y. Ayad, *Renew. Energy* 56 (2013) 64.

[2] A. Beicha, *J. Power Sources* 205 (2012) 335.

[3] W. Schmittinger, A. Vahidi, *J. Power Sources* 180 (2008) 1.
[4] M. W. Fowler, R. F. Mann, J. C. Amphlett, B. A. Peppley, P. R. Roberge, *J. Power Sources* 106 (2002) 274.
[5] R. F. Mann, J. C. Amphlett, M. A. I. Hooper, H. M. Jensen, B. A. Peppley, P. R. Roberge, *J. Power Sources* 86 (2000) 173.

# *Heterogeneous catalysis*

# *and*

# *Photocatalysis*

# SYSTEMATIC DFT STUDY OF BIMETALLIC DIMERS SUPPORTED BY MgO(001)

I. Pašti[1], L. P. Granda Marulanda,[1] N. V. Skorodumova[2,3]

[1]*University of Belgrade, Faculty of Physical Chemistry, Studentski trg 12-16, 11158 Belgrade, Serbia*
[2]*Multiscale Materials Modelling, Materials Science and Engineering, School of Industrial Engineering and Management, KTH - Royal Institute of Technology, Brinellvägen 23, 100 44 Stockholm, Sweden*
[3]*Department of Physics and Astronomy, Uppsala University, Box 516, 751 20 Uppsala, Sweden*

Bimetallic M1M2 dimers (M1, M2 = Ru, Rh, Pd, Ir and Pt) supported on MgO(001) were studied using DFT-GGA approach with the aim to investigate their stability, electronic structure and reactivity and provide new insights into the possibility of rational design of multimetallic supported catalysts. Studied dimers are stable on MgO(001). Charge state and the electronic structure of adsorbed dimers are determined by dimer composition and the orientation with respect to MgO(001) surface plane. CO chemisorptions properties of dimer constituents could be effectively linked to its electronic structure, which provides a basis for the search of new supported bimetallic catalytic systems.

## Introduction

Catalytic processes present one of the foundations of contemporary technologies, stimulating constant research and development. Most of the real life catalytic materials are consisted of catalytically active component dispersed over suitably chosen support. Magnesium-oxide, MgO, is one of the most common catalyst supports. Current literature contains large body of work conducted on MgO-supported metal clusters, including both theoretical and experimental studies [1-2]. This especially holds for metal atoms and small monometallic clusters (dimers, trimers, tetramers) supported on MgO(001) surface. However, practice has taught us that multimetallic catalysts are usually superior to their monometallic counterparts. A well known example which found many practical applications is a bifunctional mechanism of alcohol oxidation on PtRu surface where CO, intermediately formed at Pt sites, is oxidized by the mediation of OH groups formed on adjacent Ru sites [3]. In this sense, MgO-supported bimetallic dimers present the smallest possible model systems for supported bimetallic catalysts.
With the aim to understand the interactions, stability, the electronic structure and the reactivity of supported bimetallic dimers on MgO, this contribution presents a combinatorial study of bimetallic M1M2 dimers (M1, M2 = Ru, Rh, Pd, Ir and Pt) with the defect-free MgO(001).

## Computational details

DFT-GGA calculations were performed using the PWscf code of Quantum ESPRESSO distribution [4]. Ultra soft pseudopotentials were used for the treatment of core electrons and the kinetic energy cutoff for the selection of the plane-wave basis set was 28 Ry. The MgO (001) surface has been modeled by a three layers slab with (2×2) unit cell. The surface slabs were separated by a vacuum region of 12 Å with the dipole correction included. As a probe molecule, CO was used to assess the reactivity of metal monomers and dimers. The charge transfer was analyzed on the basis of "Atoms in Molecules" theory of Bader.

## Results

Studied metal monomers adsorb at oxygen sites of MgO(001) with adsorption energies between −0.75 eV (Ru) and −2.27 eV (Pt). Adsorption of bimetallic dimers is also preferred at oxygen sites of MgO(001). $Pt_2$, $Ir_2$ and PtIr dimers prefer adsorption in vertical mode with one atom attached to O surface site while others are parallel to the surface. Relatively large cohesive energies of M1M2+MgO(001) adsorption complexes point that such structures are more stable than formation of adsorbed monomers. This indicates that under realistic growth conditions formation of metal agglomerates on MgO(001) is expected, which is governed by stronger M1-M2 interaction compared to M-MgO(001) interaction. Using Bader analysis significant charge transfer to adsorbed metal atoms was observed, reaching −0.47e for the case of Ir monomer. For the case of supported bimetallic dimers, charge transfer depends on the dimer orientation with respect to MgO(001) surface plane and the position of M1 and M2 in the Periodic Table of Elements.

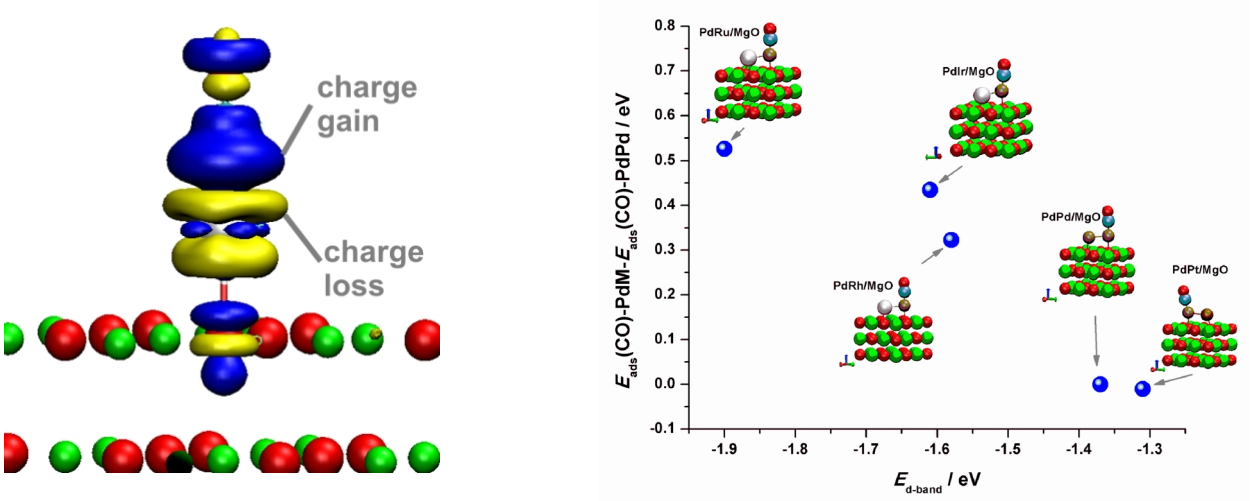


**Figure 1.** Charge redistribution upon CO adsorption on $Ir_{ads}$/MgO(001) (left) and correlation of CO binding energy to Pd atom of PdM2/MgO(001) with the d-band center of respective Pd atom ($E_{d\text{-}band}$).

Adsorption of CO on supported metal monomers and selected bimetallic dimers was investigated to reveal the electronic structure parameters which determine dimer reactivity. CO binds to Ir monomer the most strongly, with the adsorption energy of −3.79 eV, while the weakest bond is established with Pd monomer (−2.49 eV). CO adsorption is followed by significant charge redistribution (Fig. 1, left). In the case of supported dimers, chemisorption properties of dimer and dimer constituents are affects by dimer composition and also dimer orientation with respect to MgO(001) surface plane. Clear linear relationship between CO adsorption energy and the d-band center position of a reactive atom in the dimer was observed (Fig 1, right).
Presented results extend the d-band center model of Hammer and Nørskov [5] to highly under-coordinated metal atoms and infer to a conclusion that is possible to tune/optimize chemisorptions properties of supported bimetallic clusters to maximize catalytic performance.

**Conclusion**

Bimetallic M1M2 dimers (M1, M2 = Ru, Rh, Pd, Ir and Pt) supported on defect-free MgO(001) are expected to be stable and preferred over adsorbed M1 and M2 monomers. These species interact preferentially with O centers of Mg(001) and, with the exceptions of $Pt_2$, $Ir_2$ and PtIr, prefer parallel orientation with respect to MgO(001) surface plane. The electronic structure and the charge state of adsorbed dimers depend on dimer composition and orientation. CO chemisorption properties can be tuned by dimer composition, while d-band center position can be correlated to CO adsorption properties of a given atom in supported M1M2 dimer.

**References**

[1] M. Amft, N.V. Skorodumova, *Phys. Rev. B* 81 (2010) 195443.
[2] F. Frusteri, S. Freni, L. Spadaro, V. Chiodo, G. Bonura, S. Donato, S. Cavallaro, *Catal. Commun.* 5 (2004) 611.
[3] M. Watanabe, S. Motoo, *J. Electroanal. Chem.* 60 (1975) 267.
[4] P. Giannozzi, et al. *J. Phys.: Condens. Matter* 21 (2009) 395502.
[5] B. Hammer, J.K. Nørskov, *Surf. Sci.* 343 (1995) 211.

## ADATOM CHARGING ON METAL SUPPORTED THIN FILMS: MECHANISM AND PERSPECTIVES FOR CATALYSIS

P. A. Žguns[1], I. Pašti[2], M. Wessel[3], N. V. Skorodumova[1,3]

*[1] Multiscale Materials Modelling, Department of Materials Science and Engineering, Royal Institute of Technology, SE-100 44 Stockholm, Sweden*
*[2] Faculty of Physical Chemistry, University of Belgrade, Studentski Trg 12-16, 11158 Belgrade, Serbia*
*[3] Department of Physics and Astronomy, Uppsala University, Box 516, 75121 Uppsala, Sweden*

Over the past years adatom charging on metal supported thin films had been studied intensively (see, e.g. [1-3]). The main feature being in the centre of attention is a charge transfer from support metal to adatom through insulating film. However, the detailed mechanism is still under the debate [1-3].
Here we report our study on AB/Mo (AB = ScN, MgO, NaF), as well as Cu atom adsorption on them. The prerequisites for adatom charging and the mechanism of charge redistribution is discussed. In order to examine the applicability of Cu/AB/Mo systems in catalysis, we investigate the adsorption of small molecules on Cu/AB/Mo.

**References**

[1] G. Pacchioni, L. Giordano, M. Baistrocchi, Phys. Rev. Lett. 94 (2005) 226104.
[2] K. Honkala, H. Häkkinen, J. Phys. Chem. C 111 (2007) 4319.
[3] P. Frondelius, A. Hellman, K. Honkala, H. Häkkinen, H. Grönbeck, Phys. Rev. B 78 (2008) 085426.

# SYNTHESIS AND TESTING OF HETEROGENEOUS CATALYST FOR BIODIESEL

Ž. Kesić,[1] I. Lukić,[1] M. Zdujić,[2] Lj. Mojović,[1] D. Skala[1]

[1]*University of Belgrade, Faculty of Technology and Metallurgy*
[2]*Institute of Technical Sciences of the Serbian Academy of Sciences and Arts*

In the present work, biodiesel production from the transesterification of the sunflower oil with methanol over a calcium based catalysts has been studied. Catalysts were prepared using a mechanochemical method. Basic aim of this paper is to explore effect of type and quantities of catalyst on transesterification process.

## Introduction

The use of biodiesel is of great interest during the past decade due to the diminishing petroleum reserves and environmental concerns. Biodiesel, also known as fatty acid methyl esters (FAME), which is produced by transesterification of vegetable oil with methanol, can be used as an alternative to fossil diesel fuel [1].
Among the heterogeneous catalysts that are being used in transesterification, calcium oxide (CaO) has a promising place. CaO catalyst is one of the most studied systems for biodiesel production due to high activity, availability and low cost [2]. Also, mixed metal oxides i.e. the oxides containing two or more different kinds of metal cations, represent an interesting class of heterogeneous catalysts and catalyst supports for alkali metals [3]. The CaO·ZnO mixed oxide has been found to be active catalysts for methanolysis of sunflower oil, while $K_2CO_3$ is usually used as promoter to modify the base properties of alumina, alumina/silica, cinder or hydrotalcite as support [4]. $CaTiO_3$ prepared by the calcination of $TiO_2/CaCO_3$ mixture at 1323 K showed high activity for the transesterification of rapeseed oil to biodiesel, but it was easy to be deactivated [5].

## Experimental

In order to study solid base catalyst for biodiesel production, transesterification of edible sunflower oil with methanol was carried out in the presence of calcium type oxides. Powder mixtures of CaO and ZnO, in the molar ratio of 1:2 with water, with as well as without addition of $K_2CO_3$ (molar ratio of $K_2CO_3$ to CaO 2:10) were used as starting materials for mechanochemical treatment and then calcined at 700 °C for 3 h. The perovskite $CaTiO_3$ was prepared by calcination of precursor, obtained by the mechanochemical activation of starting powders $CaCO_3$ and $TiO_2$ at 700 $^oC$ for 24 h. In addition, $CaTiO_3$ was synthesized by

conventional solid-state reaction, which involves mixing the $CaCO_3$ and $TiO_2$ in the desired proportion followed by calcination at 1050 $^oC$.

The prepared catalysts were characterized by X-ray diffraction (XRD) and base strength using Hammett indicator method. The effect of mechanochemical activation was assessed after carrying out transesterification reaction. All the experiments were done in 300 $cm^3$ batch autoclave equipped with a heater and a mixer at 70 $^oC$ and 1.84 bar, with the molar ratio of methanol to sunflower oil of 10:1 and with 2 wt% of catalyst based on oil weight.

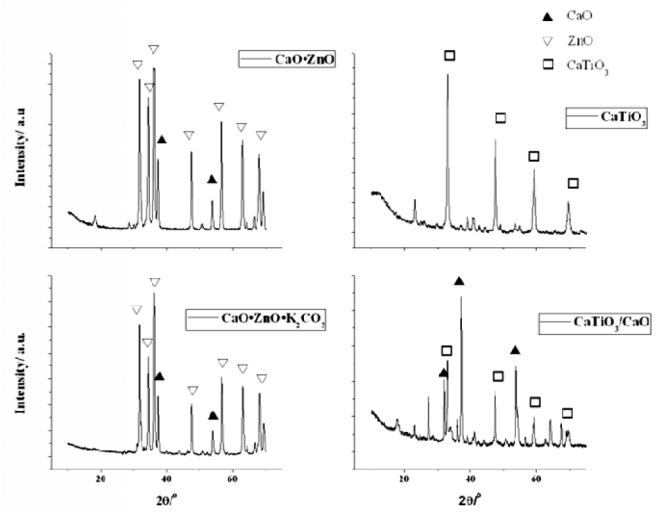


**Figure 1.** XRD patterns of synthesized catalysts.

**Results and discussion**

XRD patterns of the CaO·ZnO mixed oxides prepared with or without addition of $K_2CO_3$ are quite similar suggesting that $K_2CO_3$ didn't have a significant effect on the phase formation during heat treatment. XRD analysis of the mechanochemically activated and calcined $CaTiO_3$ sample reveals only the characteristic peaks of the perovskite type structure of $CaTiO_3$. For the sample synthesized by conventional solid-state reaction, characteristic peaks of $CaTiO_3$ and CaO could be identified on the XRD pattern, indicating a mixture of these components ($CaTiO_3$/CaO). The basicity and basic strength ($H\_$) of the solids are the most important properties regarding their application as catalysts for the methanolysis of triglycerides. The results of the characterization with methods based on the use of Hammett indicators are included in Table 1.

**Table 1.** Basic strength of the prepared catalysts

| Sample | Basic strength |
|---|---|
| CaO·ZnO | $11.0 < H\_ < 18.4$ |
| $CaO·ZnO·K_2CO_3$ | $11.0 < H\_ < 18.4$ |
| $CaTiO_3$ | $6.8 < H\_ < 9.3$ |
| $CaTiO_3$/CaO | $9.3 < H\_ < 10$ |

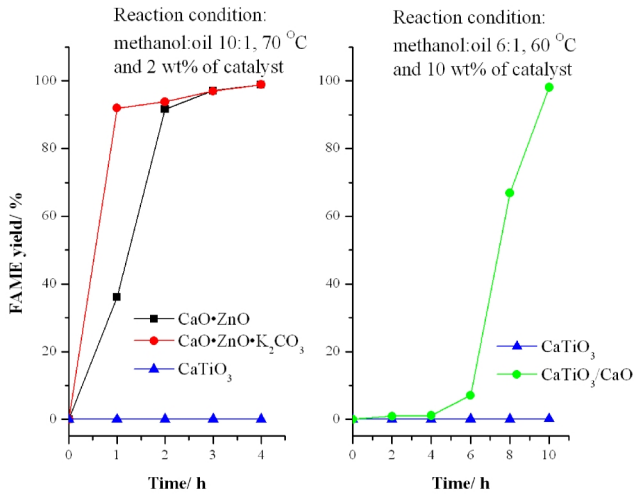


**Figure 2.** FAME yield versus time obtained with calcium based catalysts.

CaO·ZnO and CaO·ZnO·$K_2CO_3$ possess a high activity at 70 °C (molar ratio of methanol to oil 10:1 and 2 wt% of catalyst). It was found that pure perovskite $CaTiO_3$ phase exhibited no catalytic activity under the same reaction conditions, as well as under the reaction conditions reported by Kawashima [5]. Using $CaTiO_3$/CaO mixture resulted in FAME yield of 98.1% at 60 °C, molar ratio of methanol to oil 6:1 and 10 wt% of catalyst, probably due to present CaO phase.

## Conclusion

CaO·ZnO showed a high catalytic activity for methanolysis of sunflower oil at 70 °C using methanol to oil molar ratio of 10:1 and 2 wt% of catalyst. Addition of potassium carbonate accelerated the transesterification reaction. Under these conditions, pure perovskite phase exhibited no catalytic activity.

## Acknowledgements

Financial support of the Ministry of Education and Science of the Republic of Serbia (Grant No. 45001) is gratefully acknowledged.

## References

[1] M. Kouzu, S.Yamanaka, J. Hidaka, M. Tsunomori, *Appl. Catal. A* 355 (2009) 94.
[2] K. Urasaki, S. Takagi, T. Mukoyama, J. Christopher, K. Urasaki, S. Kato, A. Yamasaki, T. Kojima, S. Satokawa, *Appl. Catal. A* 411-412 (2012) 44.
[3] V. Mutreja, S. Singh, A. Ali, *Renew. Energy* 62 (2014) 226.
[4] Ž. Kesić, I. Lukić, M. Zdujić, Č. Jovalekić, H. Liu, D. Skala, *Chem. Ind. Chem. Eng. Q.*, 2014, doi:10.2298/CICEQ131026041K
[5] A. Kawashima, K. Matsubara, K. Honda, *Bioresour. Technol.* 99 (2008) 3439.

# PHOTOCATALYTIC PERFORMANCE OF $Mg_2TiO_4$ NANOPOWDER

Mina Medić,[1] Aleksandra Zarubica,[2] Scott P. Ahrenkiel,[3] Vesna Lojpur,[1] Ivana Vukoje,[1] Miroslav D. Dramićanin,[1] Jovan M. Nedeljković[1]

[1]*Institute of Nuclear Sciences Vinča, P.O. Box 522, 11001 Belgrade, Serbia*
[2]*Department of Chemistry, Faculty of Science and Mathematics, University of Niš, Višegradska 33, 18000 Niš, Serbia*
[3]*South Dakota School of Mines and Technology, 501 E. Saint Joseph Street, Rapid City, SD 57701, USA*

Magnesium-orthotitanate ($Mg_2TiO_4$) powder consisting of loosely agglomerated $Mg_2TiO_4$ nanoparticles with the size of about 10 nm was prepared using Pechini-type synthetic route. Obtained material was characterized using transmission electron microscopy and X-ray diffraction measurements. Band gap value of $Mg_2TiO_4$ powder was estimated from diffuse reflection data. Possibility to use $Mg_2TiO_4$ material for photocatalytic purposes was demonstrated in degradation reaction of organic dye crystal violet.

## Introduction

Magnesium-orthotitanate ($Mg_2TiO_4$) is widely used as a heat resistor, dielectric for microwave technology, capacitor for temperature compensation and as refractory material [1]. $Mg_2TiO_4$ has an inverse spinel structure, in which the titanium atoms occupy octahedral sites and the magnesium atoms occupy both tetrahedral and octahedral sites. $Mg_2TiO_4$ is a wide band gap material with the reported value for onset of optical absorption at 335 nm [2]. So far, the smallest $Mg_2TiO_4$ particles (~40 nm) were obtained using wet chemical method [3].
In this study attempt was made to synthesize $Mg_2TiO_4$ powder consisting of nanoparticles with average size of about 10 nm using Pechini-type synthetic route. The obtained material was thoroughly analyzed using microstructural (TEM and XRD) and spectroscopic (diffuse reflection) techniques. In this study, for the first time, photocatalytic ability, as an additional function of $Mg_2TiO_4$, was demonstrated, and its photocatalytic performance was tested using degradation kinetics of organic dye crystal violet as a model system.

## Experimental

$Mg_2TiO_4$ nano-powders were synthesized using Pechini-type polymerized complex route, described elsewhere [4].

Transmission electron microscopy (TEM) and scanning TEM (STEM) analyses were performed in a JEOL JEM-2100 $LaB_6$ instrument operated at 200 KV. X-ray diffraction (XRD) analysis of $Mg_2TiO_4$ powder was performed using Rigaku SmartLab diffractometer. Optical properties of $Mg_2TiO_4$ powder was studied using diffuse reflectance measurements (Thermo Evolution 600 spectrophotometer equipped with Labsphere RSA-PE-19).
Photocatalytic ability of $Mg_2TiO_4$ powder was studied using degradation of the organic dye crystal violet (CV). The photocatalytic reactions were induced using UV lamp (Roth Co., 16 W, 2.5 $mW/cm^2$) with maximum of light emission at 254 nm. Initial concentration of organic dye, as well as its decrease during photodegradation reactions were determined by measuring absorption at the peak position of CV ($\lambda_{max}$ = 590 nm; $\varepsilon_{590} = 8.7x10^4$ $M^{-1}cm^{-1}$).

**Results and Discussion**

A representative TEM image of $Mg_2TiO_4$ powder is shown in Figure 1. Detailed inspection of the sample indicated that $Mg_2TiO_4$ powder consists of well-crystallized, loosely agglomerated $Mg_2TiO_4$ nanoparticles with the size of about 10 nm. It should be emphasized that, to the best of our knowledge, synthetic route providing $Mg_2TiO_4$ particles with size of about 10 nm has not been previously reported in literature.

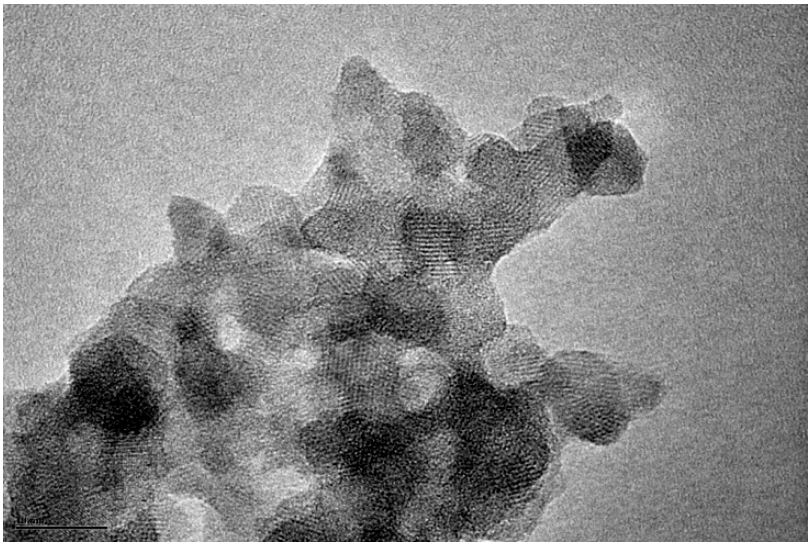

**Figure 1.** High-resolution TEM image of $Mg_2TiO_4$ powder.

The XRD measurements (results not shown) revealed that $Mg_2TiO_4$ powder has cubic crystal structure (ICDD 01-072-6968 card). It should be mentioned that there is no indication of the presence of any other crystalline phase. A grain size of 52 Å, determined from the peak broadening and Scherrer's equation, is in agreement with the size of nanoparticles by TEM analysis.

Steep rise of absorption was observed in UV spectral range bellow 350 nm after Kubelka-Munk transformation of diffuse reflection data of $Mg_2TiO_4$ powder (results not shown). Corresponding band gap energy of 3.55 eV is in agreement with reported data in literature for $Mg_2TiO_4$ [2].

Photocatalytic performance of $Mg_2TiO_4$ nanopowders was tested using degradation of organic dye CV. Degradation kinetics of CV for different initial concentrations (5-10 μM) are shown in Figure 2. As expected, decrease of initial concentration lead to faster degradation kinetics, and almost complete decolorization of CV was achieved for the lowest initial concentration after 1 day of illumination. It is important to emphasized that, to the best of our knowledge, $Mg_2TiO_4$ never been used before for photocatalytic purposes.

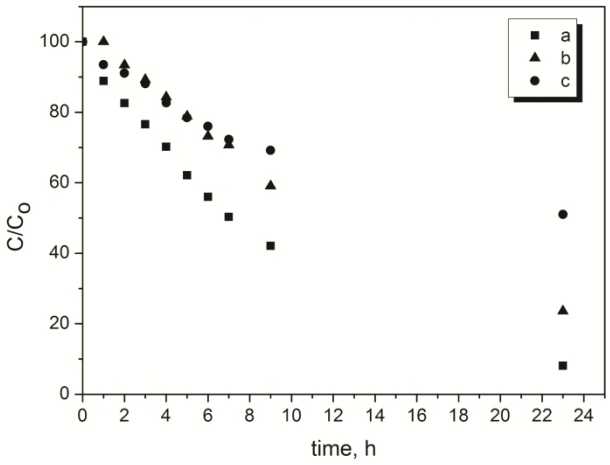


**Figure 2.** Degradation kinetic of CV over $Mg_2TiO_4$ nanopowder as a function of initial concentration of organic dye: (a) 5.0 μM, (b) 7,5 μM, and (c) 10.0 μM.

## Conclusion

Photocatalytic ability, as an additional function of $Mg_2TiO_4$, is demonstrated using degradation of organic dye crystal violet. Thorough study concerning improvement of optical and charge separation properties of $Mg_2TiO_4$ nanopowders by surface modification with bidentate benzene derivatives is underway in our laboratories.

## References

[1] T. Ye, S. Li, X. Wu, M. Xu, X. Wei, K. Wang, H. Bao, J. Wang, J. Chen, *J. Mater. Chem. C* 1 (2013) 4327.

[2] Y-D. Ho, C-H. Su, C-L. Huang, *J. Am. Ceram. Soc.* 97 (2014) 358.

[3] G. Pfaff, *Ceram. Int.* 20 (1994) 111.

[4] Ž. Antić, R. Krsmanović, M. G. Nikolić, M. Marinović-Cincović, M. Mitrić, S. Polizzi, M. D. Dramićanin, *Mater. Chem. Phys.* 135 (2012) 1064.

# *Hydrogen storage*

# HYDROGEN STORAGE PROPERTIES OF $MgH_2$ BASED HYDRIDES DOPED WITH SiC, $TiB_2$ AND $LiAlH_4$

I. Milanović,* R. Vujasin, Lj. Matović, A. Đukić, B. Paskaš Mamula, J. Grbović Novaković and N. Novaković

*Vinča Insitute of Nuclear Sciences, University of Belgrade, Belgrade, Serbia*
**e-mail: igorm@vinca.rs*

It is proven that different kinds of additives could decrease hydrogen desorption temperature of $MgH_2$ and accelerate it's kinetics. Goal of this research was destabilization of $MgH_2$ structure by three different kinds of additives: small amounts of SiC, $TiB_2$ and $LiAlH_4$ (5wt.%) by mechanical milling. $MgH_2$-SiC-$TiB_2$ system shows worse desorption properties than pure $MgH_2$. In case of $MgH_2$-$LiAlH_4$ composite, hydrogen desorption temperature is shifted under 400°C (15 min milled composite).

## Introduction

Magnesium hydride is one of the most promising materials for hydrogen storage [1]. This compound characterize sluggish kinetics and high desorption temperature. Because of that, structure of $MgH_2$ must be destabilized by addition of another compounds. This compounds are in our case: SiC [2] and $TiB_2$ [3] (separately and together) and $LiAlH_4$. Investigations of $LiAlH_4$ complex hydrides for hydrogen storage purposes, dates from works of Andreasen [4], Balema [5] and Ares [6]. Beside hydrogen storage in pure $LiAlH_4$, it is noticed that $LiAlH_4$ could be also used for destabilization of the $MgH_2$ structure [7].

## Experimental

Desorption properties of $MgH_2$ based composites are prepared by mechanical milling. The samples that were synthesized for 10h milling are: 95wt.%$MgH_2$+ 5wt.% $TiB_2$, 95wt.%$MgH_2$ + 4.5wt.%$TiB_2$ + 0.5wt.%SiC and 95wt.%$MgH_2$ + 4.5wt.% SiC + 0.5wt.%$TiB_2$. Grinding of $MgH_2$-$LiAlH_4$ composites (95wt.%$MgH_2$ + 5wt.% $LiAlH_4$ mixture) was carried out for 15, 30 and 60 minutes. Thermal desorption properties of all composites was done by temperature programmed desorption (TPD) (Fig. 1. and 3.). Morphology of samples was analyzed by scanning electron microscopy (SEM), shown at the Fig. 2.

## Results and Discussion

From Fig. 1. we can conclude that whole hydrogen desorption process is divided at three parts: low-temperature part (LT-$H_2$), intermediate-temperature part (IT-$H_2$) and high-temperature part (HT-$H_2$). The third peak has three orders of magnitude greater intensity than other two peaks. This peak represents hydrogen desorption at high temperature and it's position is dependent on the aditive type. With increasing $TiB_2$ concentration, position of HT peak is shifted towards higher temperatures. Dobrovolsky at al. [3] concluded that presence of $TiB_2$ could increase sensitivity of composite on catalitic inhibitors. Beside this drawback, $TiB_2$ has good influence on kinetic behavior by increasing rate of hydrogen desorption. From Fig. 2 it is obvious that milling process has influence on particle size. Particle size of composites reduces with the increase of SiC quantity [2]. As a consequence, decrease of hydrogen desorption temperature is noticed.

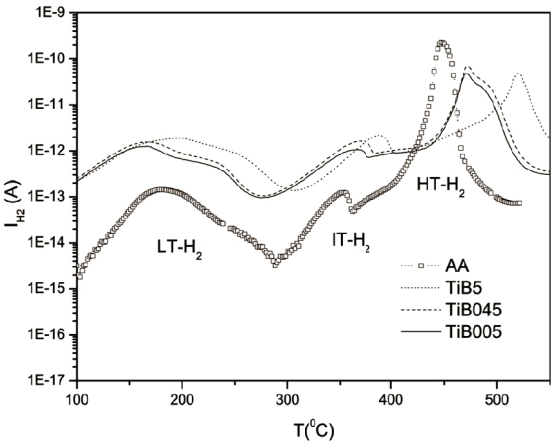


**Figure 1.** Desorption (TPD) curves of 95wt.%$MgH_2$ + 5wt.%$TiB_2$ (TiB5), 95wt.%$MgH_2$ + 4.5wt.%$TiB_2$ + 0.5wt.%SiC (TiB045) and 95wt.%$MgH_2$ + 4.5wt.% SiC + 0.5wt.%$TiB_2$ (TiB005) composites and pure unmilled $MgH_2$ (AA).

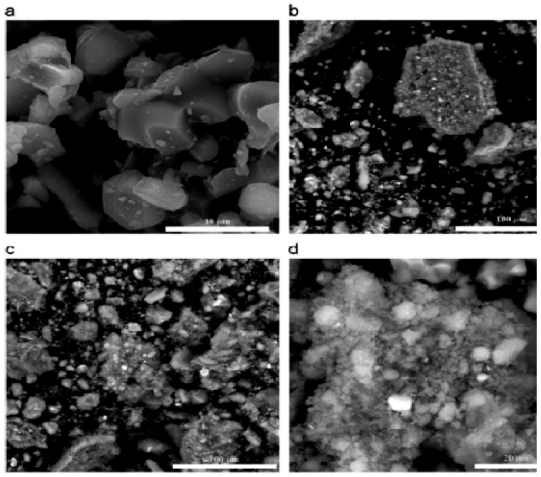


**Figure 2.** SEM micrographs of: a)AA, b)TiB5, c)TiB045 and d)TiB005 composites.

All synthesized $LiAlH_4$ composites show better desorption characteristics (Fig. 3.) than pure and milled $MgH_2$. Hydrogen desorption temperature is shifted under 400°C for 15 min milled composite. Another two composites (30 and 60 min milled) shows higher desorption temperatures. These facts are in the direct correlation with decomposition of $LiAlH_4$ with increase of milling time. Also, addition of $LiAlH_4$ accelerates the kinetics of $MgH_2$-$LiAlH_4$ composites in comparison to pure $MgH_2$.

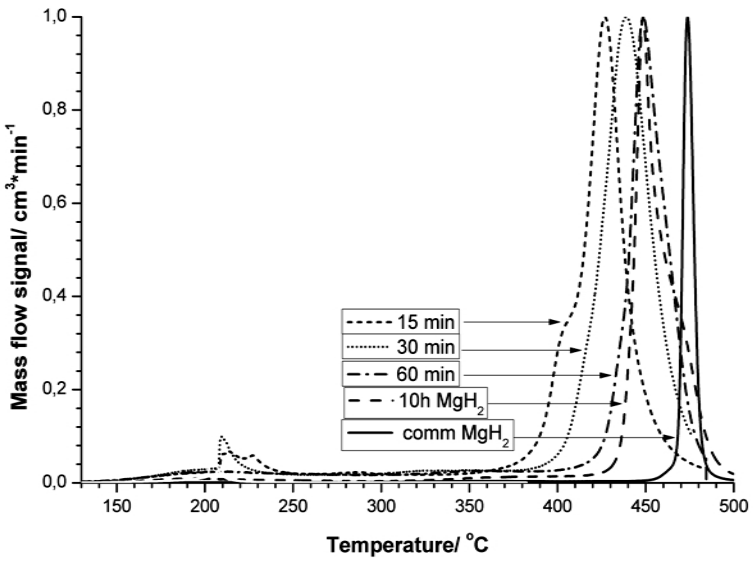


**Figure 3.** Desorption (TPD) curves of: $MgH_2$-$LiAlH_4$ composites milled for 15, 30 and 60 minutes, 10h milled $MgH_2$ and as received $MgH_2$ (comm $MgH_2$).

## Conclusion

It has been shown in both cases ($SiC+TiB_2$ and $LiAlH_4$) that small amounts of additives could improve hydrogen desorption temperatures of $MgH_2$ based composites. Beside additive concentration, important role in destabilization of $MgH_2$ plays mechanical milling which induce decrease in particle size of composites.

## Acknowledgement

This work is financially supported by Ministry of Education and Science of Republic of Serbia under grant III45012.

## References

[1] L. Schlapbach, A. Züttel, *Nature* 414 (2001) 353.
[2] A. Ranjbar, Z. P. Guo, X. B. Yu, D. Attard, A. Calka, H. K. Liu, *Int. J. Hydrogen Energy* 34 (2009) 7263.
[3] V. D. Dobrovolsky, O. G. Ershova, Y. M. Solonin, O. Y. Khyzhun, V. Paul-Boncour, *J. Alloys Compd.* 465 (2008) 177.
[4] A. Andreasen, T. Vegge, A. Pedersen, *J. Solid State Chem.* 178 (2005) 3672.
[5] V. P. Balema, V. K. Pecharsky, K. W. Dennis, *J. Alloys Compd.* 313 (2000) 69.
[6] J. R. Ares, K.-F. Aguey-Zinsou, M. Porcu, J. M. Sykes, M. Dornheim, T. Klassen, R. Bormann, *Mater. Res. Bull.* 43 (2008) 1263.
[7] Y. Zhang, Q.-F. Tian, S.-S. Liu, and L.-X. Sun, *J. Power Sources* 185 (2008) 1514.

# EFFECTS OF VACANCIES ON HYDROGEN DESORPTION PROPERTIES OF $MgH_2$

S. Kurko,* R. Vujasin, Lj. Matović, A. Đukić, B. Paskaš Mamula, J. Grbović Novaković, N. Novaković

*Vinča Institute for Nuclear Sciences, University of Belgrade, P.O. Box 522, 11000 Belgrade, Serbia*
**e-mail: skumric@vinca.rs*

The effect of surface and near-surface vacancies on hydrogen desorption properties of $MgH_2$ were investigated both experimentally and theoretically. Irradiation with $Ar^{8+}$ and $Xe^{8+}$ ions was used to introduce vacancies into subsurface layers of $MgH_2$. Theoretical calculations were performed using DFT approach within Abinit code. Results showed that there are several mechanisms involved in desorption process, which depend on defect concentration, their position and their interaction and ordering. It has been demonstrated that the changes in near-surface area play the crucial role in desorption kinetics.

## Introduction

Magnesium and magnesium based alloys have a great potential as rechargeable hydrogen storage materials since its high hydrogen storage capacity (7.6 wt %) and reversible, relatively simple, endothermic hydrogen desorption reaction. However, slow kinetics and relatively high dehydrogenation temperature still limit its practical application [1]. Severe attempts have been made to overcome these drawbacks. The most used method is nanostructuring of material by mechanical milling with different types of dopants like transition metals, intermetallics, oxides, carbides [2-5], etc.
The other way to destabilize the $MgH_2$ structure and improve its hydrogen desorption kinetics is ion irradiation. By inert, heavy ion irradiation it is possible to create a considerable amount of defects, particularly vacancies and to control their quantity and depth distribution through the sample [6]. On the other hand, DFT calculations can give an insight in the stability of the system and consequently, the possible mechanism of desorption process. From these calculations one can also determine the influence of vacancy position and concentration on the hydrogen desorption energy [7].In this paper, mechanism of hydrogen desorption from $MgH_2$ irradiated with $Ar^{8+}$ and $Xe^{8+}$ ions is investigated and correlated with DFT calculation findings.

## Experimental

Commercial (Alfa Aeser, (AA), of purity 98%) $MgH_2$ powder was prepared as explained in our previous work and homogeneously irradiated using 120 keV and $Ar^{+8}$ (sample A16) and $Xe^{+8}$

(sample S16) ions with fluence of $10^{16}$ ions/cm$^2$[6]. Interaction of incident ions with material was calculated using Monte Carlo method as implemented in SRIM package. X-ray analysis was done by Siemens KRISTALLOFLEX D-500 device. Malvern 2000SM Mastersizer laser scattering particle size analysis system was used to obtain the quantitative $MgH_2$ particle size distributions. Homemade apparatus with a quadruple mass spectrometer EXTORR XT300 was used for TPD measurements. For DFT calculations Abinit code and Troulliere Martins pseudopotentials were used. (110) plane was exposed and the supercell consists of 12 parallel atomic planes with total of 96 atoms, with H two-fold bonded surface atoms exposed to 1.5 nm thick vacuum.

**Results and Discussion**

It can be seen from table 1 that the $Xe^{8+}$ ions produce about 50 % more vacancies than $Ar^{8+}$ which are deposited nearer to the surface. XRD data showed small decrease in crystallite size for irradiated samples and shift of peaks towards higher angles as a consequence of material disordering. Mean particle size of irradiated samples is also reduced. Hydrogen desorption temperatures are 720, 643 and 665 K for samples AA, S16 and A16 consequently. The best fitting of thermal data was achieved by using Avrami-Erofeev nucleation models and results given in Table 1 show significant decrease in apparent activation energy that is more pronounced for the sample S16.

**Table 1.** SRIM, XRD, laser scattering and kinetic data for commercial (AA) and samples irradiated with $Xe^{8+}$ (S16) and $Ar^{8+}$ (A16) ions with fluence of $10^{16}$ ions/cm$^2$

| Sample | Produced vacancies per ion | Range maximum position (nm) | Crystallite size (nm) | Mean particle size (μm) | Avrami-parameter | $E_a^{des}$ (kJ/mol) |
|---|---|---|---|---|---|---|
| AA | - | - | 83 | 38 | 3 | 372 |
| S16 | 1818 | 85 | 45 | 21.7 | 4 | 97 |
| A16 | 1244 | 175 | 76 | 22.6 | 2 | 215 |

There is also change in the dimensionality of nucleus growth from 3D in sample AA to 2D for A16 and random in S16. These effects are result of hydrogen diffusion coefficient increase in subsurface layers and increase in the number of active sites for hydrogen molecule recombination because of the vacant surface structure. This explanation is supported by Park et al. on type and behavior of defects in the magnesium hydride in conditions of extremely poor hydrogen, existing during dehydrogenation process [8]. These effects are dominant for the sample S16 that has more vacancies closer to the sample surface. So, the concentration of defects has effect on desorption temperature and activation energy, while their position influences the reaction mechanism. Results of DFT calculation sowed that H-desorption energy strongly

depends on number of surface H atoms and their configuration. Surface vacancies considerably lower the H-vacancy formation energies as well in the sub-surface layers. These results suggest that the role of surface hydrogen concentration and distribution is decisive for the H-desorption kinetics, not only because of lowering the potential barrier for further H-desorption, but an increased number of surface hydrogen vacancies supports creation of the sub-surface vacancies network and make diffusion of bulk hydrogen atoms toward the surface easier.

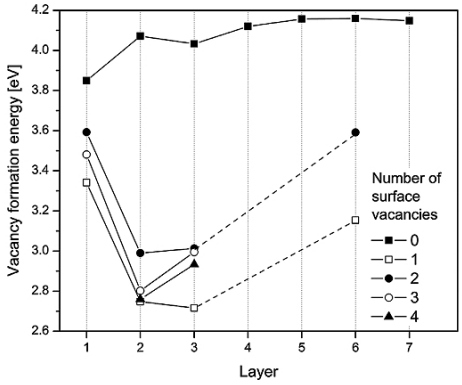


**Figure 1.** The H-vacancy formation energies in the (110) $MgH_2$sub-surface layers as a function of surface coverage with H atoms. Configurations with 1 and 3H vacancies in 3rd and 6th layer are connected with dashed line.

## Conclusion

It has been shown that the large concentration of the surface and near-surface vacancies promotes diffusion of H atoms toward the surfaces of grains, which lowers temperature and activation energy of $H_2$ desorption. Not only that concentration, but also the depth distribution of vacancies have strong influence on the desorption process.


## Acknowledgement

This work is financially supported by Ministry of Education and Science of Republic of Serbia under grant III45012.


## References


[1] L. Schlapbach, A. Züttel, *Nature* 414 (2001) 353.

[2] J. Huot, G. Liang, S. Boily, A. Van Neste, R. Schulz, *J. Alloys Compd.* 293 (1999) 495.

[3] C. Suryanarayana, *Prog. Mater. Sci.* 46 (2001) 1.

[4] S. Milošević, Ž. Rašković-Lovre, S. Kurko, R. Vujasin, N. Cvjetićanin, Lj. Matović, J. Grbović Novaković, *Ceram. Int.* 39 (2013) 51.

[5] J. Gulicovski, Ž. Rašković-Lovre, S. Kurko, R. Vujasin, Z. Jovanović, Lj. Matović, J. Grbović Novaković, *Ceram. Int.* 38 (2012) 1181.

[6] J. Grbović Novaković, Lj. Matović, S. Milovanović, M. Drvendžija, N. Novaković, D. Rajnović, M. Šiljegović, Z. Kačarević Popović, N. Ivanović, *Int. J. Hydrogen Energy* 33 (2008) 1876.

[7] A. J. Du, S. C. Smith, G. Q. Lu, *J. Phys. Chem. C* 111 (2007) 8360.

[8] M. S. Park, A. Janotti, C. G. Van de Walle, *Phys Rev B* 80 (2009) 064102.

# ENHANCED HYDROGEN SORPTION PROPERTIES OF $MgH_2$ CATALYZED WITH $VO_2$(B)

S. Milošević,[1]* R. Vujasin,[1] S. Kumrić,[1] Lj. Matović,[1] Ž. Rašković-Lovre,[1] L. Pasquini,[2] J. Grbović Novaković[1]

[1]*Vinča Institute of Nuclear Sciences, POB 522, 11000 Belgrade, Serbia*
[2]*Department of Physics and Astronomy, University of Bologna, v.le Berti Pichat 6/2,I-40127 Bologna, Italy*
**e-mail: sanjam@vinca.rs*

$MgH_2$-$VO_2$(B) composite was synthesized by high-energy mechanical milling. The differential scanning calorimetry and Sievert's apparatus for sorption analysis were used for analysing sorption properties of produced composite. Results show that desorption temperature was reduced and that sorption reaction is notable enhanced at relatively low temperature. Complete desorption of pure $MgH_2$ at 350°C could not be reached even after 100 minutes, while composite material fully desorbs in less than 3 minutes even at lower temperatures.

## Introduction

Much effort has been devoted on studies of metal hydrides for hydrogen storage. Since magnesium is an abundant, cheap and light metal with a high hydrogen sorption capacity (7.6 wt.%), metallic magnesium and magnesium based compounds were considered as a promising candidate for hydrogen storage. Still, sorption kinetics is main drawback of this material. It has been shown that high energy ball milling of magnesium hydride with various additives (oxide, non-oxide ceramics, amines etc.) improves the hydrogen sorption properties [1–3]. In contrast to bulk hydride, the form of fine powder has many advantages such large surface-to-volume ratio which enhances hydrogen diffusion and nucleation of $MgH_2$. Regarding additives, metal oxide are both catalysts and very efficient milling agents that can create defects in magnesium hydride [4]. A wide range of different metal oxide was used to improve the properties of $MgH_2$ [5–7]. Bobet et al. reported the beneficial effect $CeO_2$ on $MgH_2$ sorption kinetics. Bormann et al. proposed that oxide interfaces attached to the oxide catalysts might locally destabilize the magnesium hydride phase [6]. Oelerich et al. investigated the influence of metal oxides on the sorption behaviour of nanocrystalline Mg-based systems [5]. The highest desorption rates are achieved with $V_2O_5$ and $Fe_3O_4$. Metal oxides, compared to the $MgH_2$/transition metals composites, are dispersed homogeneously due to the brittleness. Oxides improves desorption kinetics even in very small doses. The fast sorption kinetics of composite may originate form a very high defect density, introduced at the surface of the metal oxide particles during high–

energy ball milling [8]. On the other hand the catalytic nature of oxides originate from their vacant structure, therefore in this paper we have used $VO_2$(B) to enhance sorption properties of $MgH_2$.

## Experimental

Composite material was synthesized by high-energy ball milling using Spex 8000M mixer mill. Composite contains 95 mass% of commercial $MgH_2$ (Alpha Aesar 98%) and 5 mass% of previously hydrothermally synthesized $VO_2$(B) (from $V_2O_5$ Merck as a precursor). Milling was performed for 2h with ball to powder ratio 10:1. All samples were kept and handled in Ar atmosphere. DSC measurements were performed in temperature interval 80-500ºC, using 10K/min step. Desorption/absorption cycling were performed at different temperatures and corresponding pressures to determine the dependence of $H_2$ sorption concentration and temperature of activation using Hydrogen Sorption Analyser (HSA).

## Results and Discussion

DSC curves of starting material $MgH_2$ and $VO_2$(B), and of synthesized composite are shown in Figure 1. DSC curve of composite show reduction of sorption temperature comparing to commercial $MgH_2$. Onset of desorption temperature is around 370°C while in commercial $MgH_2$ is at around 450°C. Composite shows two very wide maxima at ~395°C and ~423°C. The values of enthalpy change, obtained by integration of DSC peak area, is 1380 J/g for commercial $MgH_2$ and 900 J/g for composite material. Decrease in enthalpy corresponds to decrease in hydrogen capacity which is in accordance with the results of hydrogen sorption measurements.

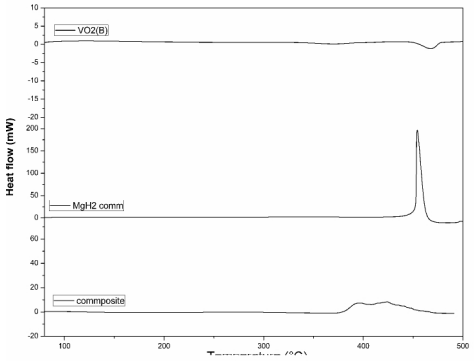


**Figure 1.** DSC curves of materials

HSA was used to examine the volume of hydrogen released from samples in a pre-set time period and temperature. In commercial $MgH_2$, at desorption temperature of 380°C, HSA curve reaches a plateau (maximum capacity of 5.7wt.%) after 30 min (see Fig. 2). At 350°C desorption begins only after 30 minutes, and after 100 minutes does not reach maximum desorption (reached ~4.5wt.%).

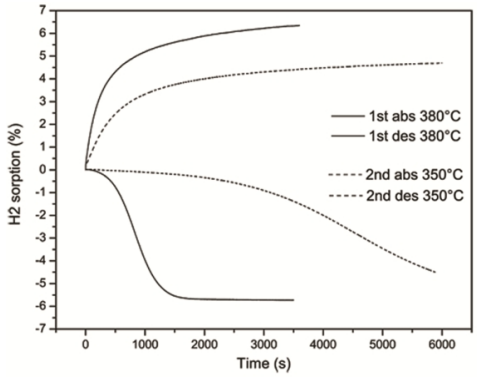


**Figure 2.** Sorption curves of commercial $MgH_2$

Also, capacity in absorption mode was significantly lower (~4.7wt.%) compared to absorption capacity at 380°C.

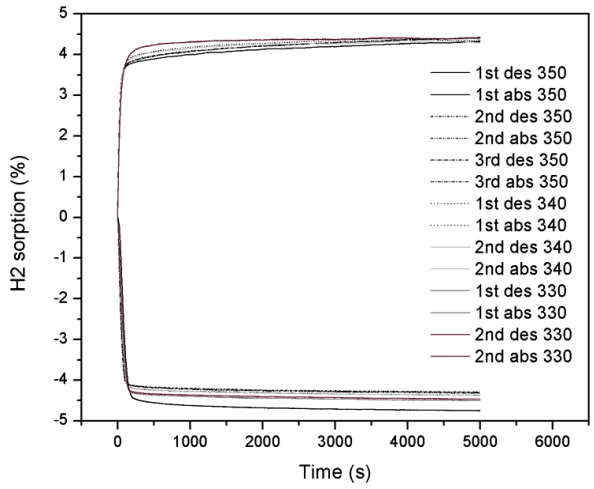


**Figure 3.** Cycling curves of composite material at 360°C

Milled composite material, with the addition of 5 mass% $VO_2$(B) shows significant acceleration of hydrogen desorption: at temperature of 350°C maximum capacity of 4.1 wt.% is reached after ~125 seconds. At 340°C, desorption capacity of 4.2 wt.% is reached after ~150 seconds, and at temperature of 330°C capacity of 4.3 wt.% is reached after ~180 seconds (see Fig. 3).

## Conclusion

$MgH_2$-$VO_2$ composite was synthesized by mechanical milling. The sorption reaction was followed by differential scanning calorimetry and sorption analysis. Results indicate excellent catalytic activity of $VO_2$(B) in both adsorption and desorption process. The temperature onset for desorption is significantly decreased. The main fact is that composite demonstrate excellent reversibility in sorption reaction. The maximum capacity of hydrogen is released in less than 3 minutes from synthesized composites, representing a dramatic speed-up of kinetics performances comparing to the unprocessed $MgH_2$.

## Acknowledgement

This research was financially supported by Ministry of Education, Science and Technology of the Republic of Serbia under grant III 45012. The authors express their gratitude to COST Action MP1103 “Nanostructured Materials for Solid-State Hydrogen Storage”.

## References

[1] L. Schlapbach, A. Zuttel, *Nature* 414 (2001) 353.
[2] A. Zuttel, *Mater. Today* 6 (2003) 24.
[3] A. Bassetti, E. Bonetti, L. Pasquini, A. Montone, J. Grbovic, M. Vittori Antisari, *Eur Phys J B* 43 (2005) 19.

[4] R. B. Gupta (Ed.), *Hydrogen Fuel-production, transport and storage*, Taylor and Francis, 2008.
[5] W. Oelerich, T. Klassen, R. Bormann, *J. Alloys Compd.* 315 (2001) 237.
[6] J. L. Bobet, S. Desmoulins-Krawiec, E. Grigorova, F. Cansell, B. Chevalier, *J. Alloys Compd.* 351 (2003) 217.
[7] A. Borgschulte, U. Bosenberg, G. Barkhordarian, M. Dornheim, R. Bormann. *Catal Today* 120 (2007) 262.
[8] A. Borgschulte, M. Bielmann, A. Zuttel, G. Barkhordarian, M. Dornheim, R. Bormann, *Appl. Surf. Sci.* 254 (2008) 2377.

# HYDROGEN DIFFUSION IN SURFACE AREA OF $TiO_2$

R. Vujasin,* B.PaskašMamula, I.Milanović, J. GrbovićNovaković, N. Novaković

*Vinča Institute of Nuclear Sciences, University of Belgrade, POB 522, 11001 Belgrade, Serbia*
**e-mail: radojka.vujasin@vinca.rs*

The hydrogen interaction with the rutile-structure $TiO_2$ (110) surface has been investigated using pseudopotential and projected augmented wave methods. The hydrogen diffusion behavior and thermodynamic properties were calculated by means of full relaxation of structure in every step of bulk diffusion. The results show the existence of potential barriers close to every atomic layer, the trends of barriers and overall system energy lowering away from surface and the occurrence of preferential H sites within each interlayer basin. These findings go in favor of previously experimental findings of $TiO_2$ low surface H coverage and observed easy diffusion of hydrogen from reduced surface into the $TiO_2$ bulk or at least in near surface region.

## Introduction

Titania attracts a lot of interest because of its many achieved and possible future applications, such as improvement of sorption properties of hydrides [1].A large number of experimental studies confirm that the addition of titania has beneficial effect on destabilization of $MgH_2$ matrix and can cause improvement of this material's kinetic properties [2-6]. Several numerical studies on hydrogen motion through oxide surface has been done to understand the mechanism of the reaction [7,8].

Yin *et al.* [9] have investigated hydrogen coverage on $TiO_2$ (110) surface under different experimental conditions of exposure to atomic hydrogen. They obtained that maximum H monolayer coverage on $TiO_2$(110) surface is only 70% at room temperature, regardless of applied partial pressure of hydrogen. They also confirmed that during the heating of the hydrogenated sample, H atoms have migrated *into* the $TiO_2$ bulk. This is unusual since desorption of $H_2$ (or $H_2O$) molecules into the gas phase is common behavior of reduced oxides surface. Filippone *et al.* carried out research which showed that hydrogen behaves as a deep donor in rutile phase and forms an $OH^+$ complex, where H forms bond with a prevailing ionic character [10]. With addition of Hubbard term U, they showed that electronic localization effects have major influence on nature of bonding and charge distribution as a consequence of hydrogen interstitial.

We have investigated the interaction of H atom with $TiO_2$ (110) surface and its behavior in the near-surface region of rutile $TiO_2$.

## Details of calculations

Investigation of atomic hydrogen behavior on rutile $TiO_2$ (110) surface and in the near-surface region were done using two methods available in Abinit code. Plane waves based calculations with Troullier-Martins norm-conserving pseudopotentials (PP) and projected augmented wave, with addition of U Hubbard term (PAW with GGA+U), method were used. The value of $U_{eff}$ was 2.0 eV. The energy cut-off of the plane wave basis set was 816 eV.

Slab supercell (2x1)(110) with 21 atomic layers and 85 atoms was constructed. The surface of the supercell was separated from its periodic image by 15 Å of vacuum. Three bottom layers were fixed to simulate the bulk. The rest of supercell atoms were subject to the relaxation of atomic positions. It is assumed that hydrogen atom forms short OH bonds and that diffusion consists of "jumps" between neighboring O sites. Calculations were performed to obtain relaxed structures with different arrangements, where H atom was bounded to O atoms in different atomic layers, as illustrated in the Figure 1.

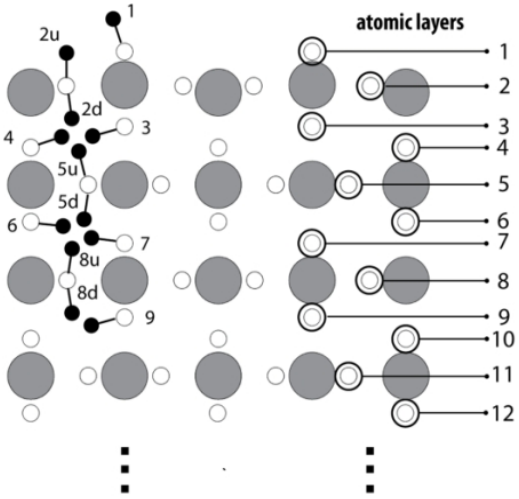


**Figure 1.** Atomic layers and positions of H atoms in slab supercell (side view).

## Results and Discussion

Figure 2 is showing the energy differences as function of H distance from surface for PP and PAW (GGA+U) calculations. Energy differences were represented on x axis, with energy of configuration 1 used as reference, marked with horizontal line. As distance reference from surface, z-coordinate of $O_{2s}$ atom in slab supercell without H was used, marked as vertical dashed line. The characteristic "periodic" dependence of energy on hydrogen position depth is visible. According to [5,6] the barriers for jump from one

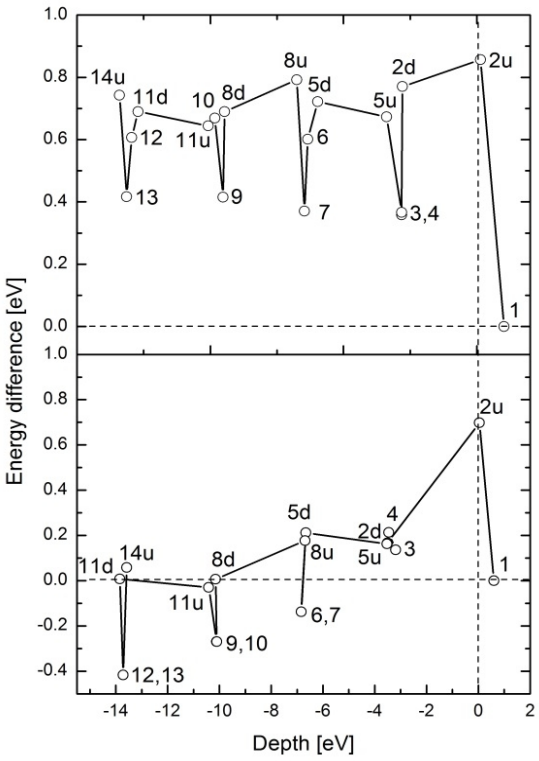


**Figure 2.** Slab system energy change as a function of hydrogen atom distance from the surface using PAW (top) and PP approach (bottom).

oxygen atom to another range from 0.5 to 1.1 eV, depending on the position of bonding oxygen atoms and distance from surface. These barriers could be overcome at modest temperatures (in accordance with [9]). The details of energy profile, like barriers, are not visible in approach presented here. However, initial and final states, corresponding to jump from one O atom to the next, can provide details and possible pathways of hydrogen drift from and to the surface.

## Conclusion

In this paper we have presented the results of electronic structure calculations of (2x1) (110) slabs of $TiO_2$ – H system. The energy profile of near-surface area shows that atomic layers parallel to the surface act like barriers for hydrogen drift into the bulk. At the same time, hydrogen should "jump" fairly easy within the same interlayer basin. Our calculations also showed that the influence of surface is constrained to only few atomic layers closest to vacuum.

## Acknowledgement

This work was supported by Serbian Ministry of Education, Science and Technological Development under the Grant III 45012. Calculations have been partially performed using ENEA-GRID facility, Italy.

## References

[1] U. Diebold, *Surf. Sci. Rep.* 48 (2003) 53.
[2] D. L. Croston, D. M. Grant, G. S. Walker, *J. Alloys Compd.* 492 (2010) 251.
[3] W. Oelerich, T. Klassen, R. Bormann, *J. Alloys Compd.* 315 (2001) 237.
[4] M. Polanski, J. Bystrzycki, *J. Alloys Compd.* 486 (2009) 697.
[5] H. Hirate et al, *J. Alloys Compd.* 509S (2011) S612.
[6] K. S. Jung, D. H. Kim, E. Y. Lee, K. S. Lee, *Catal. Today* 120 (2007) 270.
[7] J. Leconte et al, *Surf. Sci.* 497 (2002) 194.
[8] H.-T. Chen et al, *ChemPhysChem* 8 (2007) 849.
[9] X.-L. Yin et al, *ChemPhysChem* 9 (2008) 253.
[10] F. Filippone et al, *Phys Rev B* 80 (2009) 245203.

# KINETICS OF HYDROGEN ABSORPTION BY Zr-BASED ALLOYS BASED ON CHOU MODEL

D. Conić, K. Batalović

*Laboratory for nuclear and plasma physics, VINCA Institute of nuclear sciences, P.O.Box 522, Belgrade, Serbia*

Hydrogen absorption in Zr-12wt%Ta and Zr-12wt%Taat 873 K and 973 K and 1 bar hydrogen pressure is investigated. Chou model is used for kinetic analysis and to calculate activation energy for hydrogen diffusion in Zr-12wt%Ta. It is found that results strongly depend on the choice of experimental parameter in model, characteristic absorption time.

## Introduction

Zirconium and its alloys are of big importance in the various hydrogen storage applications, as well as in the nuclear technology. For this reason, kinetics of hydrogen absorption by these materials is of great interest. The process of hydrogen absorption in metals consists of large number of subsequent reactions, and therefore analysis of such process is not straightforward. Many models have been established so far to address this issue. In this study we apply the Chou model, which has proven valid for the analysis of hydrogen absorption in by metal alloy powder samples [1,2] to address the kinetics of hydrogen absorption in two Zr-based alloys.
The Chou model considers seven steps of hydride formation reaction [1].Among these, dissociation of hydrogen molecules and chemisorption on the surface, surface penetration, diffusion through the β-phase layer, and chemical reaction at the α-β boundary are considered to be potential rate controlling steps [1]. Cornerstone of Chou model application is the use of characteristic absorption time, $t_{\xi=\phi}$[2], which is experimentally measured time for the absorption of particular hydrogen fraction in the studied alloy (e.g. $t_{\phi=0.5}$is time when the half of the hydrogen amount is absorbed). This value is further used in analytical expressions for constructing absorption curves and calculating activation energies [1,2].

## Experimental

Two Zr-based alloys, Zr-12wt%Ta and Zr-2.5wt%Nb-3t%Ta, were prepared by melting a mixture of pure elements Zr, Nb and Ta (purities >99%) in an argon atmosphere in RF induction furnace. The samples were then crushed into powder and activated by annealing at the temperature above the working one, under a vacuum of $1x10^{-3}$ mbar during 2 h followed by

cooling to room temperature in hydrogen atmosphere. The hydrogen absorption process was investigated using typical, Sievert-type volumetric equipment [3] at the temperatures 873 and 973 Kand1 bar hydrogen pressure. Hydrogen absorption was monitored with time, and H/M was calculated based on the pressure change in the reaction chamber.

**Results**

Hydrogen storage capacities measured at 873 K and 973 K for Zr-12wt%Ta alloy are 0.81 H/M and 0.51 H/M respectively and for Zr-2.5wt%Nb-3wt%Ta alloy0.91 and 0.76, respectively. Zr-12wt%Ta absorbed more than 99.5% of hydrogen in less than three minutes, while Zr-2.5wt%Nb-3wt%Ta showed slower absorption process at the same conditions -same percentage of hydrogen in absorbed in ten minutes.

To analyze the hydrogen absorption kinetics, Chou model for different rate controlling steps was tested. By showing the best model - experimental results match, we established diffusion of hydrogen atoms through the β-phase as the rate controlling step in the case of hydrogen absorption in Zr-12wt%Ta alloy. At the figure 1 measured absorption curve and fits according to Chou model for different characteristic times are presented.

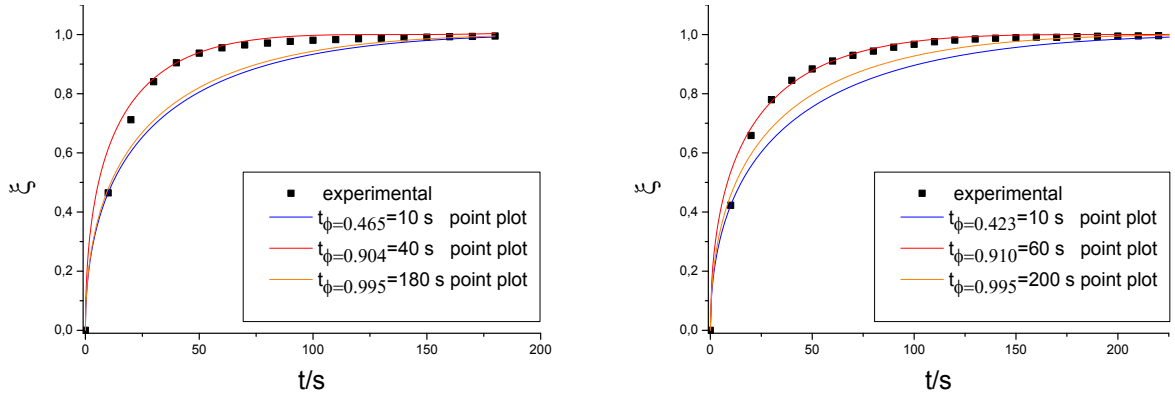


**Figure 1.** Experimental plot and Chou model fits for diffusion as rate controlling step for Zr-12wt%Ta at a) 873 K and b) 973 K

At the very beginning of hydrogen absorption (first point fit) and when absorption is almost over (≥99.5% reacted hydrogen point fit) model shows biggest mismatch with the experimental plot. For characteristic absorption times chosen in between (for reacted fraction around 90%), model curve shows good agreement to the experimental one. Calculation of activation energy by Chou analytical expression [2] is done for every measured characteristic absorption time. Activation energies obtained from the characteristic absorption times that were used for the model plots in figure 1 are presented in table 1.

**Table 1.** Activation energy for hydrogen absorption of Zr-12wt%Ta sample for diffusion of hydrogen as rate controlling step according to Chou model

| **Characteristic absorption time / s** | 10 | 40 | 60 | 180 |
|---|---|---|---|---|
| **$E_a$ / (kJ/mol)** | 16.4 | 22.5 | 21.6 | 4.0 |

Activation energies obtained from the characteristic absorption times which best fit experimental values, $t_{\xi=\phi}$=40s and $t_{\xi=\phi}$=60s, are close in values, while those obtained from $t_{\xi=\phi}$=10 s and $t_{\xi=\phi}$=180 s deviate considerably as expected. Activation energy of the hydrogen diffusion through the β-phase layer of Zr-12wt%Ta is therefore estimated on (22±1) kJ/mol, taking into account activation energy values for $t_{\xi=\phi}$=40 s and $t_{\xi=\phi}$=60 s. Previous study on hydrogen diffusion through the pure zirconium hydride layer estimated activation energy of (47.0±0.4) kJ/mol [4]. Further analysis, in the wider temperature range are needed in order to confirm the value obtained by Chou model and to prove that addition of tantalum leads to lowering of activation energy for hydrogen diffusion through zirconium.

Chou model with diffusion as the rate controlling step is also tested for the case of hydrogen absorption kinetics in Zr-2.5wt%Nb-3wt%Ta at 973 K, figure 2, for which previous study identified diffusion of hydrogen through hydride layer as the rate controlling step at the first reaction stage [3]. Similarly to the Zr-12wt%Ta sample, for the first point plot or last point plot, the biggest mismatches to the experimental values are found. For the characteristic time chosen in the middle of the first stage of hydriding reaction, in accordance with earlier research [3], model was found to be reliable for the study of hydrogen absorption kinetics.

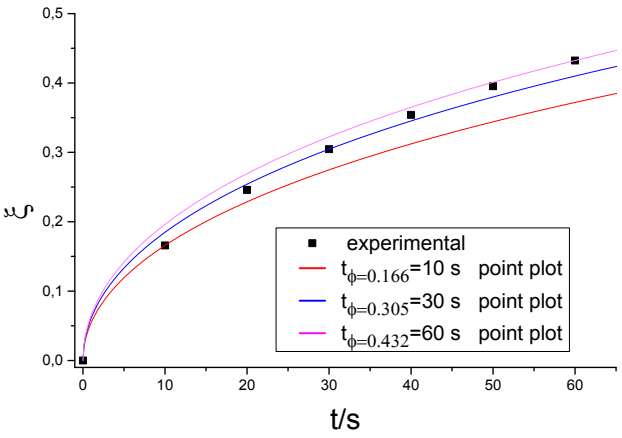


**Figure 2.** Experimental plot and Chou model fits for diffusion as rate controlling step for Zr-2.5wt%Nb-3wt%Ta at 973 K.

## Conclusion

Chou model was tested for the analysis of hydrogen absorption kinetics in Zr-based alloys. Kinetic parameters and experiment-model agreement were found to be very dependent on the selection of characteristic absorption times chosen for model fit. According to the best agreement with experimental results, for hydrogen reacted fraction around 90%, diffusion of hydrogen through β-phase layer of Zr-12wt%Ta was identified as the rate controlling step. Measurements at wider temperature range are needed to validate the preliminary results which suggest that tantalum addition lowers the activation energy for hydrogen diffusion through Zr.

**References**

[1] G. Wu, J. Zhang, Q. Li, K. Chou, *Int. J. Hydrogen Energy* 36 (2011) 12923.
[2] K.-C. Chou, Q. Li, Q. Lin, L.-J. Jiang, K.-D. Xu, *Int. J. Hydrogen Energy* 30 (2005) 301.
[3] B. Cekić, K. Ćirić, M. Iordoc, S. Marković, M. Mitrić, D. Stojić, *J. Alloys and Compd.* 559 (2013) 162.
[4] H. Wipf, B. Kappesser, R. Werner, *J. Alloys and Compd.* 310 (2000) 190.

# THERMODYNAMICS AND ELECTRONIC STRUCTURE OF HYDROGEN STORAGE MATERIALS – INSIGHT FROM DFT

Katarina Batalović, Jana Radaković, Vasil Koteski

*Laboratory for nuclear and plasma physics, Institute of Nuclear Sciences VINČA. P.O.Box 522, 11001 Belgrade, Serbia*

Thermodynamics of hydride formation and changes in the electronic structure during hydrogen absorption in binary and ternary metal alloys, as well as ternary and quaternary complex hydrides are studied using DFT methods. Useful insight into properties relevant for hydrogen storage applications, such as energy of hydride formation and band gap, is gained for $Mg_2Fe_{0.75}M_{0.25}H_6$, (M = Co, Ni, Mn, Fe) and (Ti,Zr)Ni hydrides.

## Introduction

Hydrogen is extensively studied as the ideal energy carrier for both mobile and stationary applications. One of the main unsolved problems for the wide use of hydrogen energy is finding the safe and technologically and economically feasible method of hydrogen storage. Hence, material-based hydrogen storage is the subject of numerous ongoing researches, including metal hydrides, complex hydrides, chemical hydrides, graphene-based materials etc. Design and application of various hydrides is dependent on the fundamental understanding of interaction of hydrogen with different materials. Useful insight into kinetics and thermodynamics of hydride formation/decomposition can be obtained by the use of theoretical methods.

DFT (Density Functional Theory) - based calculations are employed to assess the thermodynamic properties and electronic structure modifications, caused by changes in crystal structure, composition and hydrogen-metal interaction, for two types of hydrides. (Ti,Zr)Ni alloys belong to the class of intermetallic compounds, used for stationary hydrogen storage, in Ni-MH batteries, heat pumps, etc. TiNi- based alloys are also of interest due to the simultaneous observation of shape memory effect and possibility of reversible hydrogen absorption. $Mg_2FeH_6$ belongs to the group of Mg-based complex hydrides, interesting for their high volumetric hydrogen capacity and optical properties.

## Calculation method

The band structure calculations were performed using a Full Potential (Linearized) Augmented Plane-Waves plus local orbitals (FP (L)APW + lo) method. The exchange and correlation effects were included within the generalized gradient approximation, using the Perdew–Burke–Ernzerhof scheme. The vibrational frequencies and zero point energy (ZPE) for the investigated compounds were calculated with the Vienna Ab initio Simulation Package (VASP).

**Results and discussion**

Formation energies of the hydrides, calculated as the difference in total energy of the hydride and starting alloys (in the case of (Ti,Zr)Ni) or constituent metals (in the case of $Mg_2Fe_{0.75}M_{0.25}H_6$), are given in Table 1.

**Table 1.** Calculated formation energies and Bader charge on H atom for the studied hydrides

| | Space group | $\Delta E^f$ (kJ/molH) | AIM charge/e |
|---|---|---|---|
| TiNiH | I4/mmm | -39.6 | -0.50 |
| TiNiH | Cmcm | -11.5 | -0.45 |
| $Ti_{0.67}Zr_{0.33}NiH$ | Cmcm | -14.2[1] | -0.44 |
| $Ti_{0.67}Zr_{0.33}NiH_3$ | Cmcm | -29.6[1] | -0.40<br>-0.50 |
| $ZrNiH_3$ | Cmcm | -38.3 | -0.42<br>-0.51 |
| $Mg_2FeH_6$ | Fm-3m | -46.7[2] | -0.55 |
| $Mg_2Fe_{0.75}Mn_{0.25}$ | Fm-3m | -39.1[2] | -0.56 |
| $Mg_2Fe_{0.75}Co_{0.25}$ | Fm-3m | -40.4[2] | -0.54 |
| $Mg_2Fe_{0.75}Ni_{0.25}$ | Fm-3m | -35.0[2] | -0.54 |

Alloying of $Mg_2FeH_6$ and TiNi, is found to destabilize the hydrides. Also, TiNiH with tetragonal crystal structure was found to have lower energy than the one with orthorombic. In all studied hydrides, the Bader charge of hydrogen atom is mainly determined by the type of interstitial site hydrogen occupies. The same holds for the contribution of zero point energy change to the total energy change - in all studied Mg-based hydrides, calculated ZPE energy change is 7.3 kJ/molH [2].

Based on the calculated density of states, Fig. 1, change in the optical properties of $Mg_2FeH_6$ is considered. Doping with Ni, Mn and Co is expected to reduce the direct gap of $Mg_2FeH_6$ (calculated width of the direct band gap for $Mg_2FeH_6$ is 1.85eV[2]). Ni doping is found to cause the largest change in both thermodynamical and optical properties of $Mg_2FeH_6$.

The thermodynamics of hydride formation process in $Ti_{0.67}Zr_{0.33}Ni$ is shown in Fig.2, decomposed to elementary steps.

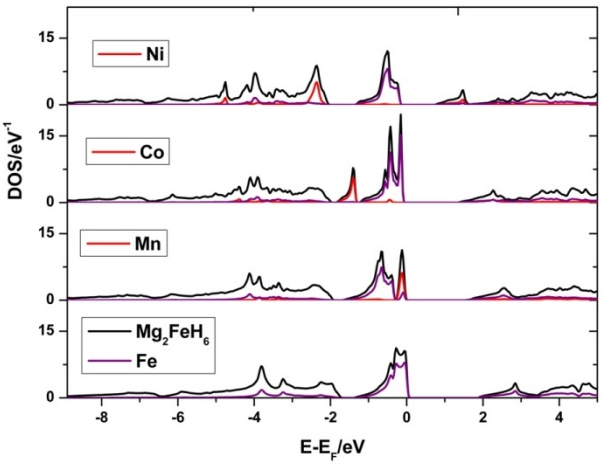


**Figure 1.** Total density of states for $Mg_2Fe_{0.75}M_{0.25}H_6$, M=Ni, Co, Mn, Fe and partial atomic contributions of the metals [2]

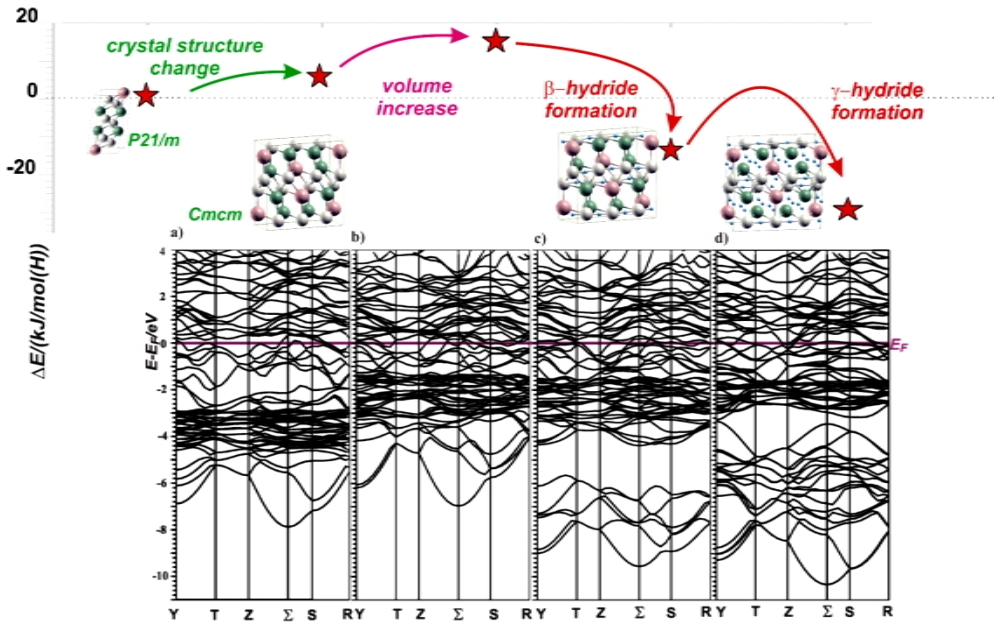


**Figure 2.** Energy change in hydride formation reaction for martensitic $Ti_{0.67}Zr_{0.33}Ni$ alloy; bottom: band structure of a) $Ti_{0.67}Zr_{0.33}Ni$, optimized; b) $Ti_{0.67}Zr_{0.33}Ni$, volume of β-hydride; c) $Ti_{0.67}Zr_{0.33}NiH$ d) $Ti_{0.67}Zr_{0.33}NiH_3$[1]

Change in the crystal structure of the starting alloy and increase of its volume cause destabilization of the martensitic $Ti_{0.67}Zr_{0.33}Ni$, while the chemical interaction of hydrogen with metals stabilize hydrides, and this is the case in formation of both β- and γ- hydride[1]. This is also seen through the changes in the band structure for the orthorhombic alloys, Fig.2. During hydride formation, some metal states are moved to the lower energies, and new band is formed at the energies of H-s states.

## Conclusion

Based on the DFT calculations, useful insight into the applicability of (Ti,Zr)Ni hydrides and $Mg_2(Fe,M)H_6$ is gain. Stability of the studied hydrides is found to be dependent on the alloy composition. Alloying $Mg_2FeH_6$ with Co, Ni and Mn destabilizes all studied hydrides. It was shown how electronic structure depends on the changes in alloy composition, volume, and crystal structure as well as how it changes during hydride formation process. The Bader charge on hydrogen atom and change in the zero point energy during hydride formation were found to be dominantly determined by the type (symmetry) of the hydrogen atom position.

## References

[1] K. Batalović, V. Koteski, D. Stojić, *J. Phys. Chem. C*, 117 (2013) 26914.
[2] K. Batalović, J. Radaković, J. Belošević-Čavor, V. Koteski, *Phys. Chem. Chem. Phys.*16 (2014)12356.

# ELECTRONIC STRUCTURE AND STABILITY OF INTERSTITIAL MONOHYDRIDES

Jana Radaković, Katarina Batalović, and Jelena Belošević-Čavor

*Laboratory for nuclear and plasma physics, Institute of Nuclear Sciences VINČA. P.O.Box 522, 11001 Belgrade, Serbia*

We present first principles calculations of the electronic structure and formation enthalpies of $HfV_2H$ interstitial monohydride. $HfV_2$ compound is a cubic Laves phase (C15), with hydrogen potentially occupying three interstitial positions: 96g, 32e, and/or 8b. Using the augmented plane waves plus local orbitals (APW+lo) method we have performed the band structure calculations in order to compare the thermodynamics of formed interstitial hydrides ($HfV_2H$ with H in 8b, 32e, or 96g). Stability of formed monohydrides is determined by calculating the enthalpy of formation for every occupied interstitial site, and the occupational site-preference of hydrogen is determined by their mutual comparison. Origin of different thermodynamic behaviour is established by estimating the differences in density of states of monohydrides, and energy position of hydrogen s band.

## Introduction

Laves phases are a large class of intermetallic compounds that exhibit high hydrogen storage capacity and favorable absorption/desorption kinetics around room temperature and ambient pressures. Consequently, they are being investigated as potential hydrogen storage materials, or electrodes for the Ni/MH batteries [1-3]. Apart from that, application of these materials in numerous fields of industry and technology requires better understanding of relationship between their electronic structure and intrinsic properties, such as, e.g., their thermodynamic stability.

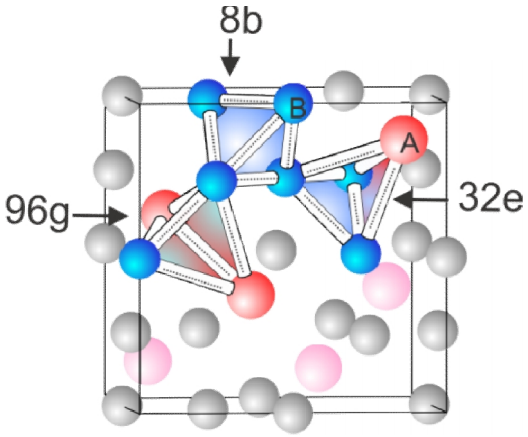


**Figure 1.** Unit cell of AB2 cubic C15 Laves phase with emphesized tetrahedral interstitial sites. (In case of HfV2 A = Hf, B = V)

In a wide range of temperatures, $HfV_2$ is a cubic Laves phase that does not undergo a phase transition with hydriding. This type of Laves phase can store hydrogen in three interstitial tetrahedra, where it can be surrounded by four V atoms (8b-Wyckoff site), three V atoms and one Hf atom (32e site), and finally by two V and two Hf atoms (96g site). The unit cell of the cubic $AB_2$ Laves phase is presented in Figure 1; it crystallizes in $MgCu_2$ structure with $Fd\bar{3}m$ space group. Distribution of hydrogen atoms in the crystal lattice, i.e., occupation of different interstitial sites is entirely affected by hydrogen concentration, as

well as the size of all interstitial tetrahedra. However, stability of formed hydride varies with respect to occupied interstitial site. To study the stability and electronic structure of $HfV_2H$ hydride, we have performed the first principles calculations, based on density functional theory.

**Calculation method**

The band structure calculations were performed using a Full Potential (Linearized) Augmented Plane-Waves plus local orbitals (FP (L)APW + lo) method, as implemented in Wien2k computational code [4]. The exchange and correlation effects were included within the generalized gradient approximation (GGA), using the Perdew–Burke–Ernzerhof (PBE) scheme. Radii of the muffin-tin, nonoverlapping, spheres centered at the atomic nucleus were set to 2.3 bohr, 1.9 bohr, and 0.9 bohr for Hf, V, and H, respectively. The number of used basis functions was determined by $R_{mt}K_{max}$ parameter, which was set to 5. The cutoff energy between the core and valence states was –6.0 Ry. Brillouin zone integration was performed via tetrahedron method, and depending on the occupied interstitial site, a mesh of 192 to 500 k points in the irreducible Brillouin zone was used. Self-consistency was achieved by demanding that the convergence of the integrated charge difference between the two successive iterations was less than $10^{-5}$ electrons. The investigated structures were relaxed until the forces acting on all atoms were less than 1 mRy/bohr.

**Results and discussion**

Formation energies of hydrides, when one hydrogen atom is positioned in 8b, 32e, or 96g interstitial site, are calculated as the difference between the total energy of the hydride $HfV_2H$, starting compound $HfV_2$, and hydrogen atom [5]. Obtained values for studied monohydrides are presented in Figure 2 (left axis). According to calculated values the most stable $HfV_2$ monohydride is formed when H occupies 96g interstitial site, while the least stable is the 8b hydride.

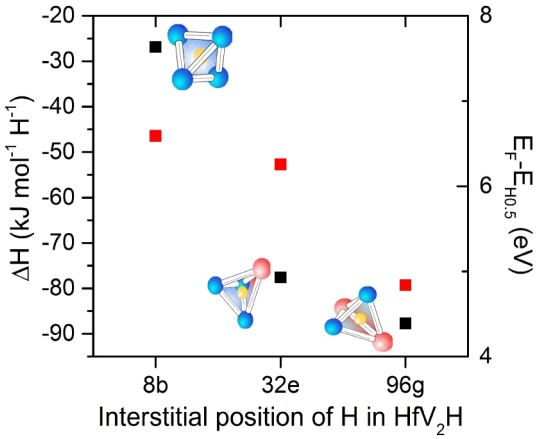


**Figure 2.** Left axis: Formation enthalpy of $HfV_2H$ with H positioned in 8b, 32e, or 96g Wyckoff site. Right axis: Energy of hydrogen s band.

To assess the origin of different thermodynamic behavior, we have studied the density of states (DOS) of all three potential hydrides. Specifically interesting was the energy position of the hydrogen s band with respect to Fermi level ($E_F$) in DOS graphs, considering that it was established that the stability of hydrides depends on the position of the hydrogen s band with respect to Fermi level [6]. The energy location of hydrogen

s band is quantified by defining the energy difference between the Fermi energy ($E_F$) and the energy for which the integrated hydrogen DOS equals 0.5 electrons ($E_{H0.5}$). Figure 3 presents the integrated hydrogen DOS in the energy range from -10 eV to Fermi energy, which is by convention set to 0 eV. Calculated energy differences for all three occupied interstitials are presented on the right axes of Figure 2, along with the formation enthalpies. It can be observed that previously determined correlation holds in the present case as well. The established trend indicates that as the energy of hydrogen electrons shifts towards the Fermi level formed hydrides are more stable, and easier to be produced. Consequently, insertion of hydrogen in 96g position will precede its accommodation by 32e, or 8b interstitial site. This conclusion confirms the previously established occupational site-preference of the atomic hydrogen in cubic Laves phases [7].

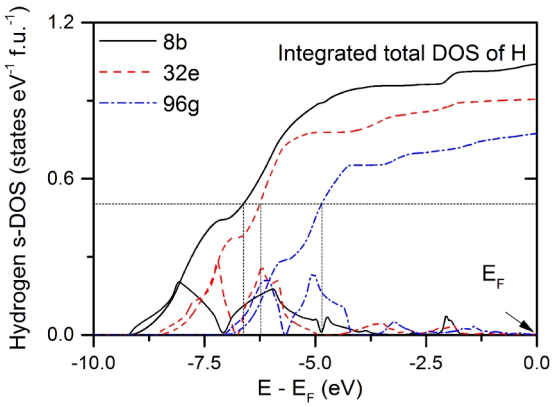


**Figure 3.** s-DOS of hydrogen in 8b, 32e, and 96g hydrides; integrated total DOS of hydrogen.

## Conclusion

First-principles calculations of the electronic structure of $HfV_2H$ cubic C15 Laves phase showed that the absorption of only one hydrogen atom in various interstitial sites substantially modifies the local electronic structure. Additionally, charge distribution of implemented hydrogen modifies according to affinity of interstitial site towards the inserted atom. Electronic charge distribution of the nearest neighbours of hydrogen atom can be associated with the hydrogen formation process as well, and stability of potential hydride.

## References

[1] S. Hong, C. L. Fu, *Phys. Rev. B* 66 (2002) 094109.
[2] J. Bodega, J. F. Fernandez, F. Leardini, J. R. Ares, C. Sanchez, *J. Phys. Chem. Solids.* 72 (2011) 1334.
[3] S. B. Gesari, M. E. Pronsato, A. Visintin, A. Juan, *J. Phys. Chem. C.* 114 (2010) 16832.
[4] P. Blaha, K. Schwarz, P. Sorantin, S. B. Trickey, *Comp. Phys. Commun.* 59 (1990) 399.
[5] K. Batalović, J. Radaković, J. Belošević-Čavor, V. Koteski, Phys. Chem. Chem. Phys.16 (2014) 12356.
[6] X. Ke, G. J. Kramer, O. M. Lovvik, *J. Phys.: Condens. Matter* 16 (2004) 6267.
[7] J. Radakovic, J. Beloševic-Čavor, V. Koteski, *Int. J. Hydrogen Energy* 38 (2013) 9229.